3 1176 01348 4747

UNCLASSIFIED [redacted]

Copy
RM L56A09

NACA RM L56A09

C2

NACA

RESEARCH MEMORANDUM

THE EFFECTS UPON BODY DRAG OF JETS EXHAUSTING FROM WING-MOUNTED NACELLES

By Robert W. Rainey

Langley Aeronautical Laboratory
Langley Field, Va.

CLASSIFICATION CHANGED
UNCLASSIFIED
To [redacted]
By authority of Nasa TPA # Effective
NB 7-6-56 Date 5-29-56

CLASSIFIED DOCUMENT

This material contains information affecting the National Defense of the United States within the meaning of the espionage laws, Title 18, U.S.C., Secs. 793 and 794, the transmission or revelation of which in any manner to an unauthorized person is prohibited by law.

NATIONAL ADVISORY COMMITTEE
FOR AERONAUTICS

WASHINGTON
April 20, 1956

[redacted]
UNCLASSIFIED

UNCLASSIFIED

[redacted]

NATIONAL ADVISORY COMMITTEE FOR AERONAUTICS

RESEARCH MEMORANDUM

THE EFFECTS UPON BODY DRAG OF JETS EXHAUSTING FROM WING-MOUNTED NACELLES

By Robert W. Rainey

SUMMARY

An investigation has been made in the Langley 9-inch supersonic tunnel to determine the effects of a sonic jet exhausting from a wing-mounted nacelle upon the body drag of a body-wing-nacelle combination for various longitudinal, spanwise, and vertical nacelle locations and jet pressure ratios. The fineness ratios of the body and nacelle were 8 and 5, respectively. The nacelle length was about 31 percent of the body length. Both the body and the nacelle consisted of forebodies and afterbodies which were parabolic arcs of revolution joined by a cylindrical midsection. The wing was untapered, swept 26.5°, and had a hexagonal airfoil section. Measurements were made at Mach numbers of 1.94 and 2.41 and at Reynolds numbers, based on body length, of about 2.61×10^6 and 2.10×10^6, respectively. Boundary-layer transition was induced artificially ahead of the body-wing juncture.

The results indicated that the maximum variations in the total and fore drags of the body due to jet interference were about one-fourth of the basic body drag. These were of the same order of magnitude as the maximum drag changes due to variation in nacelle location with the jet off. Both the jet interference and the nacelle interference upon body drag were considerably larger than the interference of the wing upon the body drag. With the nacelle at the most inboard positions and with the jet off, the body drag was reduced; operating the jet increased the body drag, however. With the nacelle located about four jet-exit diameters outboard of the body and with the jet off, the body drag values were the highest obtained; operating the jet reduced the body drag values. It was found that the entire jet-interference flow field had to be considered in the analysis of the interference upon the total, fore, and base drags of the body.

INTRODUCTION

Numerous investigations have been made at supersonic speeds to determine the effects of the addition of stores and nacelles upon the aerodynamic characteristics of individual aircraft components or entire

[redacted]

UNCLASSIFIED

configurations (for instance, refs. 1 and 2). In the majority of nacelle investigations made to date, the wing- or pylon-mounted nacelles, as well as those independently supported, did not utilize jets. Consequently, little information is available on the effects of the jet-interference flow field upon the characteristics of various components located within this flow field.

It has already been established that jet effects are important to afterbody and base drags (for instance, refs. 3 and 4), the loading on a nearby wing or surface (refs. 5, 6, and 7), and the loading on tail surfaces and afterportions of the fuselage (refs. 8 through 12). Also experimental and theoretical studies have been made of the structure of various jets exhausting into still air and into a moving airstream (refs. 13, 14, and 15). In view of the results presented in the aforementioned references, the propagation of disturbances from a jet exhausting from a wing-mounted nacelle should affect the aerodynamic characteristics of all components subjected to this jet-interference flow field.

The purpose of the present tests was to determine experimentally the effects of a jet exhausting from a sonic nozzle located within a wing-mounted nacelle upon the drag of the body of body-wing-nacelle combinations for various nacelle locations and jet pressure ratios. The nacelles were wing mounted, either directly to the wing or by use of pylons, depending upon the nacelle vertical location. The total and base drags of the body were measured with the nacelle at various spanwise and chordwise positions and at jet static-pressure ratios from the jet-off condition up to 40 (total-pressure ratios up to about 75). Tests were made in the Langley 9-inch supersonic tunnel using a semispan model installation. The tests were made at Mach numbers of 1.94 and 2.41 and at Reynolds numbers, based on fuselage length, of about 2.61×10^6 and 2.10×10^6, respectively. Boundary-layer transition was induced artificially on the body ahead of the body-wing juncture. The angle of attack and angle of yaw were 0°.

SYMBOLS

C_D drag coefficient, Drag/qS

$C_{D,b}$ base drag coefficient, $-C_{p,b} \times \frac{\text{Base area}}{S}$

ΔC_D incremental drag coefficient (jet on minus jet off or body-wing minus body)

d	diameter
K_x	longitudinal location parameter, x/d_j
K_y	spanwise location parameter, $\dfrac{\sqrt{y^2 + \left[z - \left(r_B - \frac{t}{2}\right)\right]^2} - (r_B + r_n)}{d_j}$
$\overline{K_y}$	spanwise location parameter assuming $z - \left(r_B - \frac{t}{2}\right) = 0$, $\dfrac{y - (r_B + r_n)}{d_j}$
K_z	vertical location parameter, z/d_j
M	Mach number
p	static pressure
$C_{p,b}$	base pressure coefficient, $\dfrac{p_b - p_\infty}{q_\infty}$
q	dynamic pressure
r	maximum radius
S	body frontal area
t	wing thickness
x	longitudinal distance from base of body to base of nacelle, positive upstream from base of body
x'	longitudinal distance from base of body to intersection of shock wave and body surface or plate, as seen in the schlieren photographs, positive upstream from base of body
y	spanwise distance between body and nacelle center lines, positive outboard of body
z	vertical distance from wing chord to nacelle center line, positive downward from wing chord
γ	ratio of specific heats

[redacted]

θ_N one-half of the nozzle divergence angle (fig. 4 only)

x' subscripts:

1 shock from within the jet

2 exit shock or trailing shock, for the jet on or the jet off, respectively

3 nacelle nose shock

Drag-coefficient subscripts:

b base

f fore (total minus base)

t total

Other subscripts:

b base

B body

j jet exit

n jet nacelle

∞ free stream

APPARATUS AND MODELS

Wind Tunnel

All tests were made in the Langley 9-inch supersonic tunnel which is a continuous operation, complete-return type of tunnel in which the stagnation pressure may be varied and controlled from about 1/10 atmosphere, absolute, to about 4 atmospheres, absolute. The stagnation temperature and dew point may also be varied and controlled. The Mach number is varied by interchanging nozzle blocks which form test sections approximately 9 inches square.

Models

The configuration used was a half-span installation (fig. 1). All parts were constructed of metal, and the exterior surfaces were smooth. The diameters of the body and nacelles, as well as the wing maximum thickness, were within ±0.001 inch of the specified dimensions. All other dimensions were believed to have been within ±0.005 inch of the specified dimensions with the exception of the distances from the nacelle base to the trailing edge of the wing; this varied up to 0.010 inch.

The body consisted of fore and afterbodies which were parabolic arcs of revolution and a cylindrical center section. Part of this center section was attached to the boundary-layer bypass plate and was cut out to receive the wing. The total forward and rearward gap between this wing support and the remainder of the body was about 0.020 inch; the transverse gap was about 0.005 inch. A transition strip about 1/4 inch wide and 0.006 inch thick was located on the body about 3/4 inch ahead of the body-wing leading-edge juncture. The strip consisted of fairly evenly distributed pulverized salt crystals no larger than 0.005 inch across which had passed through an 80-mesh screen. This crystal size was in order with the recommendations of reference 16.

Ten wing-nacelle assemblies were constructed and differed only in the location of the nacelle. The pertinent dimensions and designations of these assemblies are presented in figure 2. For all nacelles supported by pylons, the pylon cross section remained the same. Additional pertinent dimensions of the configurations are given in table I.

Each wing was built up of silver solder which combined three 1/4-inch-diameter copper air-supply tubes with steel leading- and trailing-edge wedges and included a jet static- and a jet stagnation-pressure tube (see fig. 2(a)). Dry air (dewpoint approximately -40° F) from a high-pressure storage tank was piped through a throttling valve into the air supply tubes at approximately atmospheric temperature.

Balance System

The body was supported by a forward flex link and the drag strain-gage beam (see fig. 1). A preloaded tension spring, adjustable from the base of the body, provided a means of varying the operational drag range of the balance system. During installation, the strain-gage beam was oriented so that the lift-on-drag interaction was negligible. It was also determined that interaction of side force and yawing moment on drag was negligible.

During the test program a sufficient number of balance calibrations were made between test runs to ascertain what small variations in

spring tension, if any, had taken place. These minor changes in spring tension have been included in the estimated probable errors in the section entitled "Precision of Data."

PRECISION OF DATA

A summary of the estimated maximum probable errors for the tests is presented in the following table:

Test Mach number, M	Maximum probable errors in -					
	M	R	$C_{D,t}$	$C_{D,b}$	$C_{D,f}$	p_j/p_∞
1.94	±0.010	±0.09 × 10^6	±0.003	±0.001	±0.004	±0.25
2.41	±.015	±.09	±.004	±.001	±.004	±.25

The spanwise nacelle locations were set within ±0.010 inch of the specified values which corresponds to a K_y value of ±0.04. The error in K_x was dictated by the model construction and was found to be less than ±0.04.

RESULTS AND DISCUSSION

Interference Considerations

For the general case of a jet exhausting into a supersonic stream, the calculation of the interference flow field is difficult and complex. One such calculation using the method of characteristics has been made by Schäfer (ref. 15). His results have been converted to isobar and streamline form and are presented in figure 3. Although the test conditions and configuration for this calculated case are different from those utilized in the present tests, the general flow phenomena of the calculated case are similar to those of the present tests at pressure ratios where the shock within the jet existed. Therefore, these more detailed calculated results will be used to define qualitatively the jet-interference flow field.

It is evident in figure 3 that significant pressure rises and changes in flow angle exist across the exit shock and are a maximum at the lip of the exit. The pressure and flow inclinations outboard and downstream of the exit are reduced as indicated by the isobars and streamlines.

It is obvious that the interference effects of the jet upon a neighboring body or surface would be dependent upon their relative locations since the distribution of interference pressures and flow angles can vary appreciably with position within the interference flow field. For the present case, as will be discussed in a later section, the gradients in pressure and flow angle within the expansion region outside of the mixing boundary and between the exit shock and the reflected shock from within the jet influenced the body drag. These gradients could not be discarded as secondary (as compared to considering only the effects of pressure rise across the exit shock and shock from within the jet) in the analyses of body drags.

A typical example in which portions of a twin-jet aircraft having wing-pylon-mounted nacelles might be subjected to this jet-interference flow field is presented in figure 4 (assuming no distortion to the flow field due to the presence of aircraft components for illustrative purposes only). It is apparent that the fuselage afterbody and tail surfaces would be subjected to various pressure variations and flow inclination angles which would have an effect on the fuselage and tail drags and the longitudinal stability characteristics. For the case of asymmetric jet flow fields (due to, for example, the aircraft at sideslip angles other than 0° or unequal jet thrusts), the directional and lateral stabilities, in addition to the longitudinal stability, would be affected.

Basic Data

The measured total and base drag coefficients are presented for several values of K_y (fig. 5) as a function of p_j/p_∞ in figures 6(a) and 6(b) for Mach numbers of 1.94 and 2.41, respectively. The drag coefficients (fig. 6) at the lowest value of p_j/p_∞ were for jet-off conditions. Due to wing sweep, K_x changed as K_y was changed. The parameter K_y was the slant distance between outer surfaces of the body and nacelle, nondimensionalized through the use of d_j (fig. 5) and is defined as the "spanwise location parameter." This distance was essentially the minimum distance between the two components for any one spanwise and vertical nacelle location and was undoubtedly an important factor in determining the existence of reflections and local choking between these two components. Also shown in figure 5 are the distances used in the longitudinal and vertical location parameters.

Measured Interference Effects

Throughout this report, reference will be made to the nacelle interference upon various other components. For the cases when the nacelle is supported by a pylon, the term "nacelle interference" is meant to include the total interferences of both pylon and nacelle.

The sources of interference upon the body, neglecting mutual interferences, were the wing, nacelle, and jet. The interference of the wing upon the body fore and total drags was beneficial at $M_\infty = 1.94$ and detrimental at $M_\infty = 2.41$ (table II); these interference drags due to the wing were small compared to the drag of the body alone. Large drag changes occurred as a result of adding the nacelle to the wing (compare jet-off results in fig. 6 to drag coefficients of body in presence of wing, table II) and as a result of operating the jet (figs. 7, 8, and 9). In figure 10 are presented changes in body fore drags and incremental fore drags at $M_\infty = 1.94$ associated with changes in shock locations obtained from schlieren photographs.

Effects of jet-interference flow field.- The incremental drags (fore, base, and total) of the body due to the jet were either beneficial or detrimental (figs. 7, 8, and 9), dependent upon the pressure ratio of the jet and its location with respect to the body. Both of these factors were of importance interferencewise. The jet pressure ratio was predominant in the formation of the interference flow field; and the distribution of this flow field upon the body was primarily dictated by the relative locations of jet and body. However, for the present tests, the schlieren studies indicated that the jet upon discharge from the exit was bent in a direction away from the body when the nacelle was located at $\overline{K_y} = 1$ and, particularly, at low jet pressure ratios. This was believed to have been the result of the reflected disturbances between the nacelle and body.

The largest of the drag increases due to jet interference took place when the nacelle was at its most inboard $\left(\overline{K_y} = 1\right)$ and forward location and highest jet pressure ratio (see, for instance, fig. 7(a), $K_Z = 2.5$). The effect of increasing the Mach number from 1.94 to 2.41 was, generally, to reduce the magnitudes of the drag increases (compare, for instance, fig. 7(a), $K_Z = 2.5$, to fig. 7(b), $K_Z = 2.5$). The basic body drags are summarized in table II to facilitate comparison with the drag increments of figures 7, 8, and 9.

Comparison of figures 7, 8, and 9 indicated that the total drag increases or decreases resulted from variations in either base or fore drags or both. No attempt will be made to analyze each individual trend of the drag variations; however, analyses will be made of three typical types of drag variations through the use of schlieren photographs in a later section.

Association of shock locations with body fore drag variations.- The results of figure 10 are presented solely to illustrate how the interference fore drag varied with shock movement. This correlation should not be construed as an attempt to isolate the individual effects of shock

waves or flow regions. These results include the data for all the longitudinal, spanwise, and vertical nacelle locations for which shock-body intersection locations could be obtained at $M_\infty = 1.94$. These shock intersections were taken as the location at which the most forward portion of the shock front appeared to intersect the contour of the body silhouetted in the schlieren photograph (or with the plate surface when the shock extended downstream of the body base). When the jet axis was directly above the body center line ($K_Z = 1.5$), the value of x' is correct. For the other K_Z values, x' is slightly in error due to the curved nature of the shock; but for the values of K_Z used and for the purposes of this correlation, this error is not important. In figures 10(a) and 10(b), the fore drag coefficients are presented as a function of the locations of the intersections of the nose and trailing shocks with the body surface for jet off. As these shock locations were shifted, the distribution of interference pressures upon the body was also changed and resulted in large variations in body fore drag. For example, in figure 10(a), the beneficial effect of the pressure rise across the nose shock upon the body drag is evident for nose shock locations of the order of -2 (where the pressure rise was felt forward through the wake and boundary layer) to about 7. At this location, the effects of the expansions propagated from the base and rearward portions of the nacelle (and pylon) reduced the pressures on the aftersurfaces of the body and increased the body fore drag. These drag variations are compared to the drag coefficients of the body alone and the body in the presence of the wing, signified by B and BW, respectively. The large interference of wing nacelle on the body as compared to the small interference of the wing on the body is evident.

The variations of incremental fore drag coefficients due to jet interference are presented in figures 10(c) and 10(d) as a function of the location of the intersections of the shock from within the jet and the exit shock with the body surface. These results indicated that the maximum change in $C_{D,f}$ due to jet interference was about 0.05. This was about 22 percent of the basic fuselage drag and was of the same order as the maximum change in $C_{D,f}$ as a result of nacelle and pylon interference with the jet off (figs. 10(a) and 10(b)). It should be noted, however, that the pylon used in the present tests was thick; for cases where thinner pylons were used, the maximum pylon-nacelle interference effects would probably be subordinate to the maximum jet-interference effects.

Correlation of Flow-Field Observations With Measured Drag Results

Presented in figure 11 are schlieren photographs of the body and body-wing combination. The various flow phenomena associated with the tests at $M_\infty = 1.94$ are indicated and should aid in the interpretation of figure 12. In figure 12 are presented three types of drag variations

due to jet interference along with schlieren photographs which show the changes in the flow field that were associated with the drag variations. The three types of drag variations are: total and base drags decreasing, fore drag near constant (model 2-C, $K_x = 8.96$, $K_y = 6.06$, $K_z = 2.50$); total and fore drags decreasing, base drag near constant (model 3-B, $K_x = 8.78$, $K_y = 3.00$, $K_z = 1.50$); and total and base drags increasing, fore drag constant (model 2-A, $K_x = 11.46$, $K_y = 1.27$, $K_z = 0$). These types of drag variations do not cover all the types which were encountered; rather, these were chosen for discussion purposes.

Model 2-C ($K_x = 8.96$, $K_y = 6.06$, $K_z = 2.50$).- In figure 12(a) the nacelle was far enough outboard ($K_y = 6.06$) so that no multiple reflections occurred and the wake of the nacelle had essentially no inclination. With the jet off, the nacelle trailing shock intersected the plate downstream of the body trailing shock. This placed the base of the body and a portion of the afterbody in the expansion regions propagated from the nacelle afterbody and base and the pylon afterportions. Therefore, $C_{D,f}$ and $C_{D,b}$ were higher than their values with no nacelle (0.220 and 0.034, respectively, as compared to 0.212 and 0.016, respectively, with no nacelle).

As p_j/p_∞ increased to 1, the nacelle trailing shock disappeared and an exit shock was created which intersected the plate closer to the base of the body. The pressure rise across this shock was felt forward within the wake of the body and reduced $C_{D,b}$ without affecting $C_{D,f}$. Further increases in p_j/p_∞ to a value of 20 magnified these effects. At $p_j/p_\infty > 20$, the exit shock progressed forward of the base of the body and reduced $C_{D,f}$ also.

Examination of this series of schlieren photographs indicated that a severe "bending" of the inboard exit shock took place as p_j/p_∞ increased. Study of other schlieren photographs of the same model but at different spanwise locations indicated that the initial exit shock angles at the lip of the jet were about the same but that a more gradual rate of change of shock inclination was prevalent for all other spanwise nacelle locations at equivalent values of p_j/p_∞. With the nacelle located as in figure 12(a), the shocks from the nacelle nose and pylon leading edge combined and reflected from the body just rearward of the wing-trailing-edge—body juncture along with the disturbances originating at this juncture. This was sufficient to cause the decrease in the rate of change of exit shock angle in the regions where these disturbances are visible and resulted in the local exit shock angles being higher than usual. At the extremity of this flow region, the shock angle decreased abruptly. The

important effect that this phenomenon has in changing the location of the intersection of the exit shock with the body surface is evident. The drag results in this figure indicate that the changes in $C_{D,f}$ and $C_{D,b}$ were largely dependent upon this location.

Model 3-B ($K_x = 8.78$, $K_y = 3.00$, $K_z = 1.50$).- In figure 12(b) the jet-off values of $C_{D,f}$ and $C_{D,b}$ are higher than the no-nacelle values (0.256 and 0.020, respectively, as compared to 0.212 and 0.016, respectively, with no nacelle). The rearward portions of the body was subjected to the low-pressure field associated with the nacelle afterbody and base; this more than canceled the combined effects of the pressure rise due to the reflections between body and nacelle and the trailing shock behind the nacelle that intersected with the wake of the body.

At jet pressure ratios greater than one, the exit shock extended from the lip of the nacelle and intersected the afterportion of the body thereby reducing $C_{D,f}$. The expansion region of flow between the exit shock and the shock from within the jet reduced the base pressure slightly; thus, a small increase in $C_{D,b}$ took place. At $p_j/p_\infty \geq 20$, however, the pressure rise through the exit shock had increased to the extent that the magnitude of the pressure in this expansion zone resulted in no further increase in $C_{D,b}$.

Model 2-A ($K_x = 11.46$, $K_y = 1.27$, $K_z = 0$).- In figure 12(e) some of the multiple reflections of disturbances between body and nacelle are visible, and it is believed that the pressure rise across these disturbances were responsible for the outboard inclination of the free jet and/or the nacelle wake behind the nacelle base for the jet-off and $p_j/p_\infty = 1$ conditions. For these conditions the momentum of the jet or wake is low and subject to changes in attitude in order to maintain a condition of equilibrium with the surrounding flow.

With the jet off, the increased pressure on the afterbody as a result of the reflections between body and nacelle reduced the fore drag coefficient from 0.212 (with no nacelle) to 0.190 with little change in $C_{D,b}$.

For this nacelle location, and with jet on, the exit shock, which was probably the strongest shock associated with the jet flow field, intersected the body near the cylindrical midsection and undoubtedly had little effect upon the local pressure drag. The distribution of pressures on the body surface behind the exit shock, combined with any aspiration effects which the jet caused, canceled the effects of the pressure rises across the exit shock and the shock from within the jet and resulted in no change in fore drag. As the jet pressure ratio increased, the shock from within the jet moved downstream; and the expansion region was lengthened. However,

the distribution of pressure upon the body remained such as to result in no increase in body fore drag. At pressure ratios greater than about 20, the shock from within the jet moved downstream of the base of the body. The increased Mach number and reduced pressure at the lip of the body base was sufficient to more than offset the effects of the pressure rise across the shock wave and established a reduced base pressure (increased base drag). This was reflected directly in the total drag increase as the fore drag remained constant.

Summation of Drag Results

Presented in figures 13, 14, and 15 are summaries of the drag variations due to changes in nacelle longitudinal, spanwise, and vertical locations, respectively, at various values of p_j/p_∞. In figures 13 and 14, two of the location parameters are held constant while the third is varied. For example, in figure 13, K_y and K_z are held constant and the drag variations with K_x are presented. These drag results include, therefore, the effects of variation in pylon sweep angle along with the effects of variation in nacelle location and jet pressure ratio. Similarly, in figure 14, in order to maintain a constant value of K_x as K_y varied, the pylon sweep angle changed as a result of the longitudinal shift in nacelle location with respect to the wing because of the sweep of the wing. In figure 15, only the results using the unswept pylons are presented; therefore, for each value of K_y, there was a different value of K_x.

In all summary figures, the measured drag of the body using the body-wing combination is shown for reference purposes (indicated by "BW"). Also, at the larger values of K_y, since the jet-interference effects were zero, a solid line is used to represent the drag results for all values of p_j/p_∞.

Varying longitudinal nacelle location.- Large drag variations were realized by varying K_x (fig. 13) for the most inboard nacelle locations, particularly for $K_z = 1.5$. These changes are probably associated with the combined effects of multireflected disturbances and changes in local skin friction. It also appears possible that some aspiration of flow from locally choked regions between the nacelle and body might have taken place. These drag changes were somewhat reduced at $M_\infty = 2.41$ (compare figs. 13(a) and 13(b)). At neither Mach number was the nacelle far enough downstream and/or outboard to result in no nacelle-body interference. However, at both Mach numbers, the jet interference effects were zero at the largest values of K_y. In general, the changes in $C_{D,t}$ and

$C_{D,b}$ due to changes in p_j/p_∞ were smaller at $M_\infty = 2.41$ than at $M_\infty = 1.94$ for $K_y \geq 5$.

Varying spanwise nacelle location.- As a result of nacelle interference, large variations in $C_{D,t}$ and $C_{D,f}$ were realized with the jet off by varying K_y at all values of K_x and K_z (fig. 14). With the nacelle inboard $(K_y \approx 1)$ and the jet off, the nacelle interference generally reduced the total and fore drags of the body; however, operating the jet generally increased these body drags from the jet-off value. With the nacelle located outboard of the body about four jet-exit diameters at $M_\infty = 1.94$ and about three jet-exit diameters at $M_\infty = 2.41$ and with the jet-off, the nacelle interference increased the body total and fore drags to the highest values obtained; operating the jet reduced these drags from the jet-off values. As a result of varying K_y or p_j/p_∞, $C_{D,b}$ variations at $M_\infty = 2.41$ were significantly less than those at $M_\infty = 1.94$ because of the smaller shock and expansion angles.

Varying vertical nacelle location.- The results presented in figure 15 were obtained using models 2-A through 2-D only (unswept pylons). No general trends were noted for the results. It is evident, however, that the vertical nacelle location was definitely important to the body drags, particularly at $M_\infty = 1.94$ where the propagation of the interference pressure fields resulted in large and varying effects upon the body $(\text{at } K_y = 1.0, \text{ for instance})$.

Examination of the data shows that at a given longitudinal position of the nacelle and at a constant radial position of the nacelle with respect to the body axis, the change in body drags with change in jet pressure ratio is not independent of the vertical position of the nacelle in relation to the wing. This indicates that the wing-pylon—interference flow field has a significant effect upon the jet interference upon body drag.

CONCLUSIONS

The results of an experimental investigation at Mach numbers of 1.94 and 2.41 to determine the effects of jet interference upon the body drag of a body-wing configuration equipped with a wing-mounted jet nacelle having a sonic exit indicate the following conclusions:

1. The maximum variations in the total and fore drags of the body due to jet interference were about one-fourth of the basic body drag. This was of the same order of magnitude as the maximum drag changes which

resulted from the variation in nacelle location with the jet off. Both the jet interference and the nacelle interference upon the body drags were considerably larger than the interference of the wing upon the body.

2. With the nacelle at the inboard locations and with the jet off, the nacelle interference reduced the body drag; however, operating the jet increased the body drag from the jet-off value.

3. With the nacelle located outboard of the body about four jet-exit diameters at a Mach number of 1.94 and about three jet-exit diameters at a Mach number of 2.41 and with the jet off, the nacelle interference increased the body drag to the highest value obtained; operating the jet reduced the body drag from the jet-off value.

4. Correlation of schlieren photographs with drag results indicated that the entire jet-interference flow field must be considered in the analysis of the effects of jet upon the total, fore, and base drags of the body. Consideration of only the locations of the exit shock and shock from within the jet with respect to the body is not sufficient to show detailed quantitative changes of these drags.

Langley Aeronautical Laboratory,
National Advisory Committee for Aeronautics,
Langley Field, Va., January 12, 1956.

REFERENCES

1. Smith, Norman F., and Carlson, Harry W.: The Origin and Distribution of Supersonic Store Interference From Measurement of Individual Forces on Several Wing-Fuselage-Store Configurations. I.- Swept-Wing Heavy-Bomber Configuration With Large Store (Nacelle). Lift and Drag; Mach Number, 1.61. NACA RM L55A13a, 1955.

2. Jacobsen, Carl R: Effects of Size of External Stores on the Aerodynamic Characteristics of an Unswept and a 45° Sweptback Wing of Aspect Ratio 4 and a 60° Delta Wing at Mach Numbers of 1.41, 1.62, and 1.96. NACA RM L52K20a, 1953.

3. Love, Eugene S.: Aerodynamic Investigation of a Parabolic Body of Revolution at Mach Number of 1.92 and Some Effects of an Annular Jet Exhausting From the Base. NACA RM L9K09, 1950.

4. Cortright, Edgar M., Jr., and Schroeder, Albert H.: Investigation at Mach Number 1.91 of Side and Base Pressure Distributions Over Conical Boattails Without and With Jet Flow Issuing From Base. NACA RM E51F26, 1951.

5. Englert, Gerald W., Wasserbauer, Joseph F., and Whalen, Paul: Interaction of a Jet and Flat Plate Located in an Airstream. NACA RM E55G19, 1955.

6. Bressette, Walter E., and Leiss, Abraham: Investigation of Jet Effects on a Flat Surface Downstream of the Exit of a Simulated Turbojet Nacelle at a Free-Stream Mach Number of 1.39. NACA RM L55L13, 1956.

7. Jonas, Julius: On the Interaction Between Multiple Jets and an Adjacent Surface. Aero. Eng. Rev., vol. 11, no. 1, Jan. 1952, pp. 21-25.

8. Hatch, John E., Jr., and Savelle, William M.: Some Effects of a Sonic Jet Exhaust on the Loading Over a Yawed Fin at a Mach Number of 3.03. NACA RM L52L02a, 1953.

9. Salmi, Reino J., and Klann, John L.: Interference Effects at Mach Number 1.9 on a Horizontal Tail Due to Trailing Shock Waves From an Axially Symmetric Body With an Exiting Jet. NACA RM E55J13a, 1956.

10. Valerino, Alfred S.: Jet Effects on Pressure Loading of All-Movable Horizontal Stabilizer. NACA RM E54C24, 1954.

11. Peck, Robert F.: Jet Effects on Longitudinal Trim of an Airplane Configuration Measured at Mach Numbers Between 1.2 and 1.8. NACA RM L54J29a, 1955.

[redacted]

12. Grigsby, Carl E.: An Investigation of the Effects of Jet Exhaust and Reynolds Number Upon the Flow Over the Vertical Stabilizer and Rudder of the Douglas D-558-II Research Airplane at Mach Numbers of 1.62, 1.93, and 2.41. NACA RM L54E03, 1954.

13. Love, Eugene S., and Grigsby, Carl E.: Some Studies of Axisymmetric Free Jets Exhausting From Sonic and Supersonic Nozzles Into Still Air and Into Supersonic Streams. NACA RM L54L31, 1955.

14. Pack, D. C.: On the Formation of Shock-Waves in Supersonic Gas Jets (Two-Dimensional Flow). Quarterly Jour. Mech. and Appl. Math., vol. I, pt 1, Mar. 1948, pp. 1-17.

15. Schäfer, M.: Steady Supersonic Flows. British M.A.P. Völkenrode. Reps. and Translations No. 995, Apr. 15, 1948. Reps. and Translations No. 996, May 1, 1948.

16. Fallis, William B.: On Distributed Roughness as a Means of Fixing Transition at High Supersonic Speeds. Jour. Aero. Sci. (Readers' Forum), vol. 22, no. 5, May 1955, p. 339.

TABLE I.- PERTINENT MODEL INFORMATION

Model no.	K_x at $\overline{K}_y = 1$	K_z	Pylon sweep angle, deg
1-B	13.18	1.5	-45
1-C	13.18	2.5	-45
1-D	14.18	3.5	-45
2-A	11.46	0	---
2-B	11.46	1.5	0
2-C	11.46	2.5	0
2-D	11.46	3.5	0
3-B	9.78	1.5	45
3-C	9.78	2.5	45
3-D	8.78	3.5	45

Distance from base of body to wing-trailing-edge—body juncture is equal to 13.87 jet-exit diameters.

Distance from nacelle nose	Nacelle radius
0	0
.100	.062
.200	.116
.300	.160
.400	.196
.500	.222
.600	.240
.750	.250
1.750	.250
2.000	.232
2.100	.222
2.200	.205
2.300	.183
2.400	.156
2.500	.125

Distance from body nose	Body radius
0	0
.250	.087
.500	.165
1.000	.297
1.500	.397
2.000	.463
2.500	.495
2.750	.500
4.750	.500
5.500	.486
6.000	.462
6.500	.428
7.000	.380
7.500	.321
8.000	.250

TABLE II.- SUMMARY OF DRAG COEFFICIENTS

FOR BODY AND BODY-WING CONFIGURATIONS

Configuration	Drag coefficient	M	
		1.94	2.41
Body	$C_{D,t}$	0.235	0.214
	$C_{D,f}$	.226	.205
	$C_{D,b}$	.009	.009
Body in presence of wing	$C_{D,t}$	0.228	0.224
	$C_{D,f}$	.212	.208
	$C_{D,b}$	.016	.016
Effect of wing on body	$\Delta C_{D,t}$	-0.007	0.010
	$\Delta C_{D,f}$	-.014	.003
	$\Delta C_{D,b}$	.007	.007

[redacted]

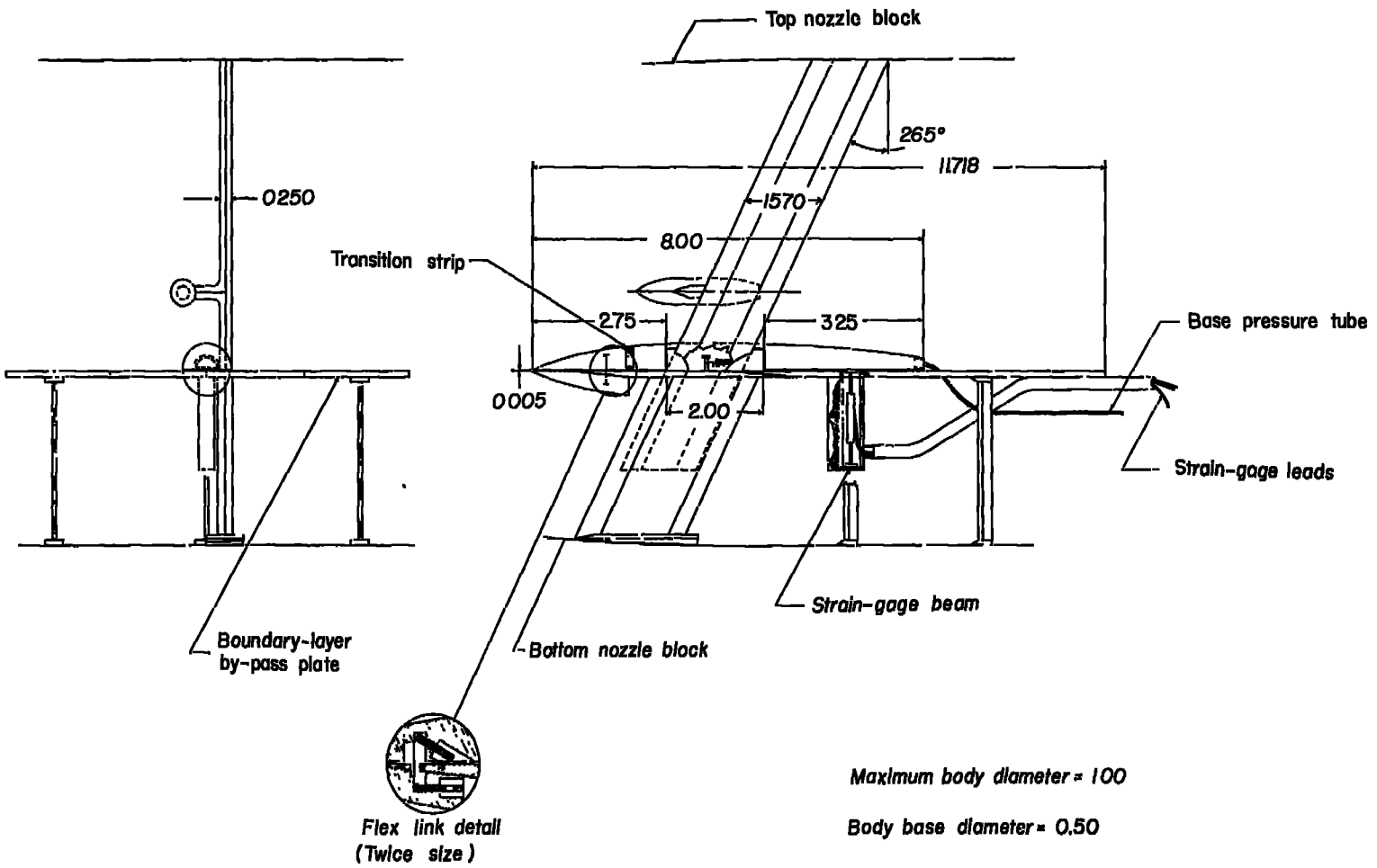

(a) Drawing of model. All dimensions are in inches.

Figure 1.- Model installation in the Langley 9-inch supersonic tunnel.

(b) Photograph of model in tunnel. L-88760.1

Figure 1.- Concluded.

[redacted]

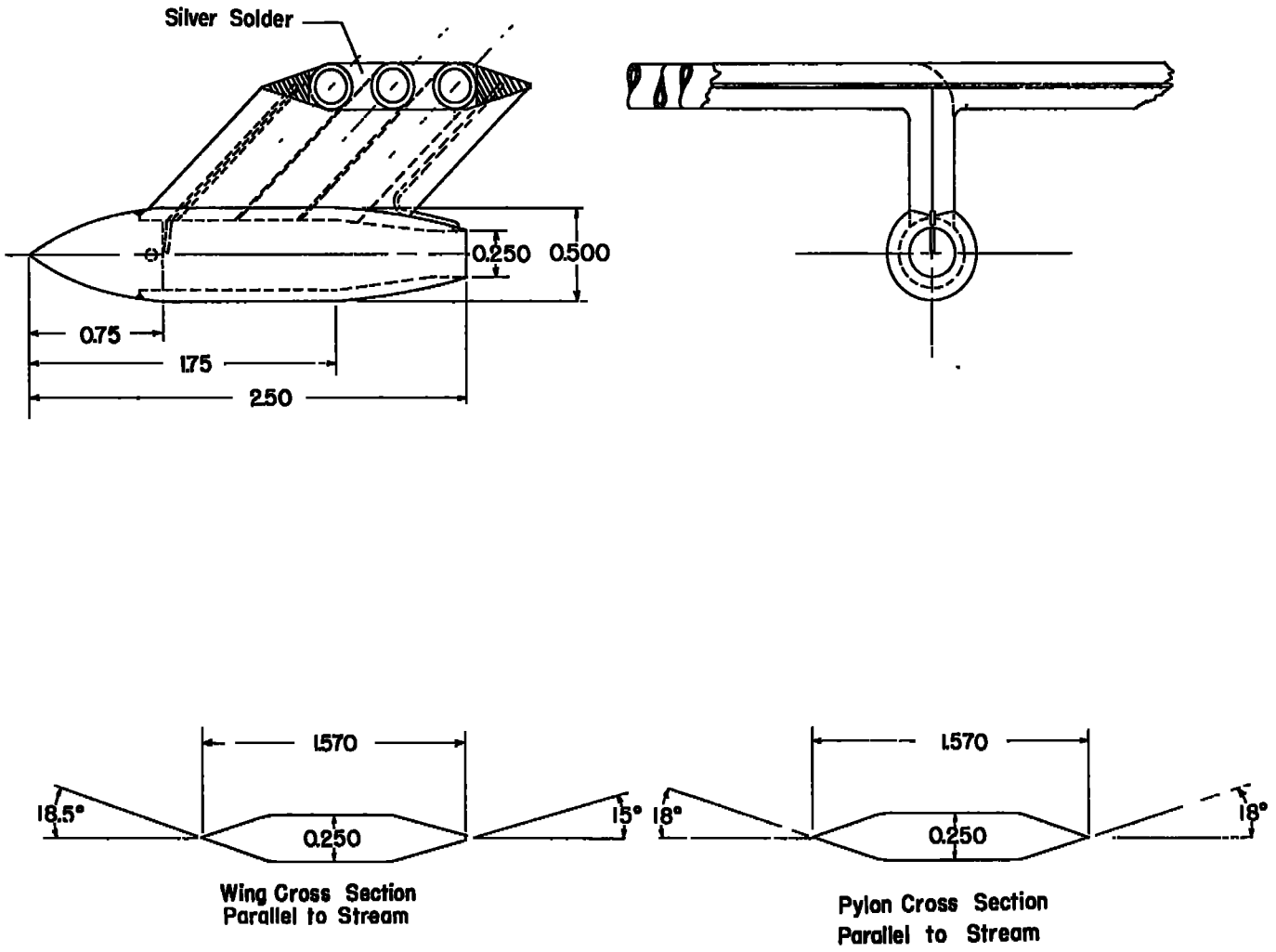

(a) Pertinent dimensions of wing-nacelle assembly (in.).

Figure 2.- Details of wing-nacelle assemblies.

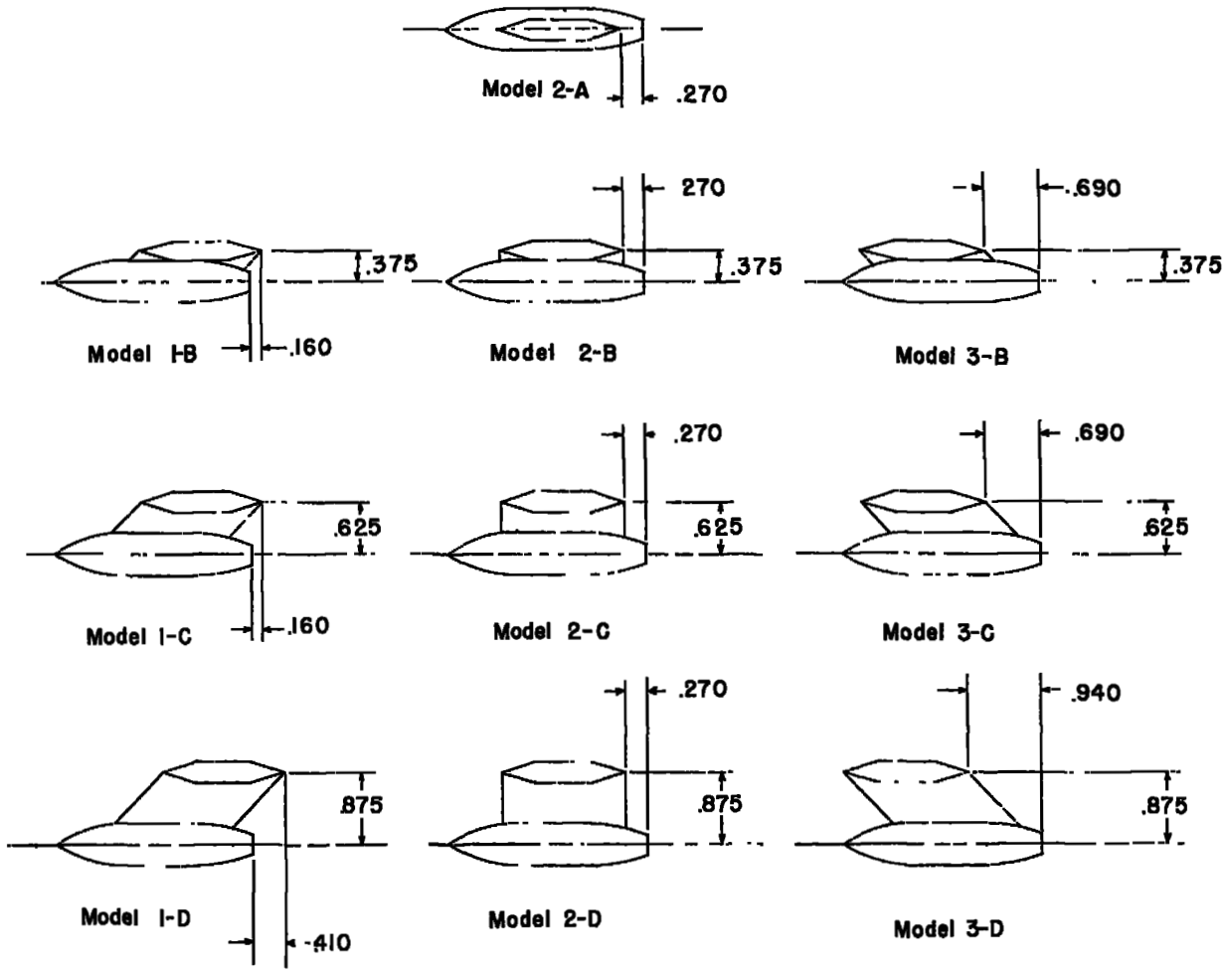

(b) Designations of wing-nacelle assemblies.
All dimensions are in inches.

Figure 2.- Concluded.

$M_\infty = 3.24$ (assumed uniform)

$M_j = 2.38$

$\frac{p_j}{p_\infty} = 8.96$

$\theta_N = 12.5°$

$\gamma_\infty = \gamma_j = 1.400$

Boattail angle = 9°

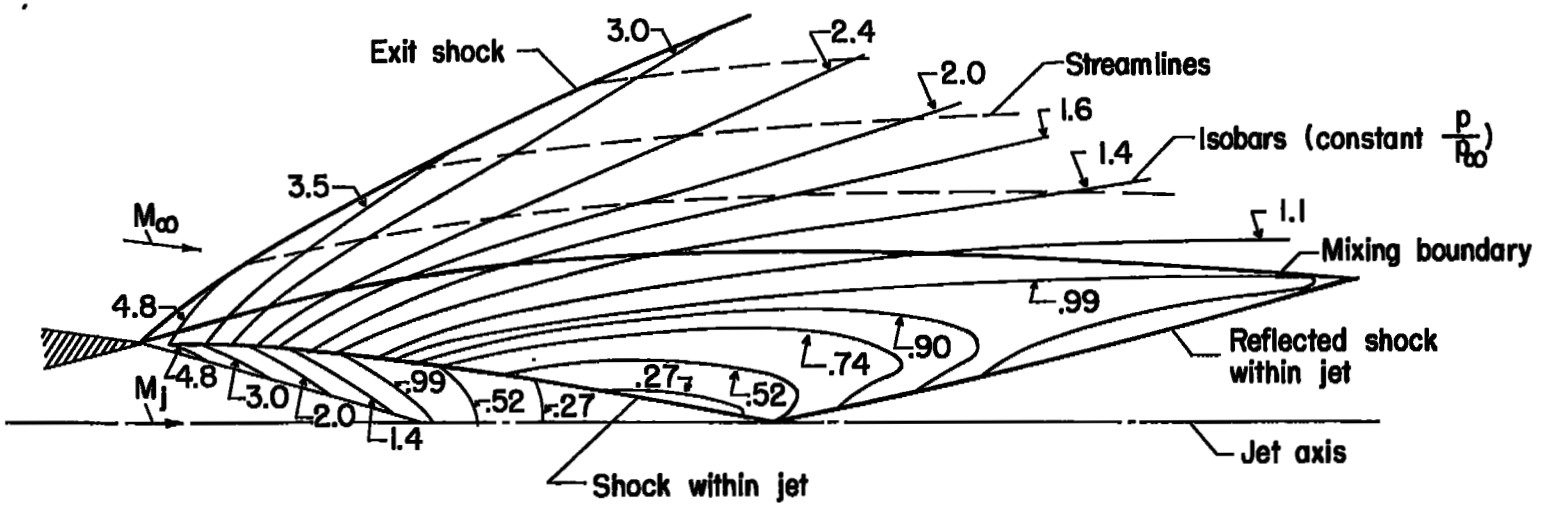

Figure 3.- Distribution of static-pressure ratio p/p_∞ associated with flow issuing from a supersonic nozzle. Obtained from calculations by Schäfer using method of characteristics (ref. 15).

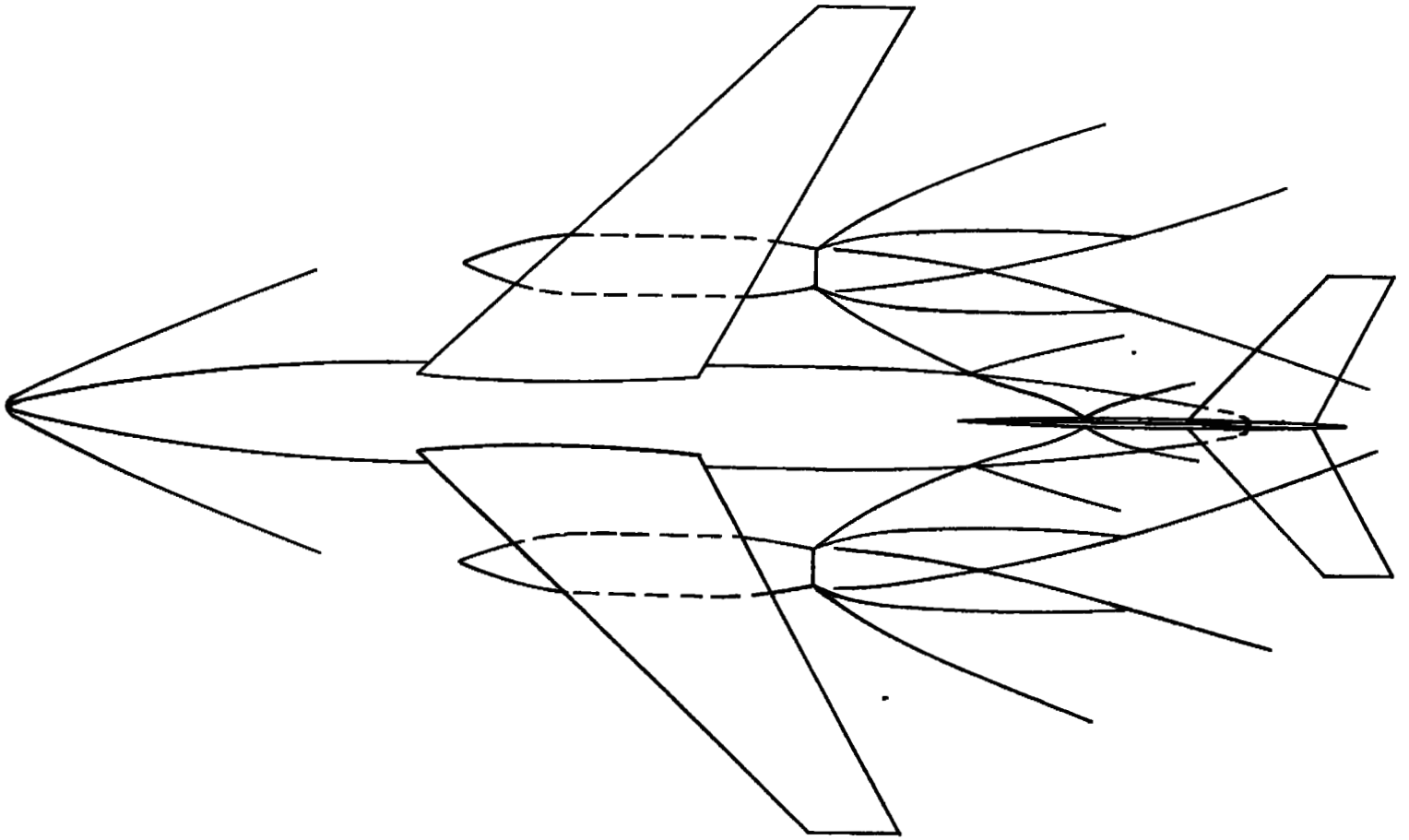

Figure 4.- Typical example of association of jet-interference flow field with aircraft components (wing-mounted nacelles). $M_\infty = 3.24$; $M_j = 2.38$; $p_j/p_\infty = 8.96$.

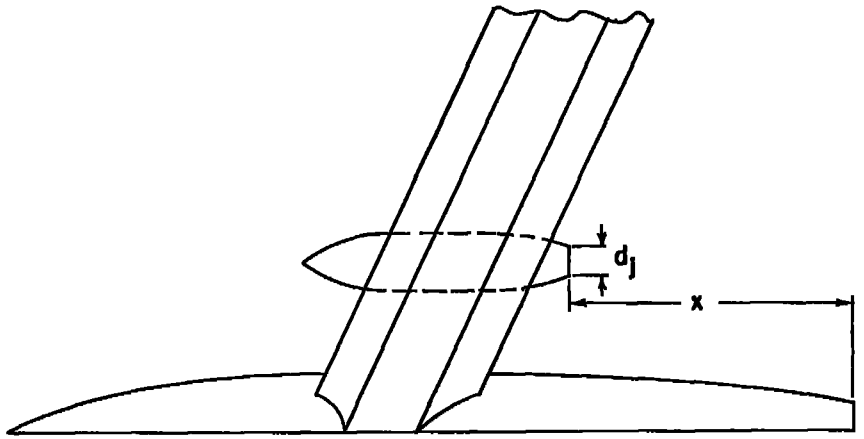

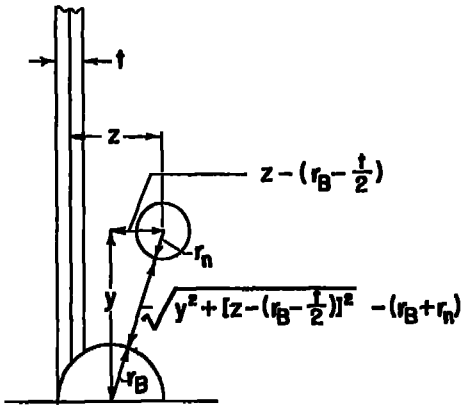

$$K_x = \frac{x}{d_j}$$

$$K_y = \frac{\sqrt{y^2+[z-(r_B-\frac{t}{2})]^2}-(r_B+r_n)}{d_j}$$

$$K_z = \frac{z}{d_j}$$

Figure 5.- Layout of model showing dimensions used in location parameters. Details are omitted for clarity.

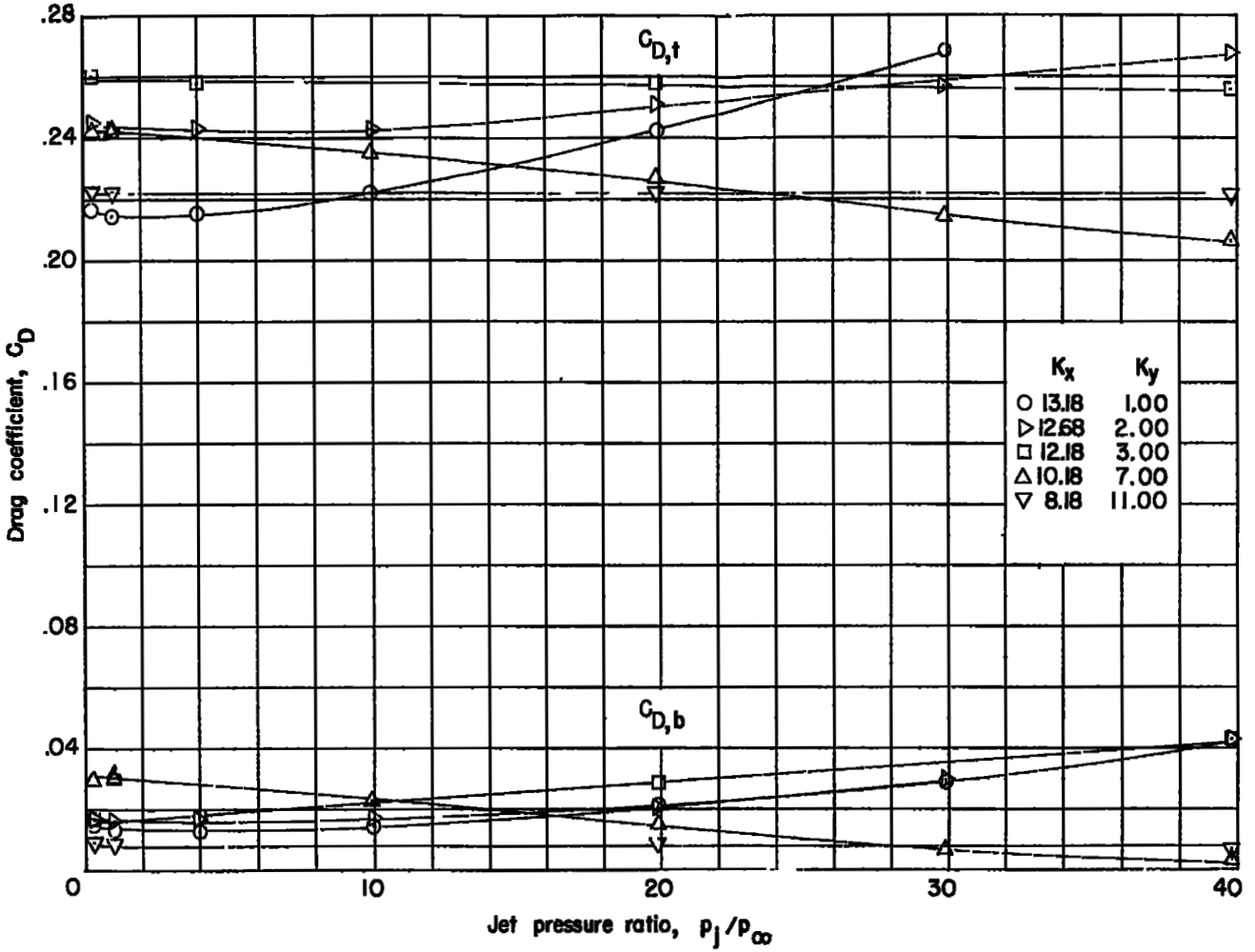

Model 1-B

(a) $M_\infty = 1.94$.

Figure 6.- Measured total and base drag coefficients.

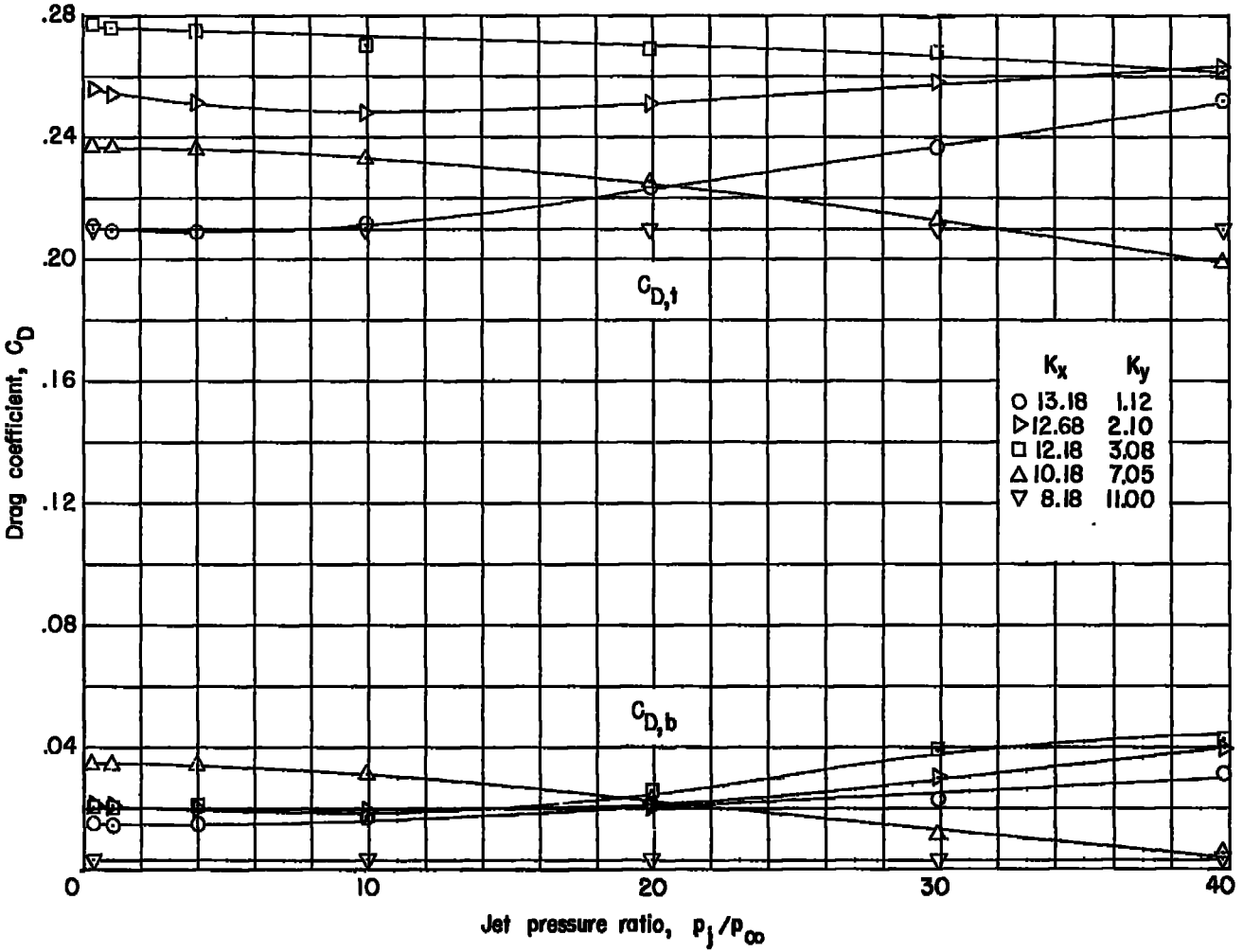

Model 1-C

(a) $M_\infty = 1.94$. Continued.

Figure 6.- Continued.

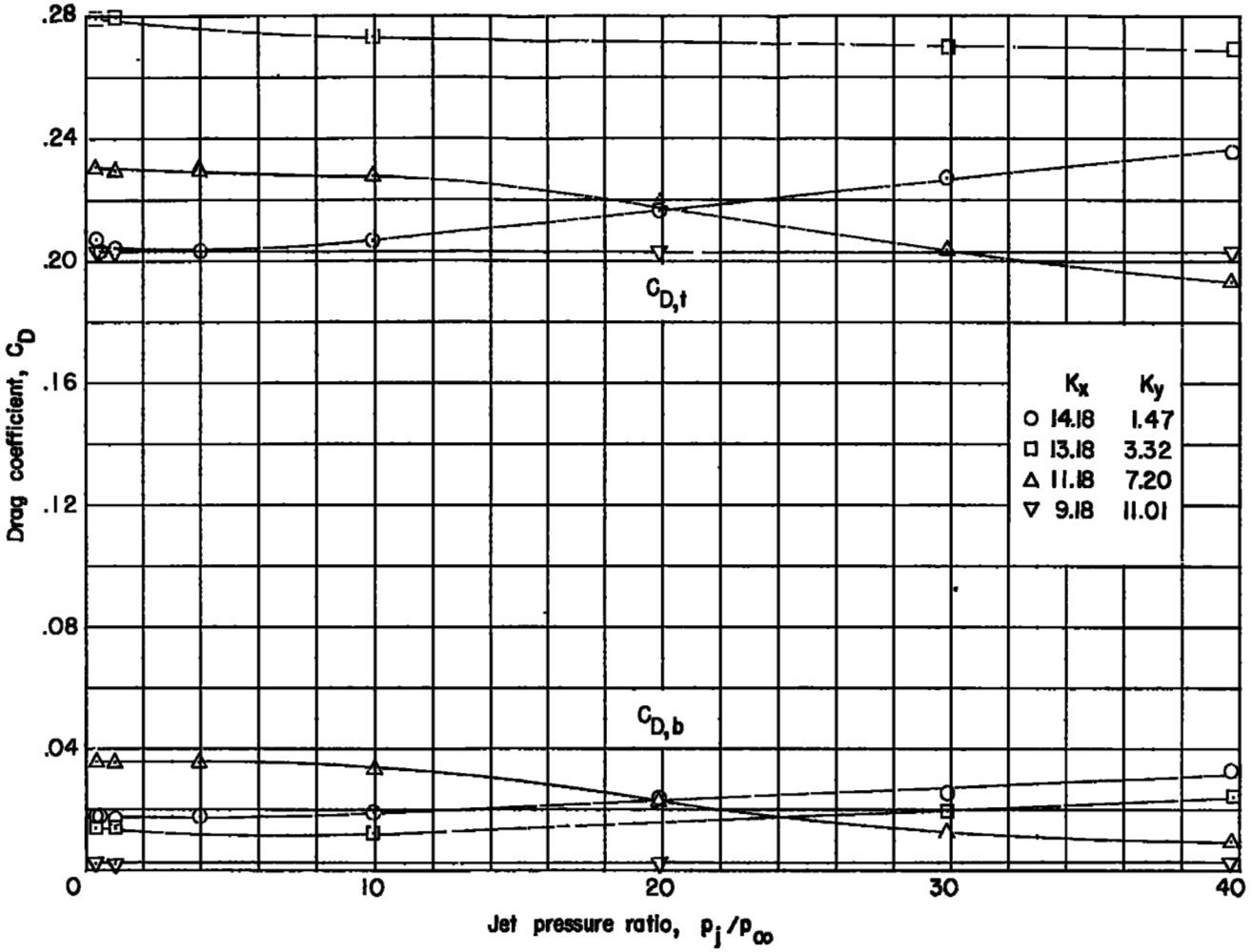

Model 1-D

(a) $M_\infty = 1.94$. Continued.

Figure 6.- Continued.

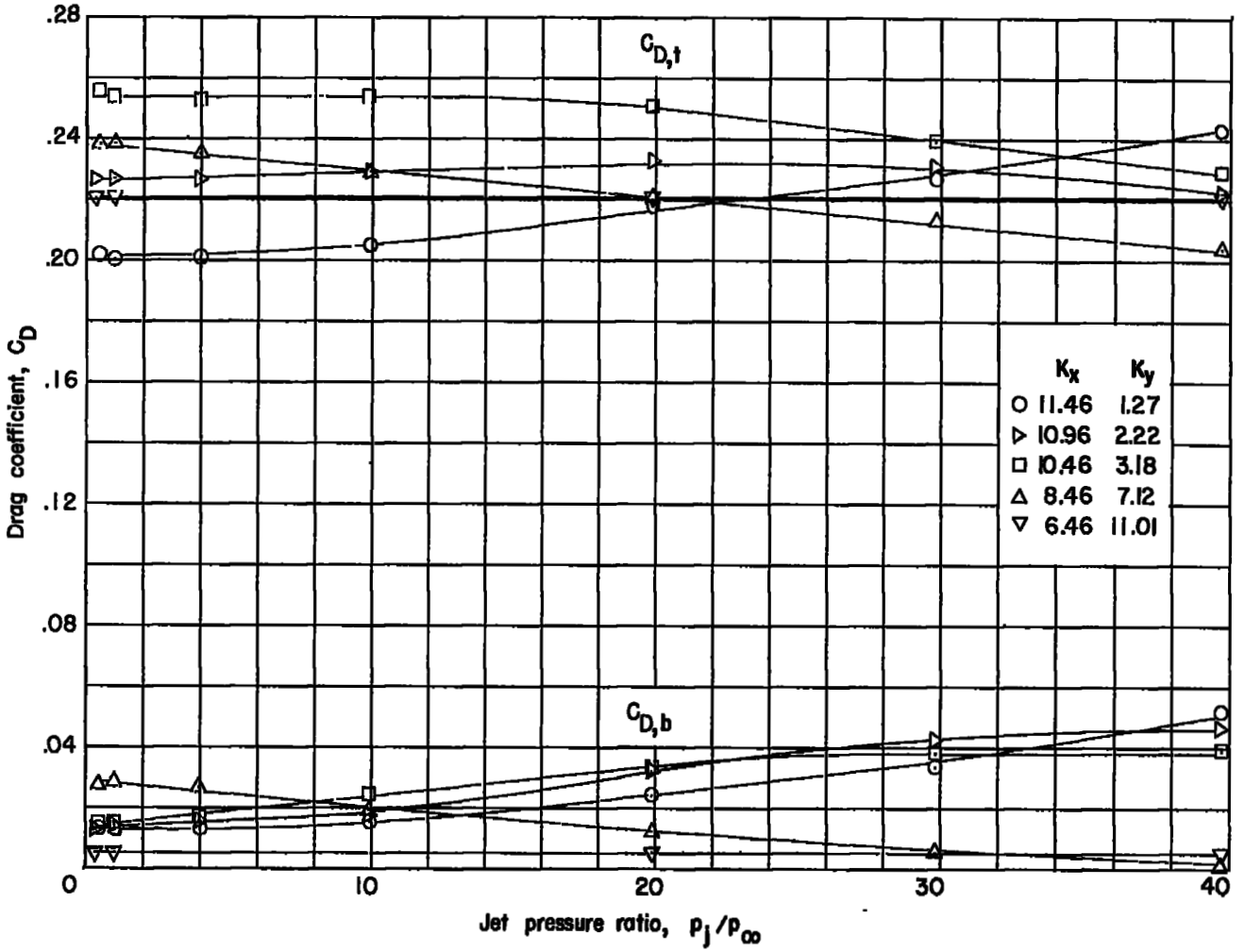

Model 2-A

(a) $M_\infty = 1.94$. Continued.

Figure 6.- Continued.

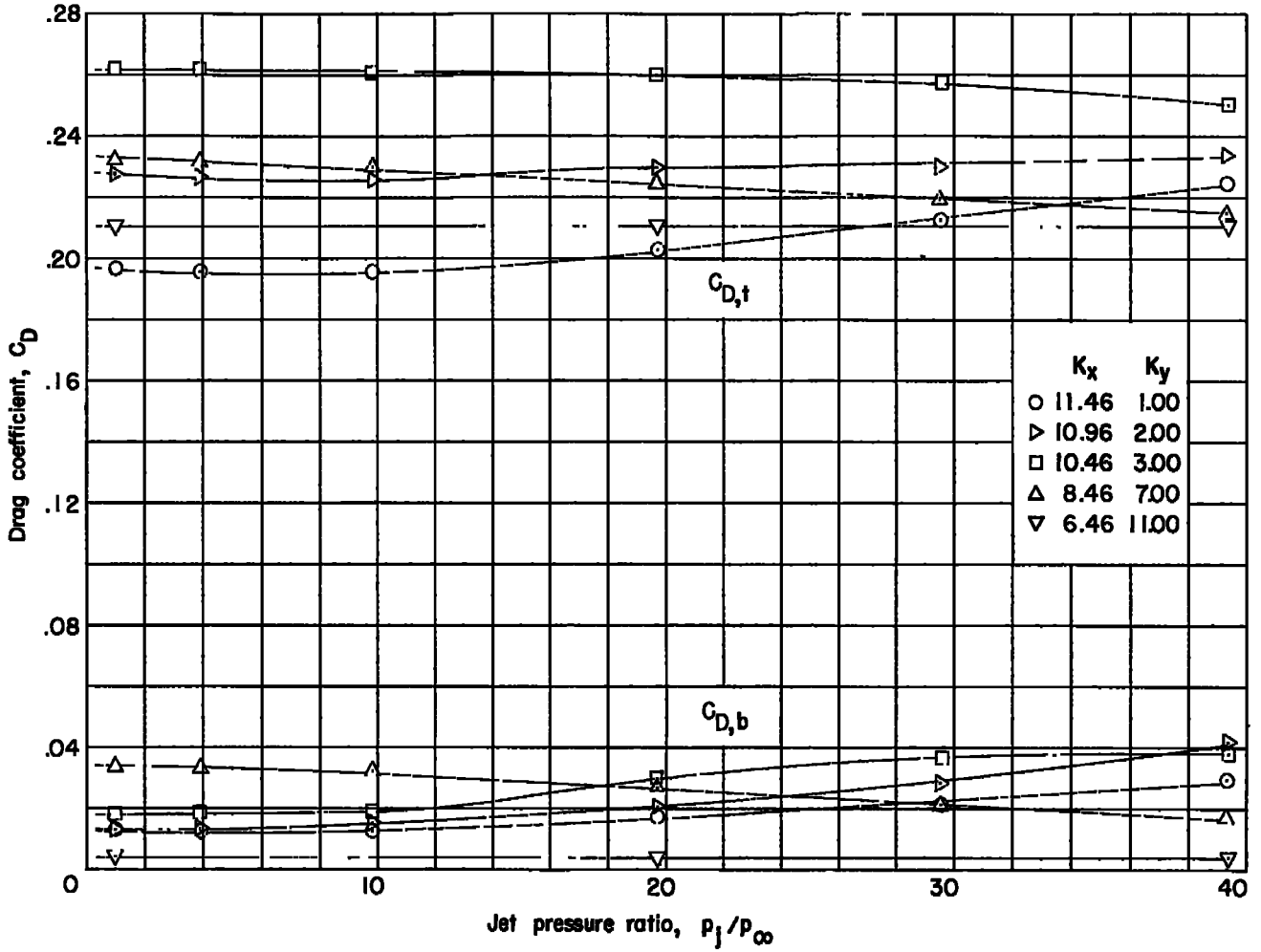

Model 2-B

(a) $M_\infty = 1.94$. Continued.

Figure 6.- Continued.

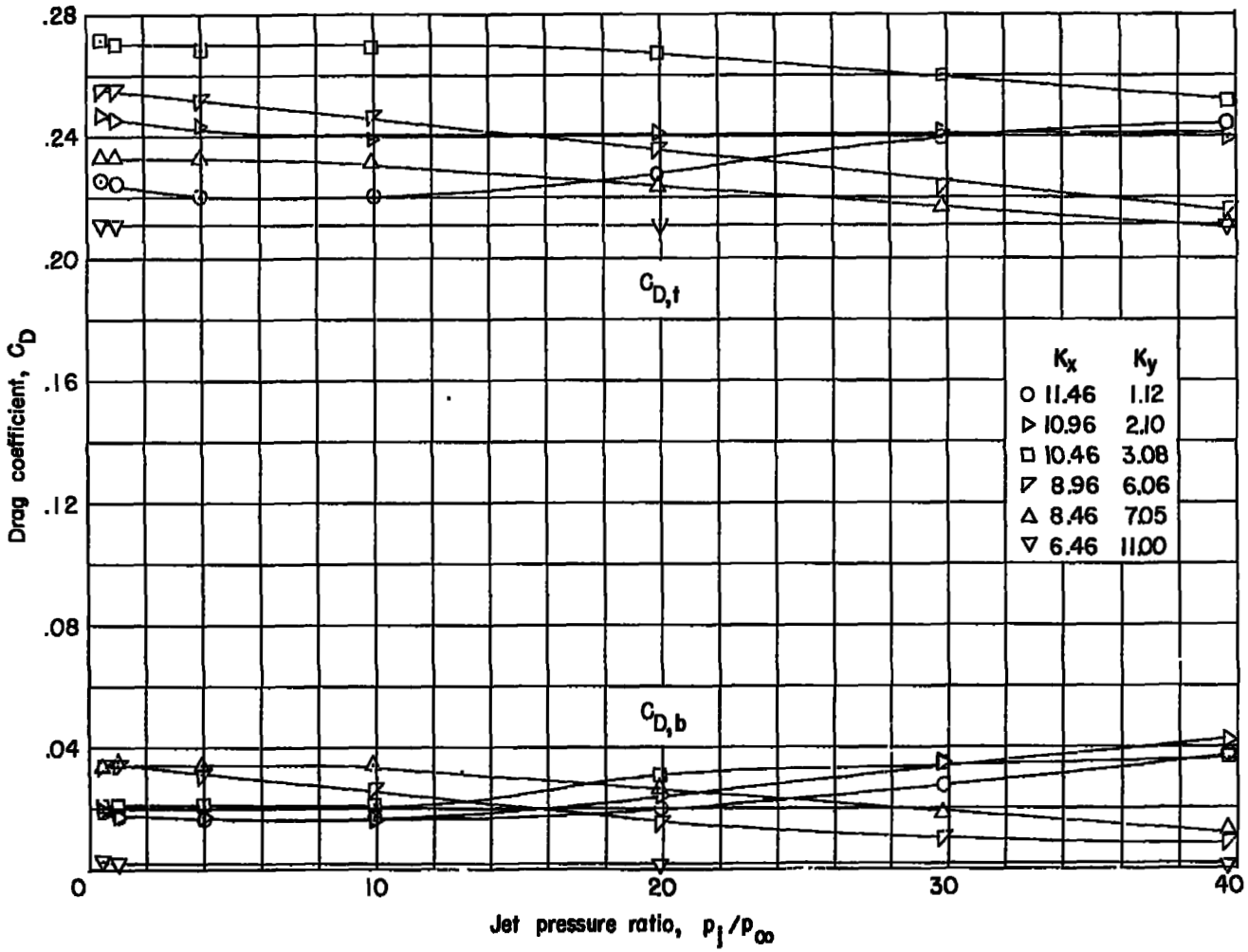

Model 2-C

(a) $M_\infty = 1.94$. Continued.

Figure 6.- Continued.

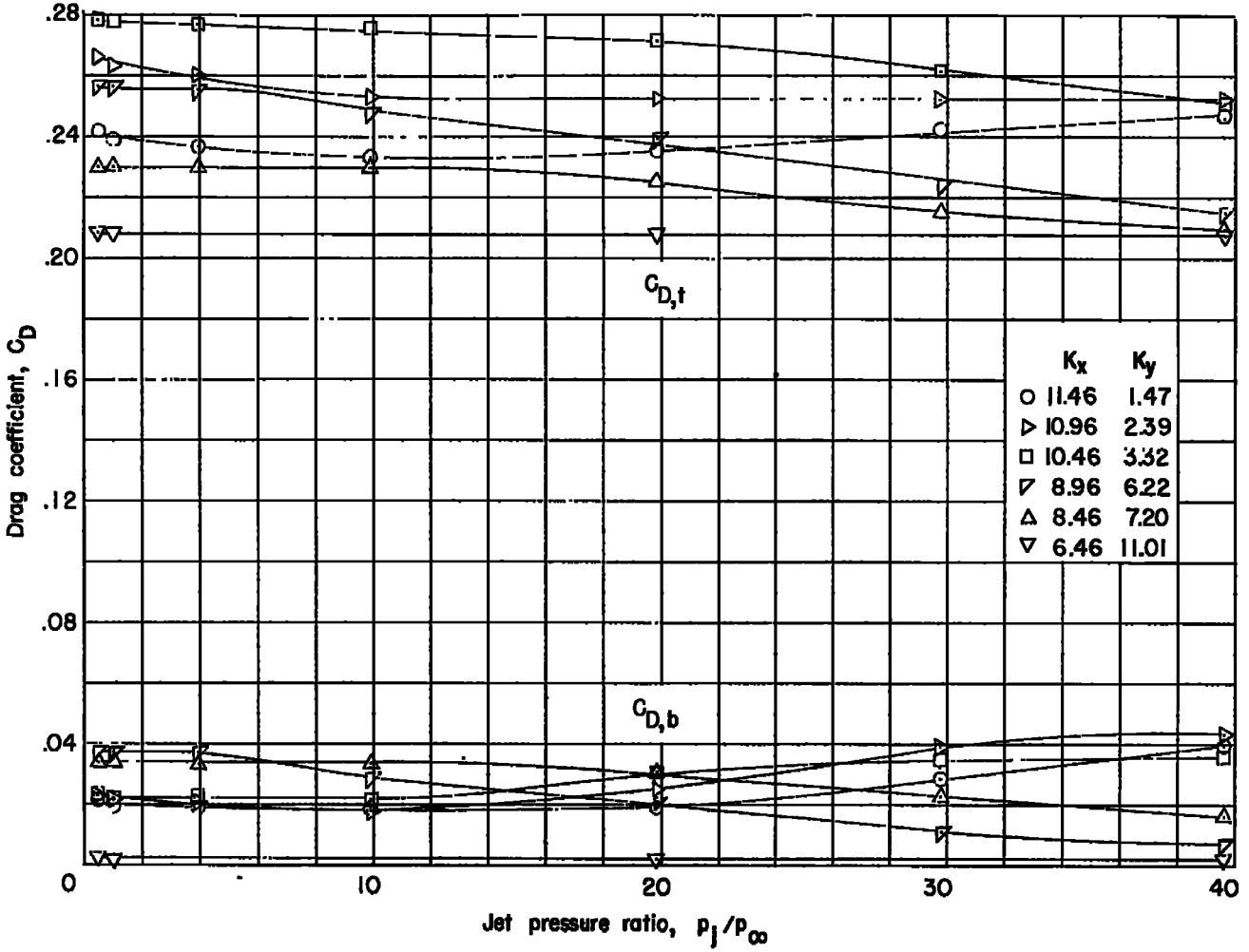

Model 2-D

(a) $M_\infty = 1.94$. Continued.

Figure 6.- Continued.

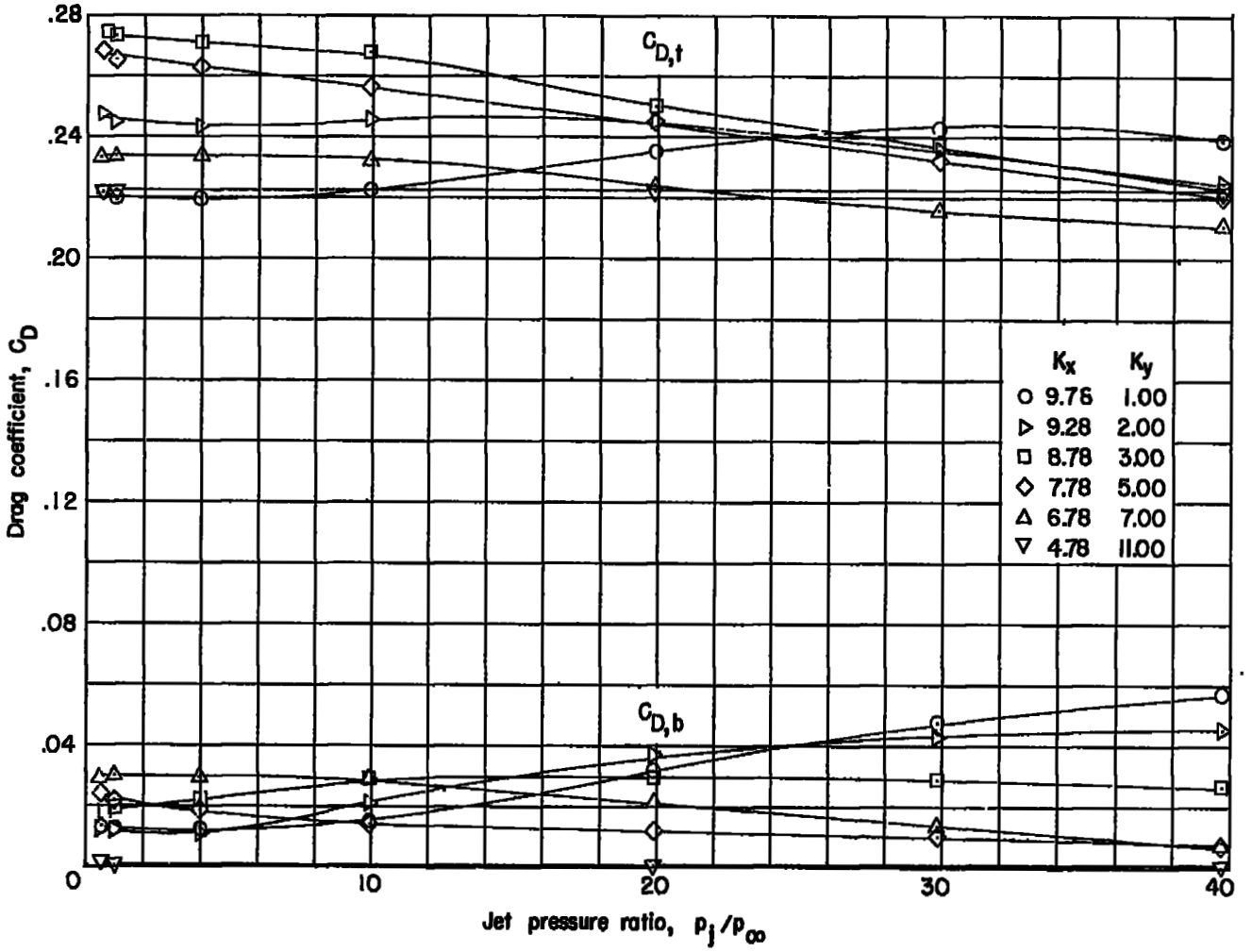

Model 3-B

(a) $M_\infty = 1.94$. Continued.

Figure 6.- Continued.

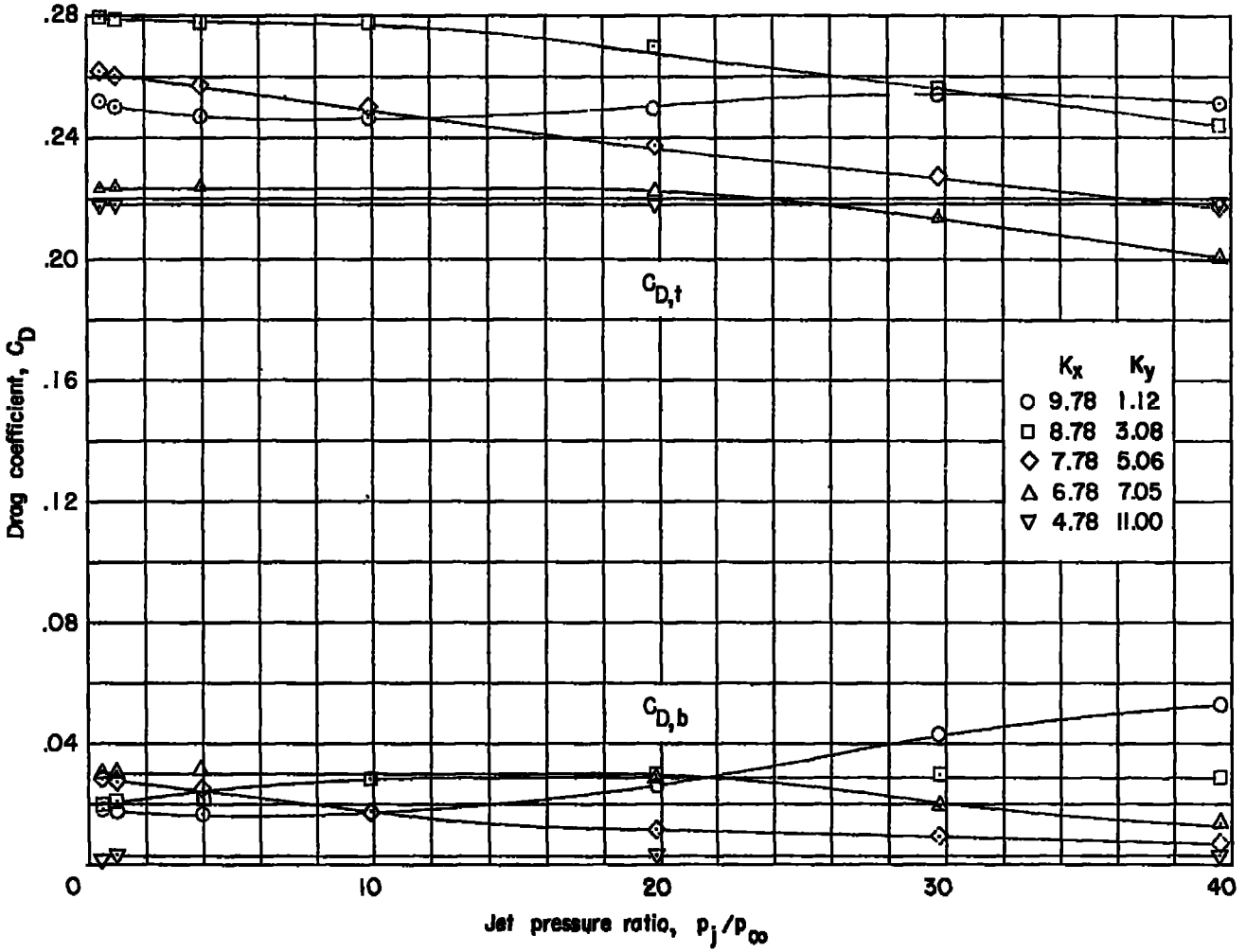

Model 3-C

(a) $M_\infty = 1.94$. Continued.

Figure 6.- Continued.

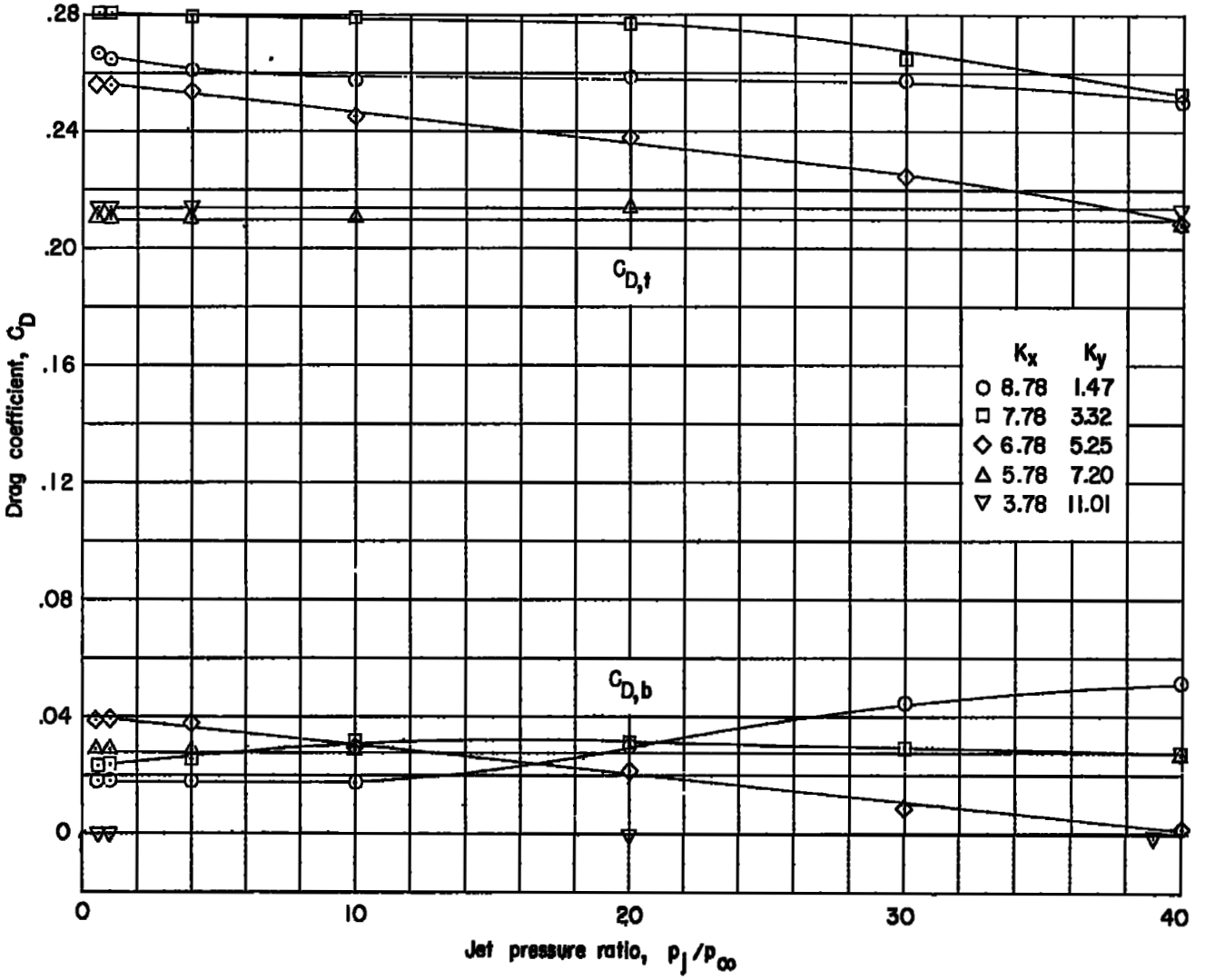

Model 3-D

(a) $M_\infty = 1.94$. Concluded.

Figure 6.- Continued.

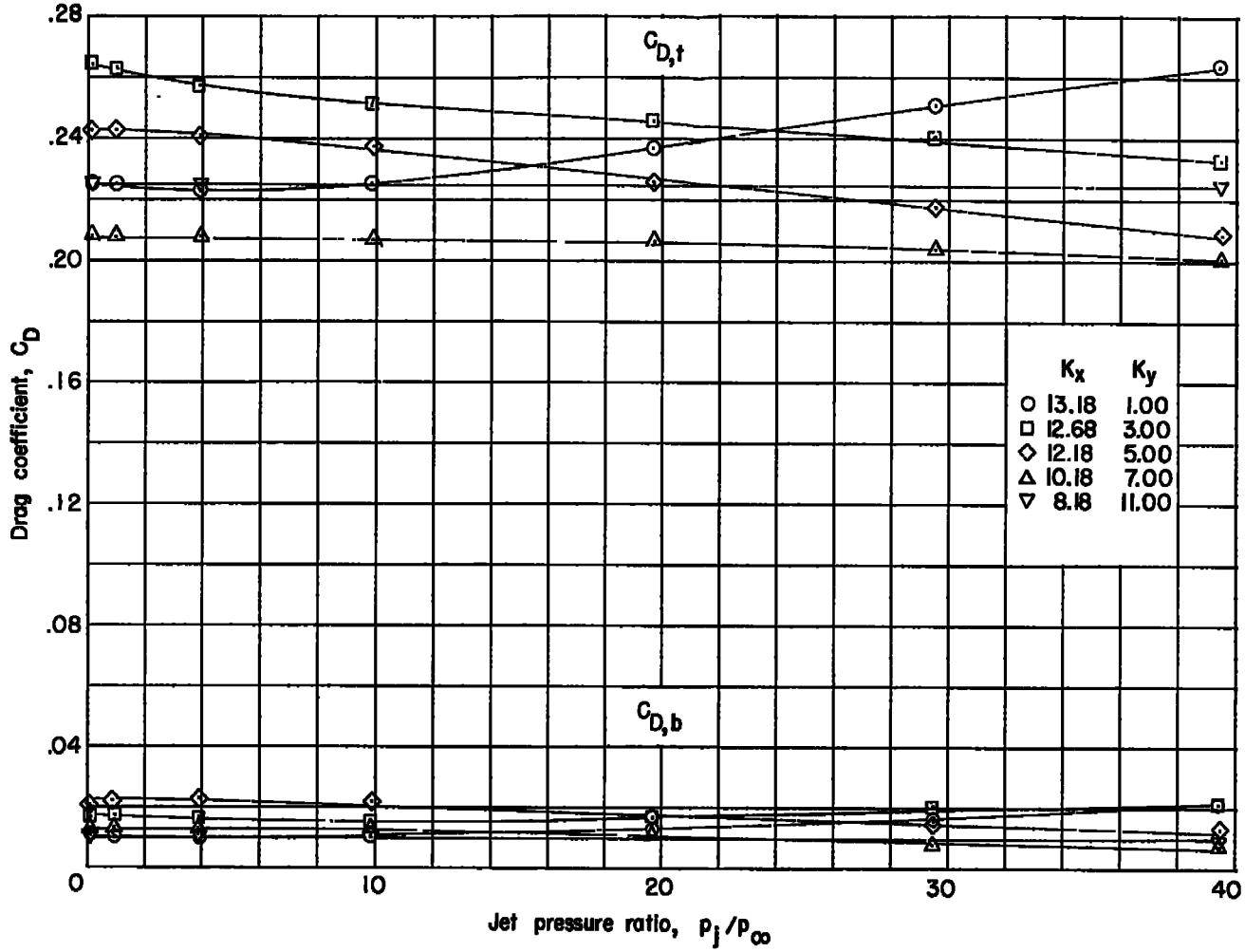

Model 1-B

(b) $M_\infty = 2.41$.

Figure 6.- Continued.

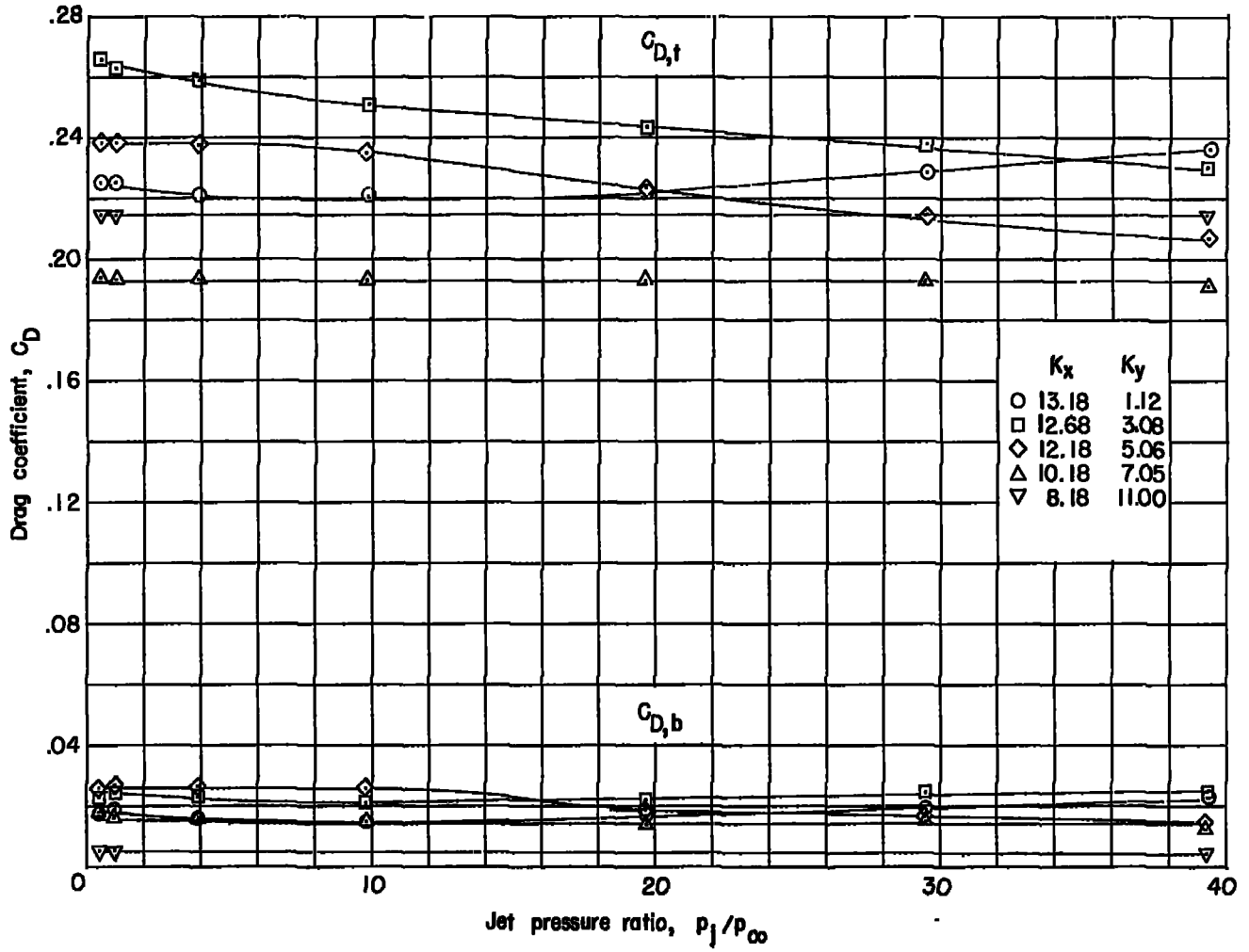

Model 1-C

(b) $M_\infty = 2.41$. Continued.

Figure 6.- Continued.

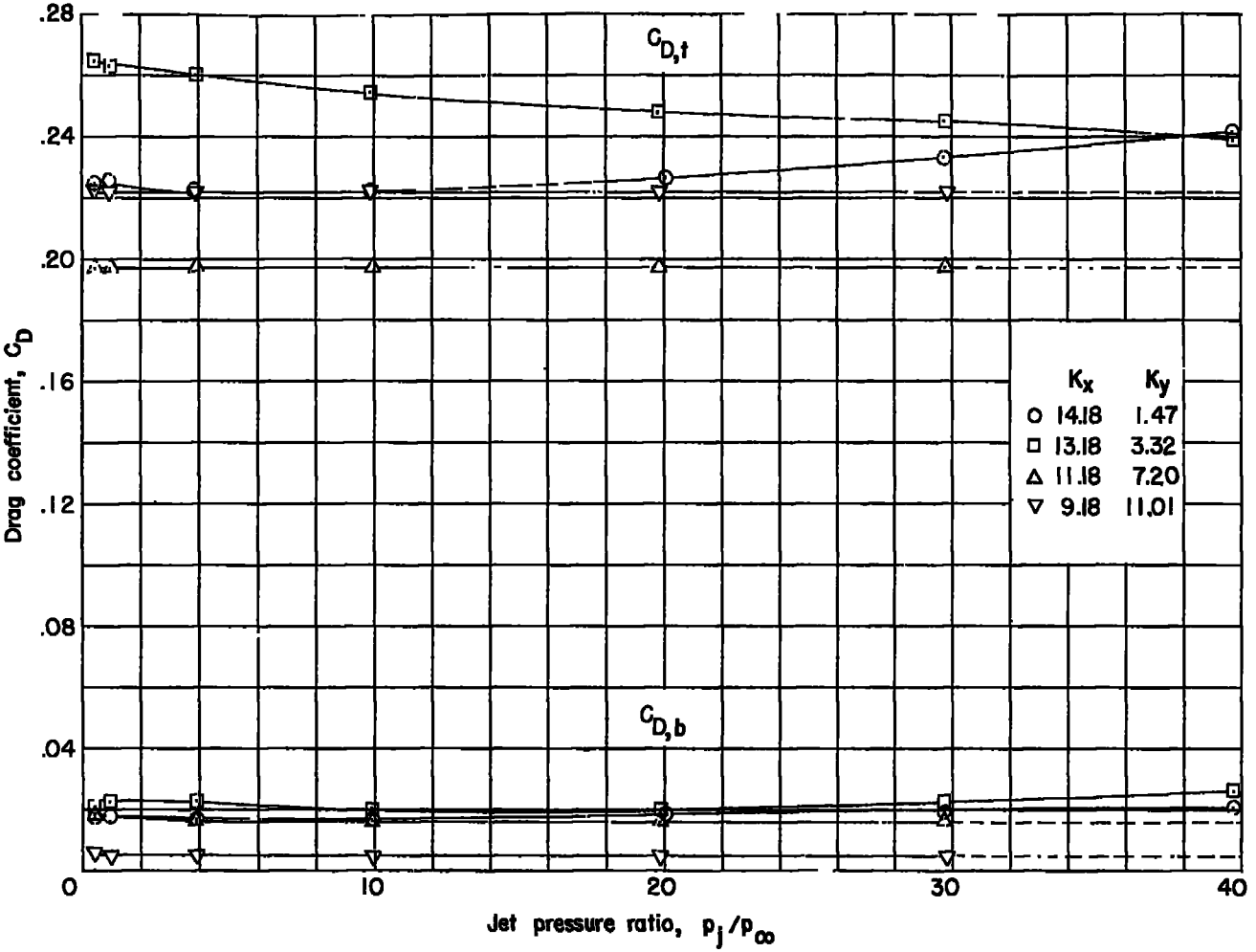

Model 1-D

(b) $M_\infty = 2.41$. Continued.

Figure 6.- Continued.

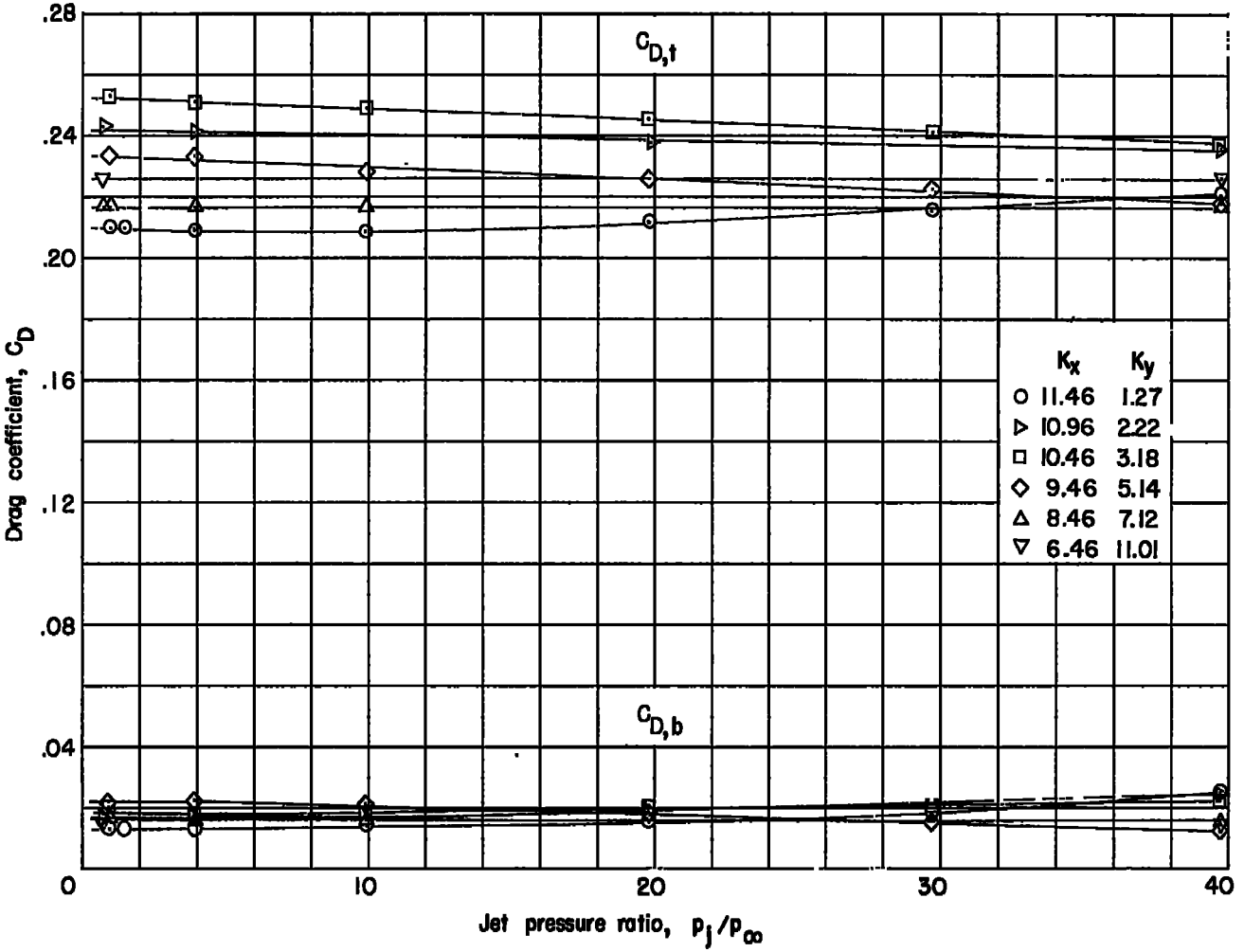

Model 2-A

(b) $M_\infty = 2.41$. Continued.

Figure 6.- Continued.

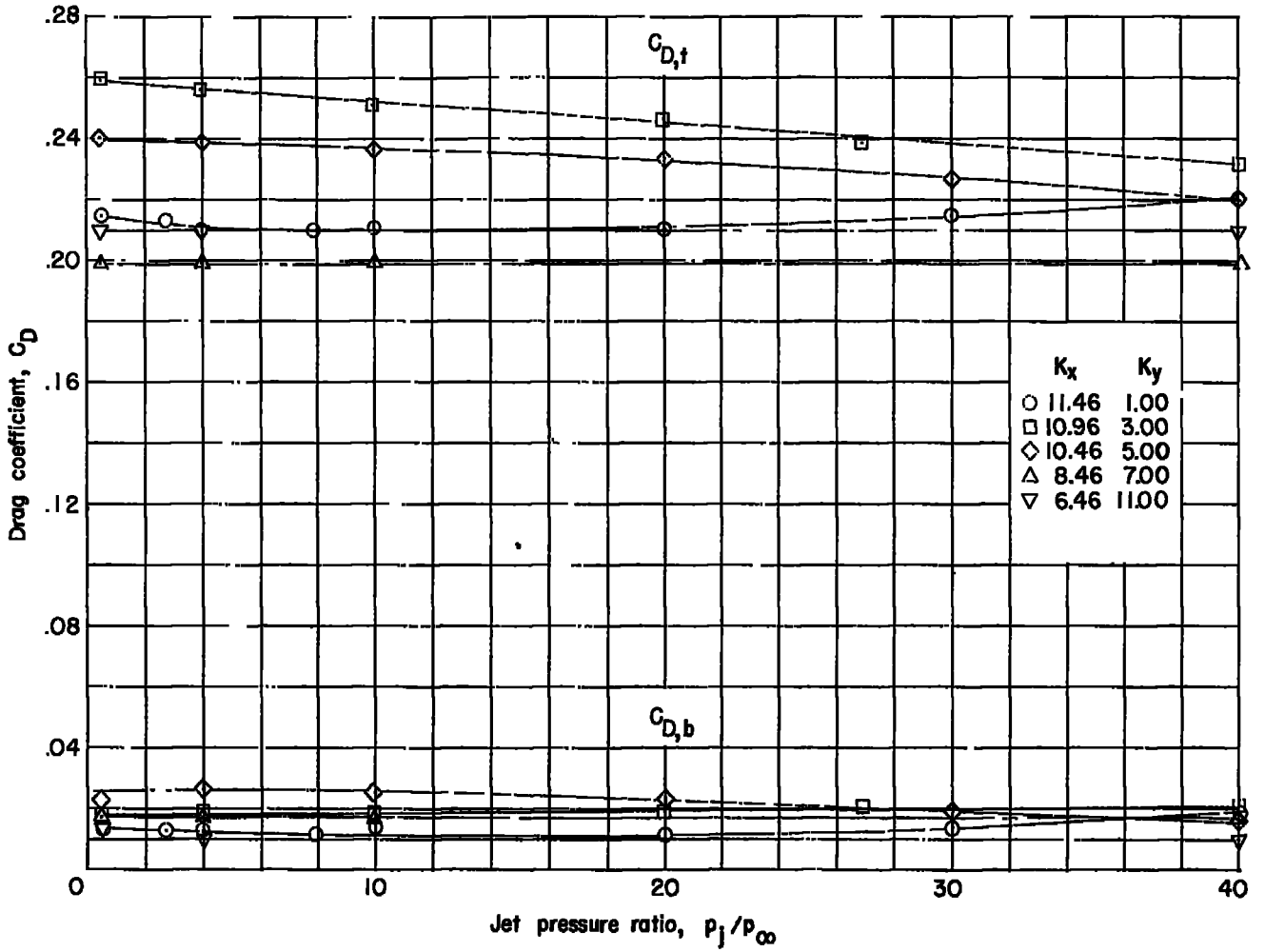

Model 2-B

(b) $M_\infty = 2.41$. Continued.

Figure 6.- Continued.

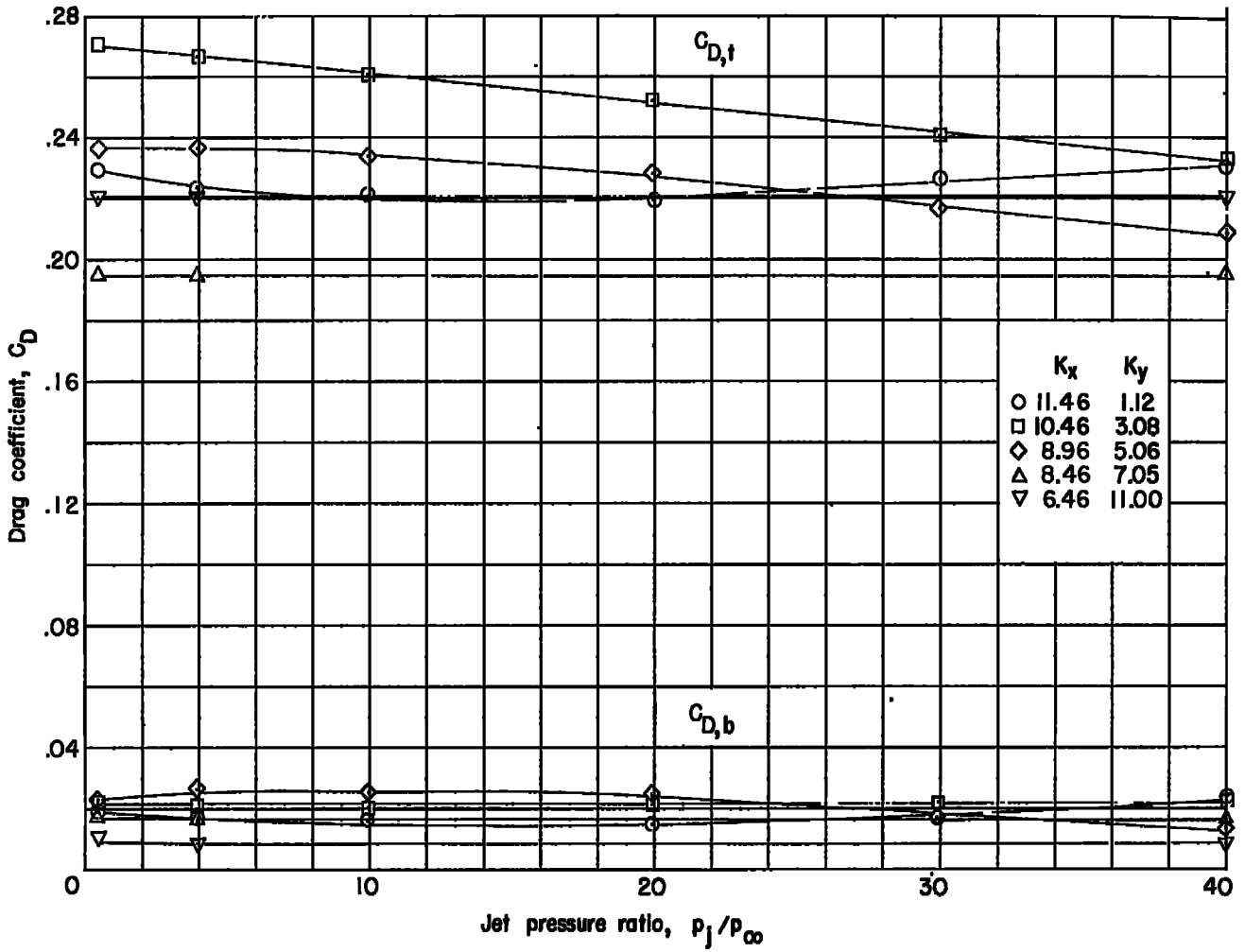

Model 2-C

(b) $M_\infty = 2.41$. Continued.

Figure 6.- Continued.

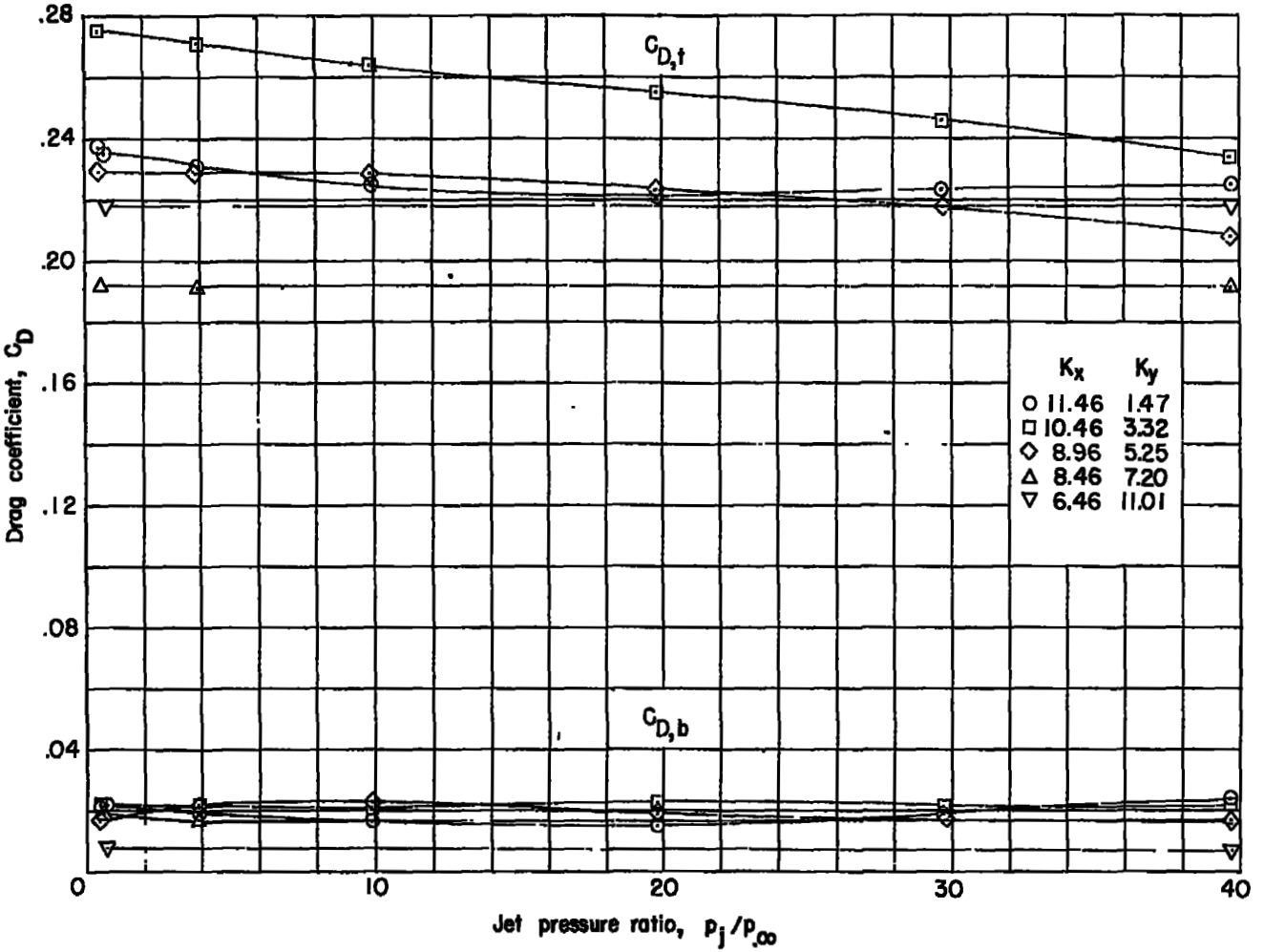

Model 2-D

(b) $M_\infty = 2.41$. Continued.

Figure 6.- Continued.

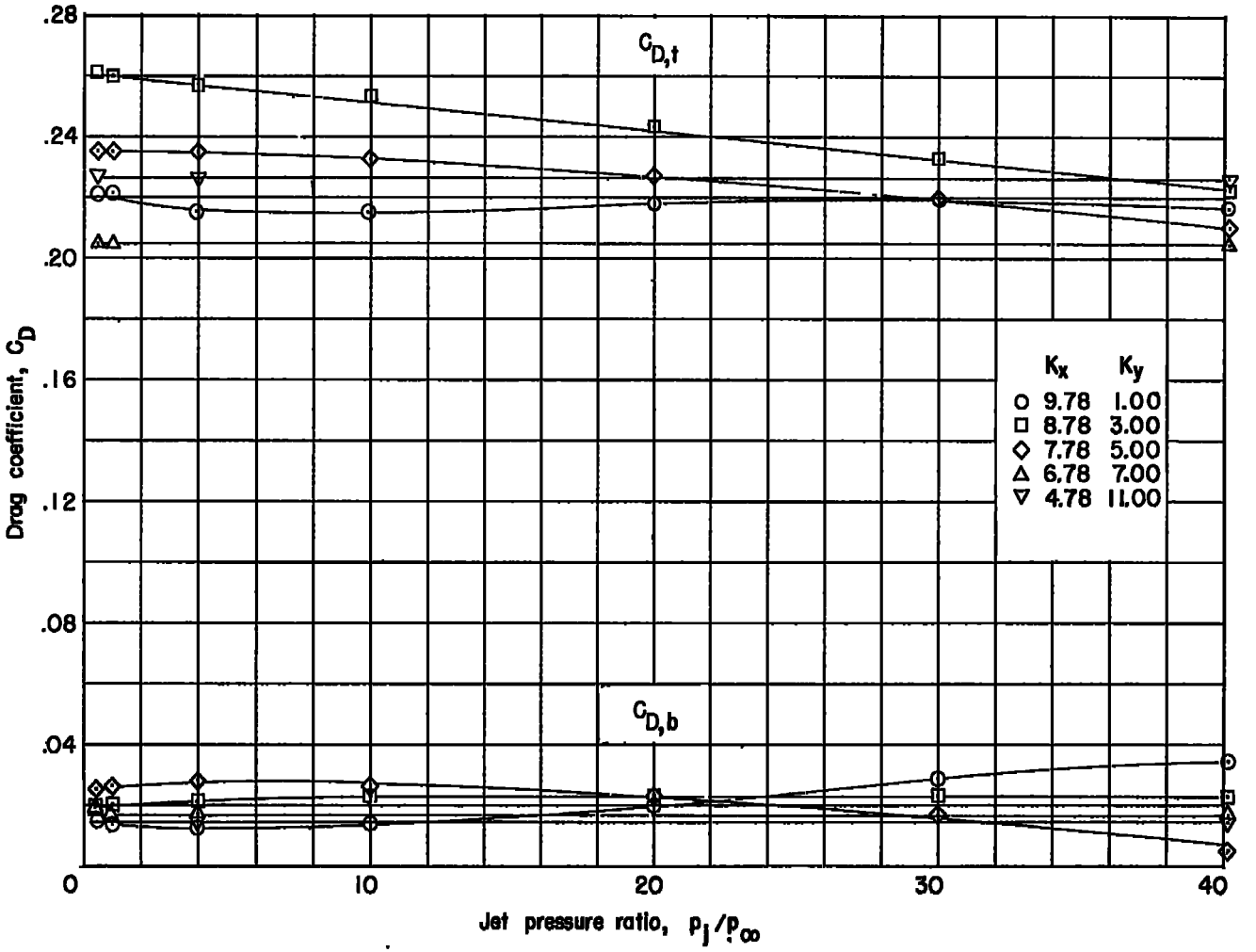

Model 3-B

(b) $M_\infty = 2.41$. Continued.

Figure 6.- Continued.

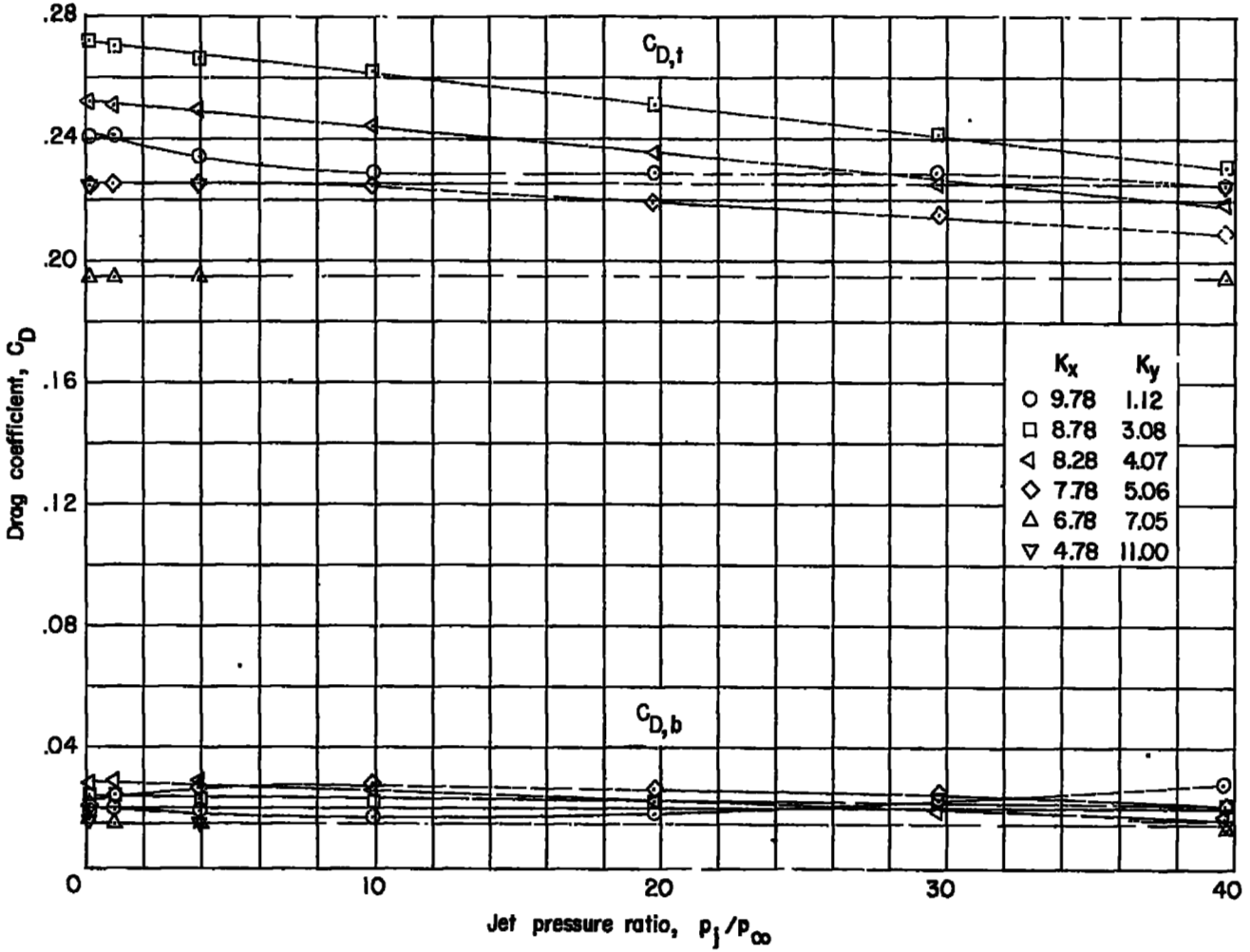

Model 3-C

(b) $M_\infty = 2.41$. Continued.

Figure 6.- Continued.

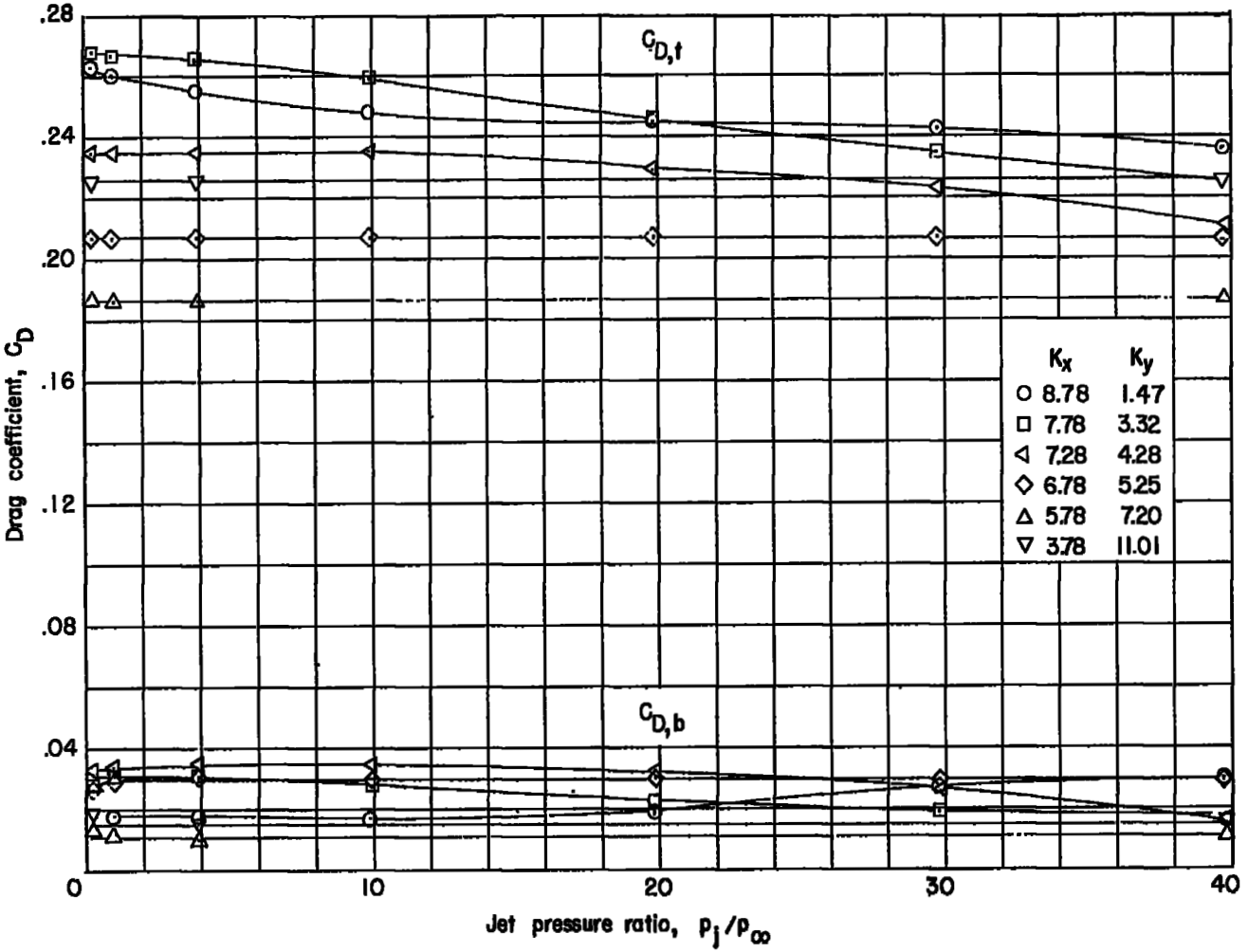

Model 3-D

(b) $M_\infty = 2.41$. Concluded.

Figure 6.- Concluded.

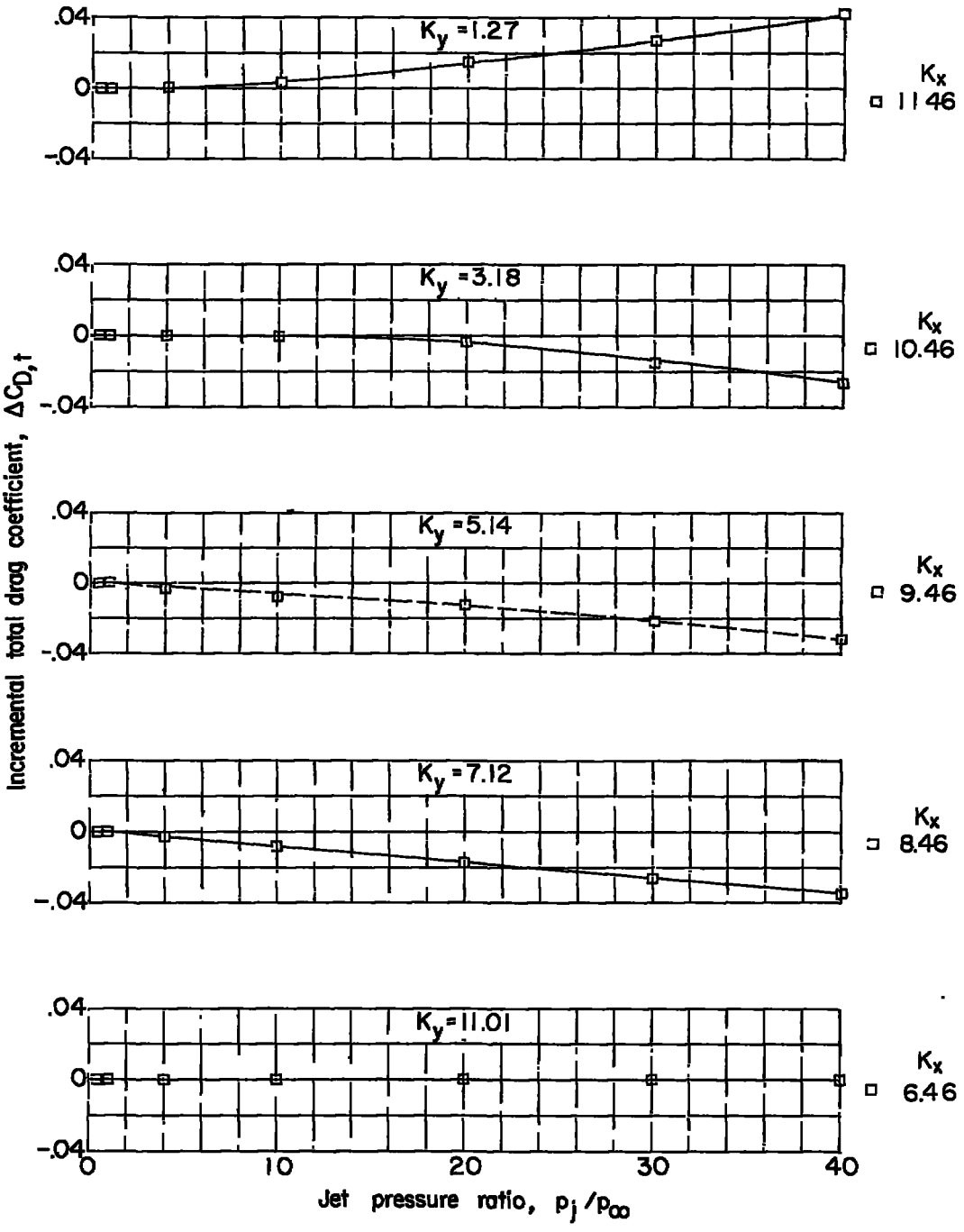

$K_z = 0$

(a) $M_\infty = 1.94$.

Figure 7.- Effects of the jet on incremental total drag coefficients. Dashed curves are from interpolated data.

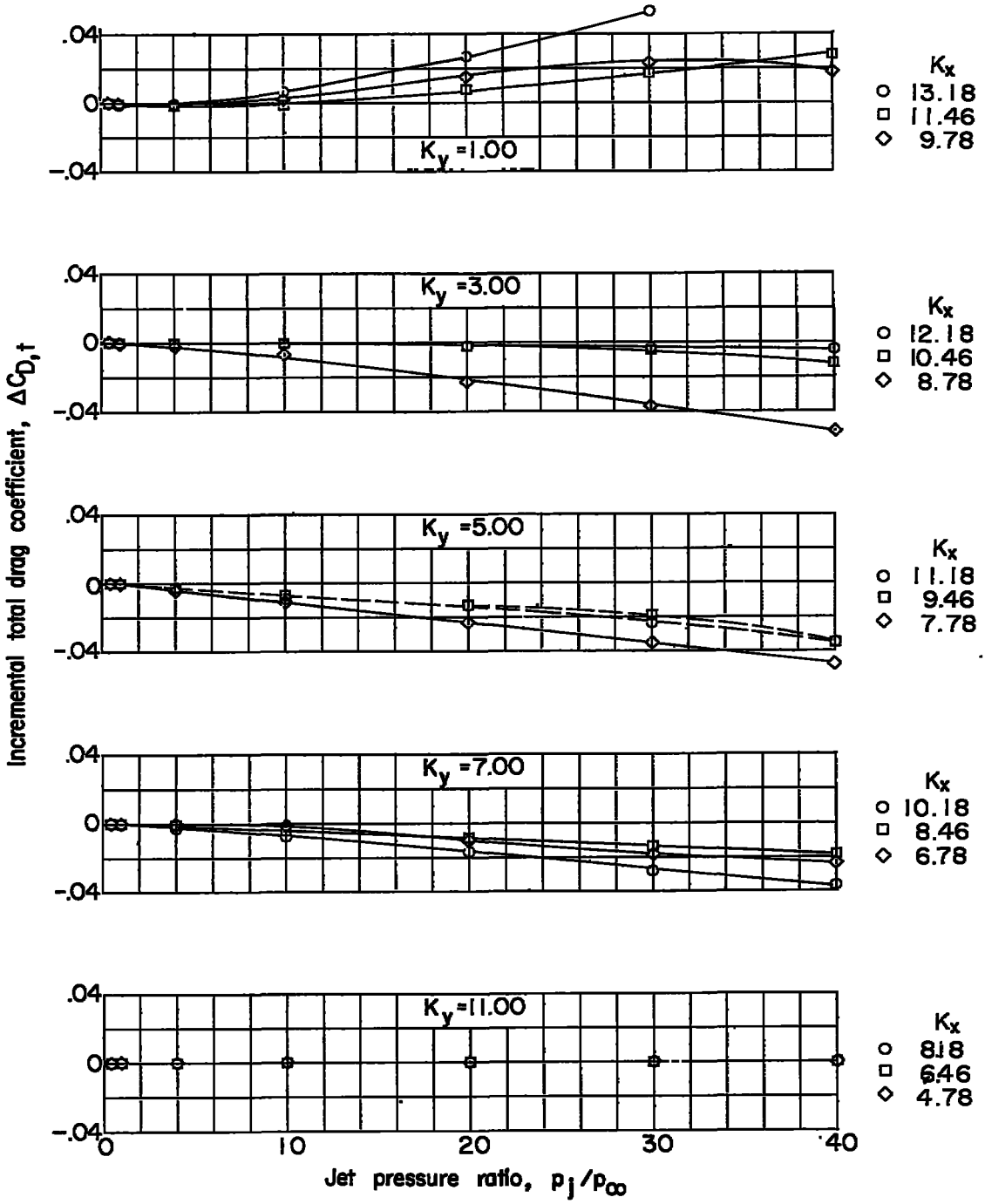

$K_z = 1.5$

(a) $M_\infty = 1.94$. Continued.

Figure 7.- Continued.

[redacted]

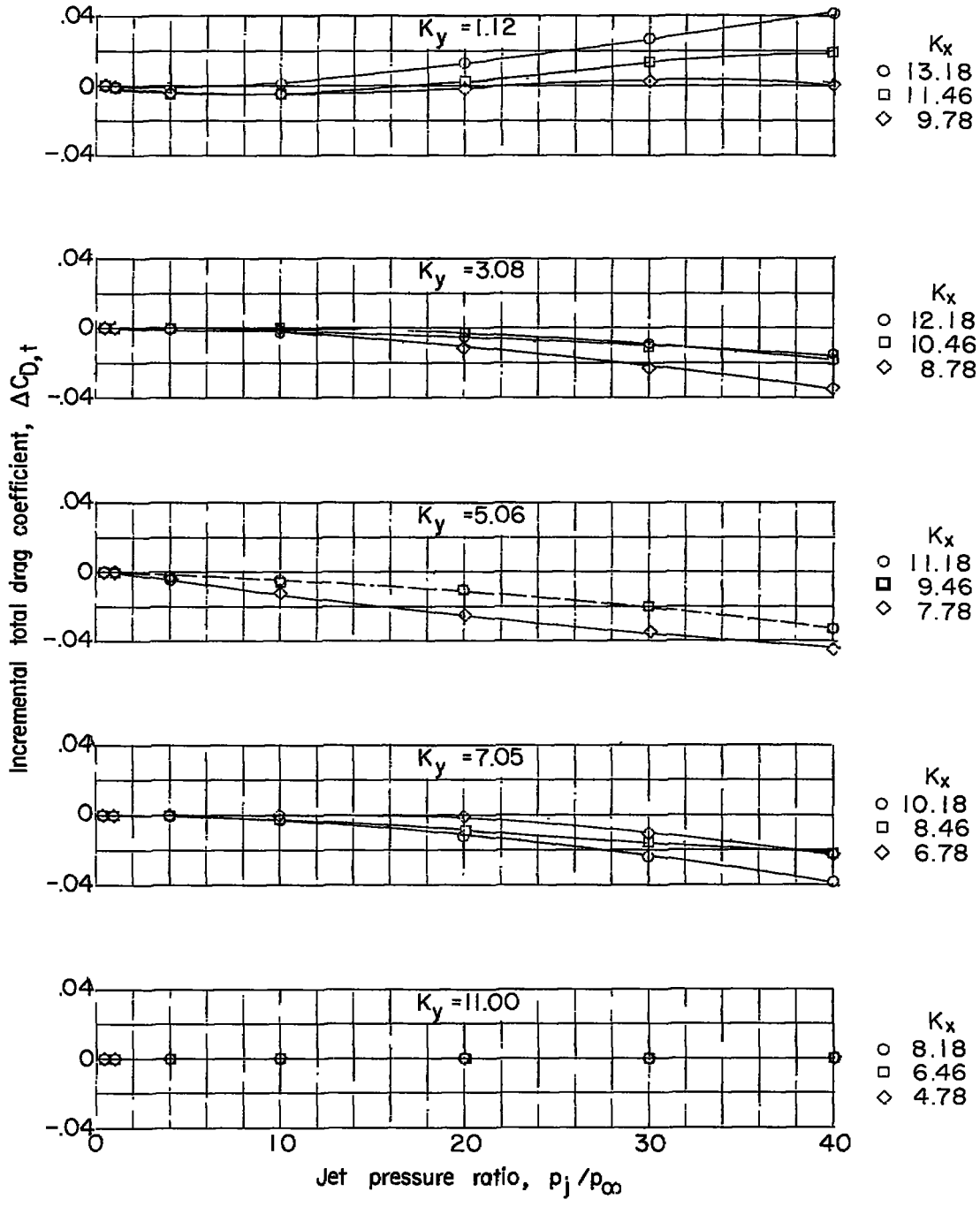

$K_z = 2.5$

(a) $M_\infty = 1.94$. Continued.

Figure 7.- Continued.

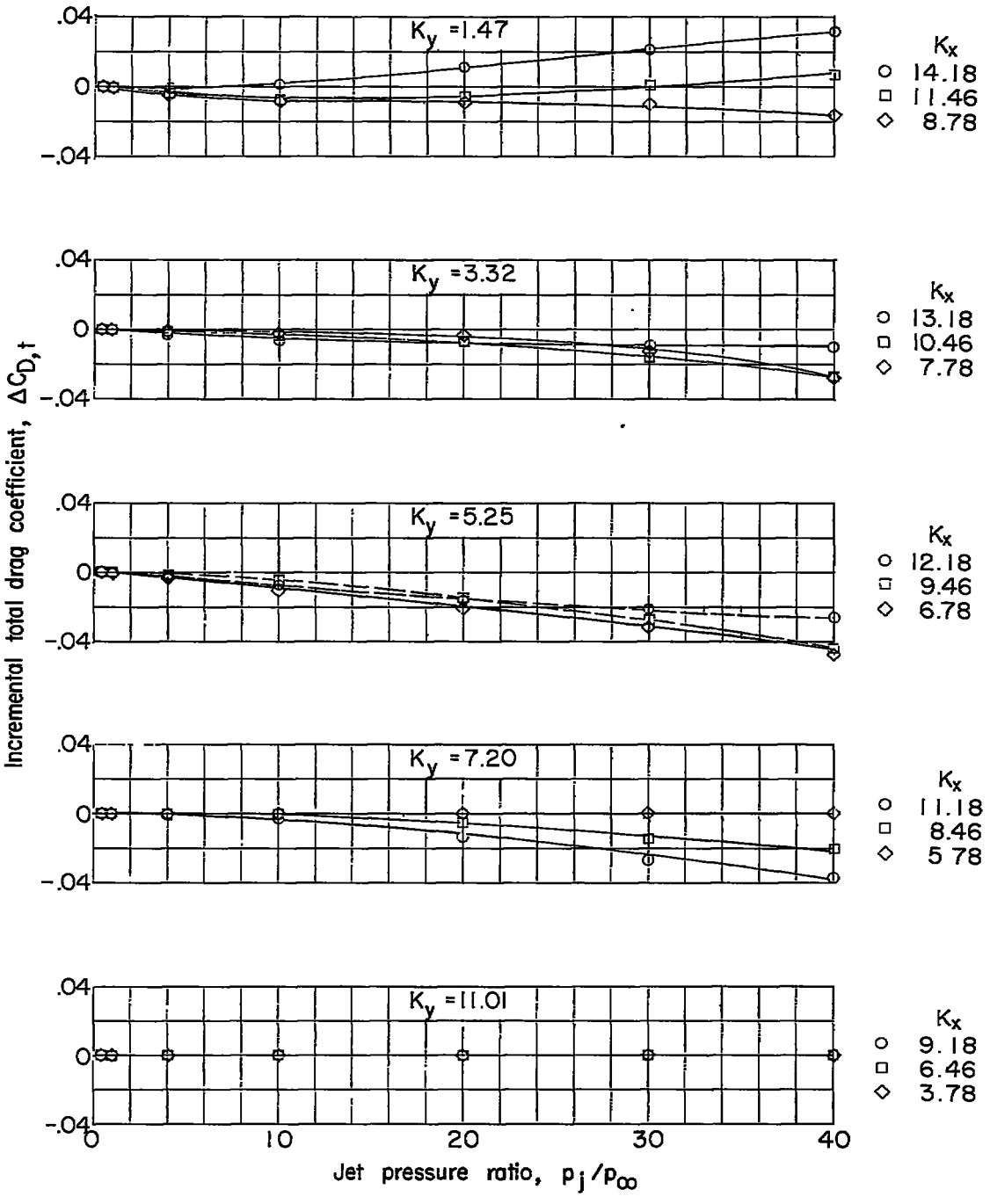

$K_z = 3.5$

(a) $M_\infty = 1.94$. Concluded.

Figure 7.- Continued.

[redacted]

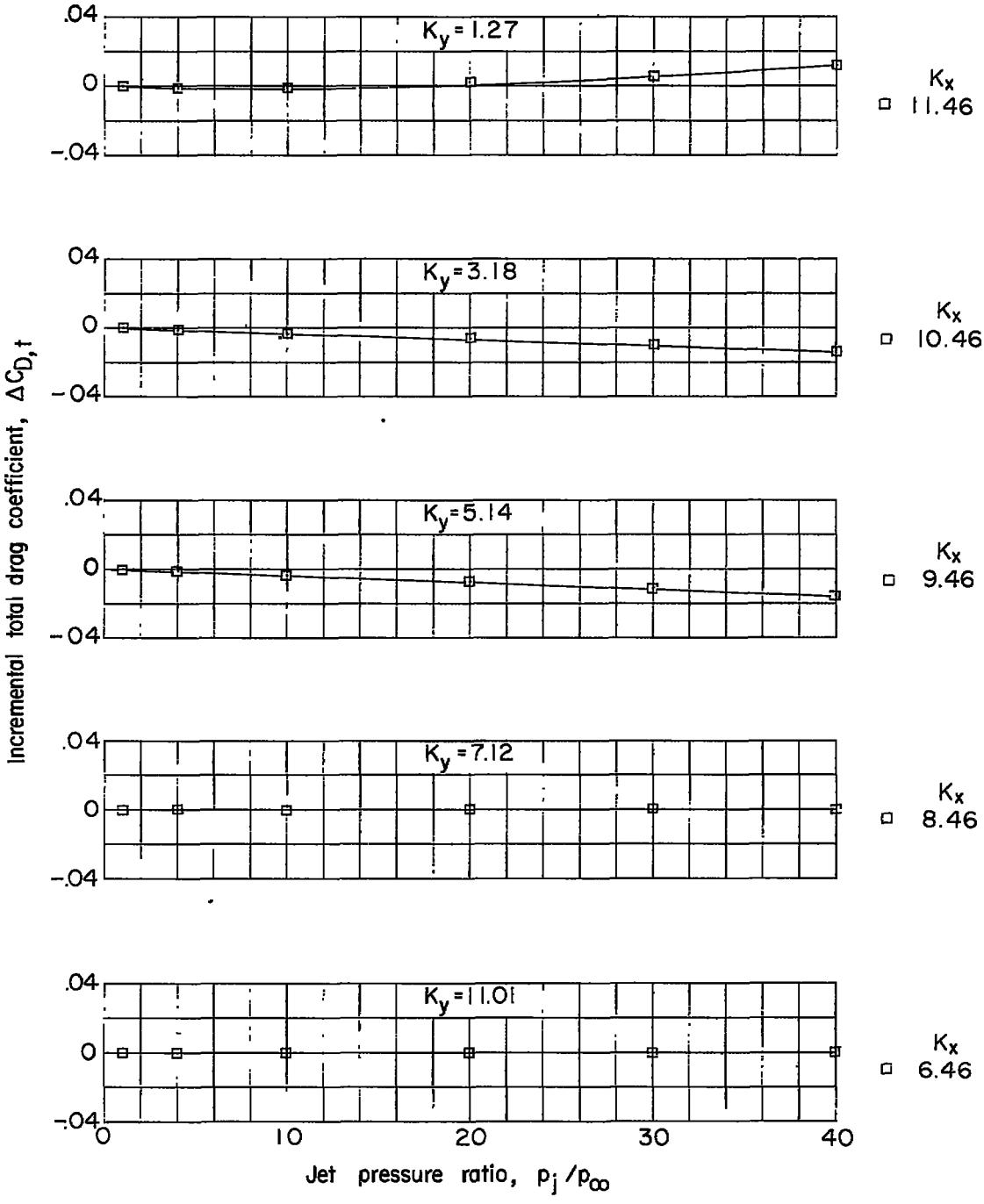

$K_z = 0$

(b) $M_\infty = 2.41$.

Figure 7.- Continued.

[redacted]

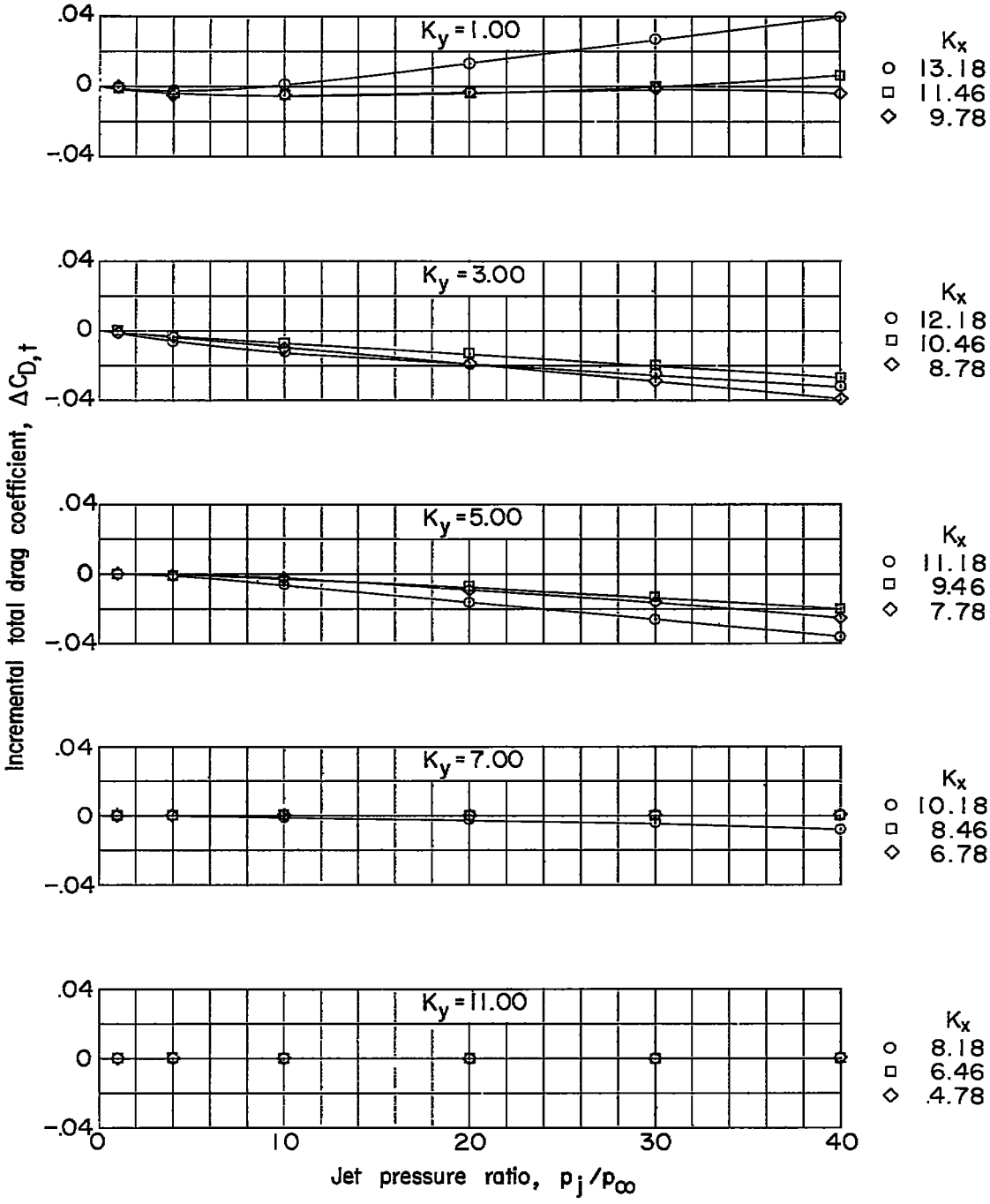

$K_z = 1.5$

(b) $M_\infty = 2.41$. Continued.

Figure 7.- Continued.

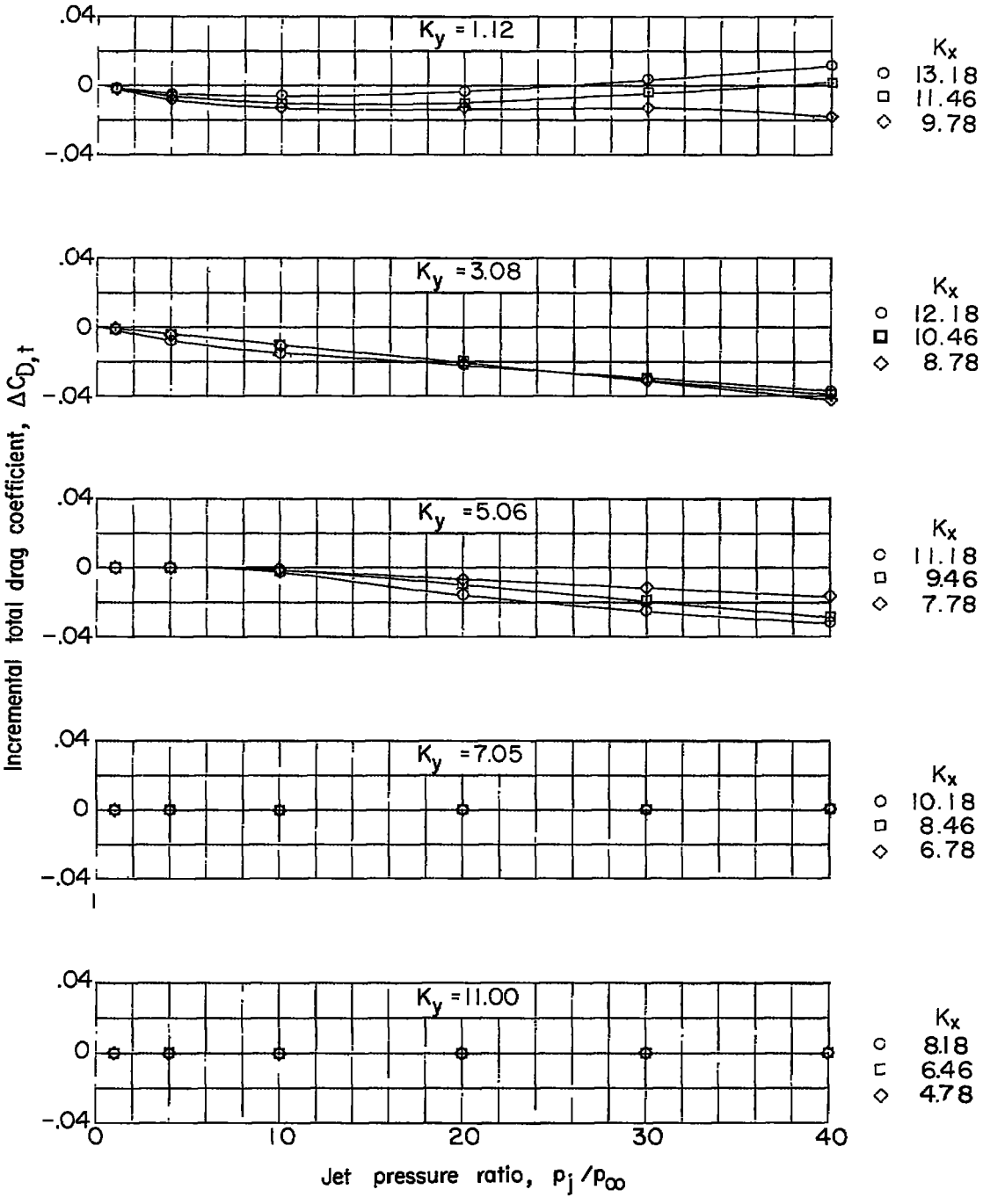

K_z = 2.5

(b) M_∞ = 2.41. Continued.

Figure 7.- Continued.

[redacted]

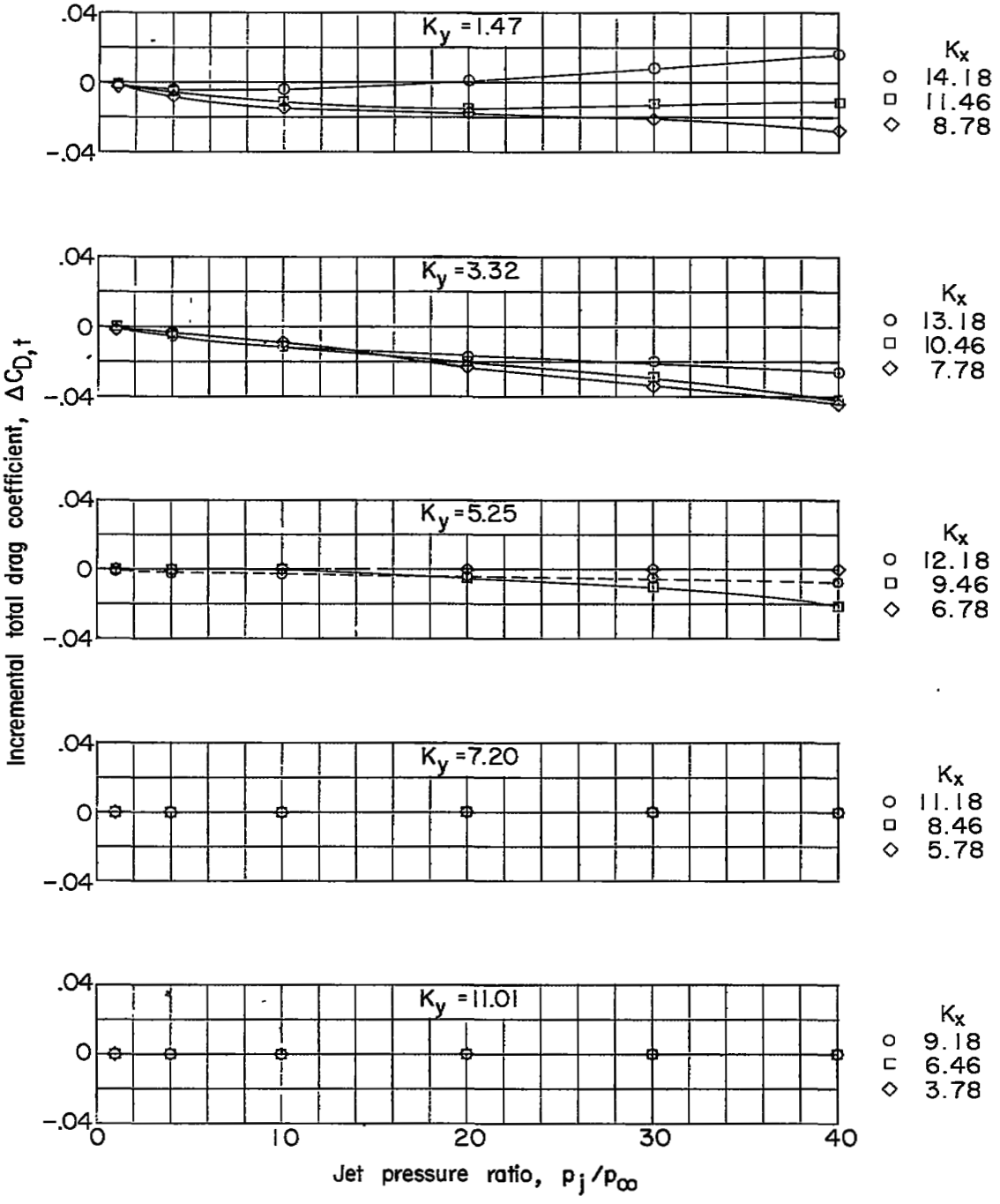

K_z = 3.5

(b) M_∞ = 2.41. Concluded.

Figure 7.- Concluded.

[redacted]

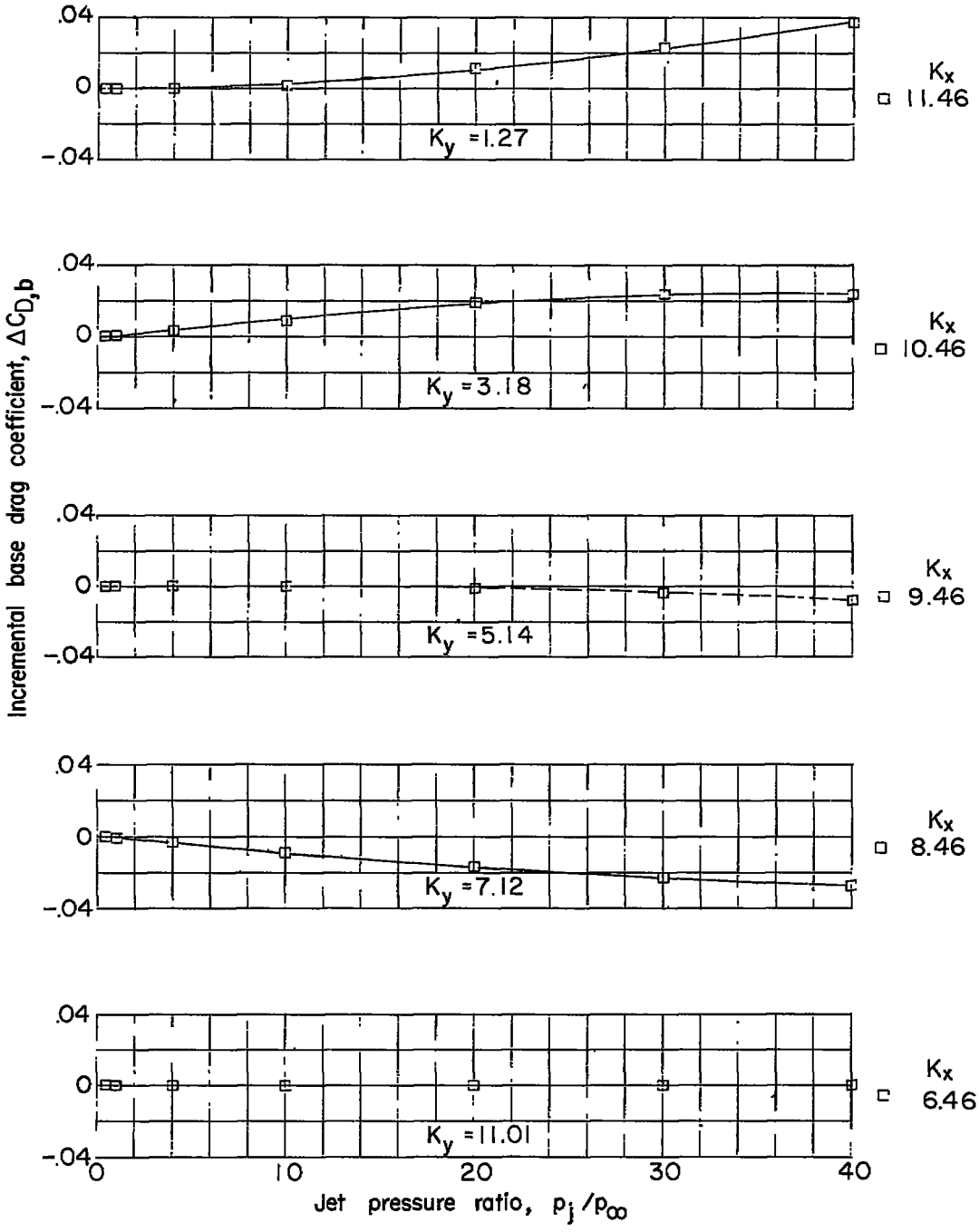

$K_z = 0$

(a) $M_\infty = 1.94$.

Figure 8.- Effects of the jet on incremental base drag coefficients. Dashed curves are from interpolated data.

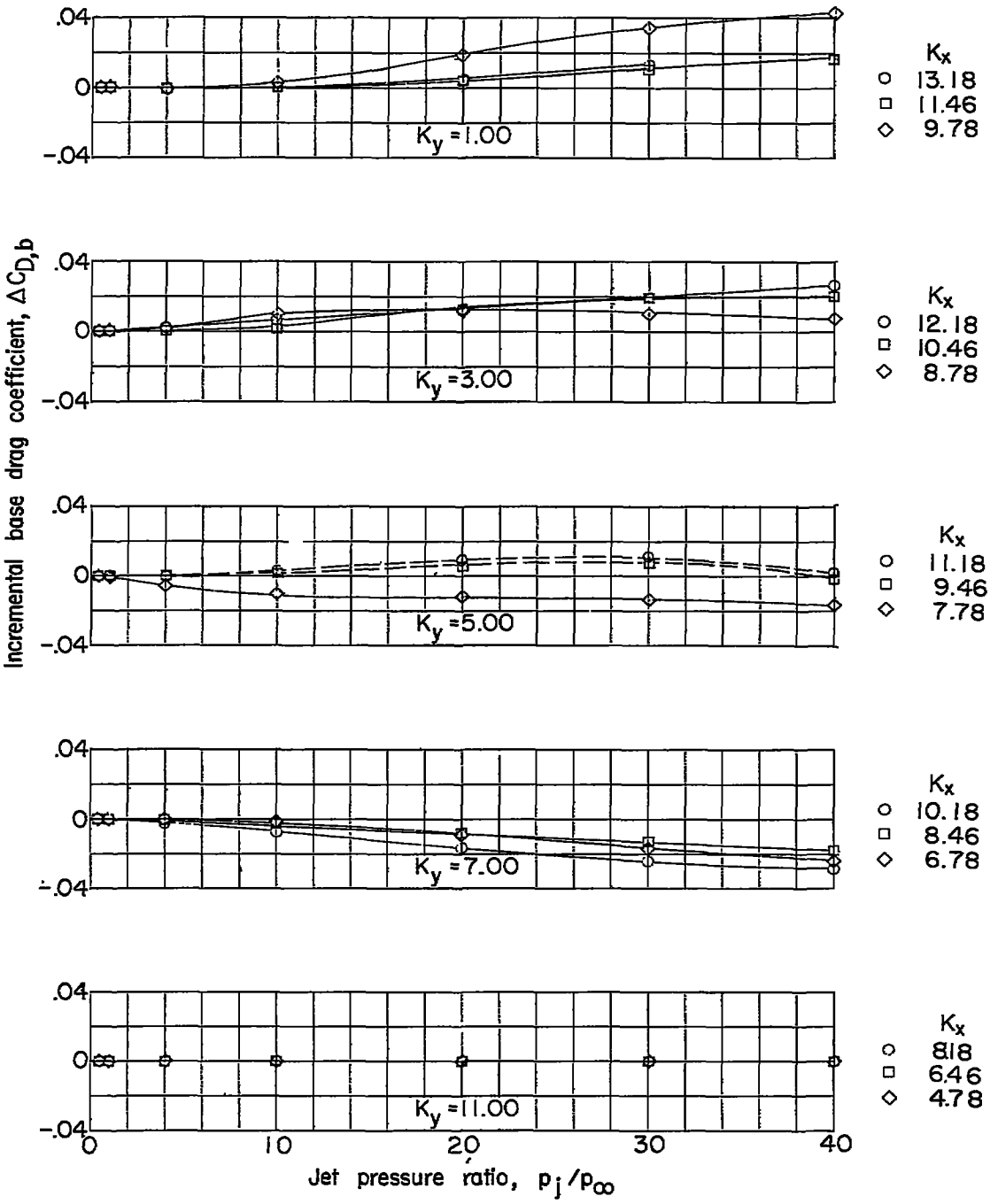

$K_z = 1.5$

(a) $M_\infty = 1.94$. Continued.

Figure 8.- Continued.

[redacted]

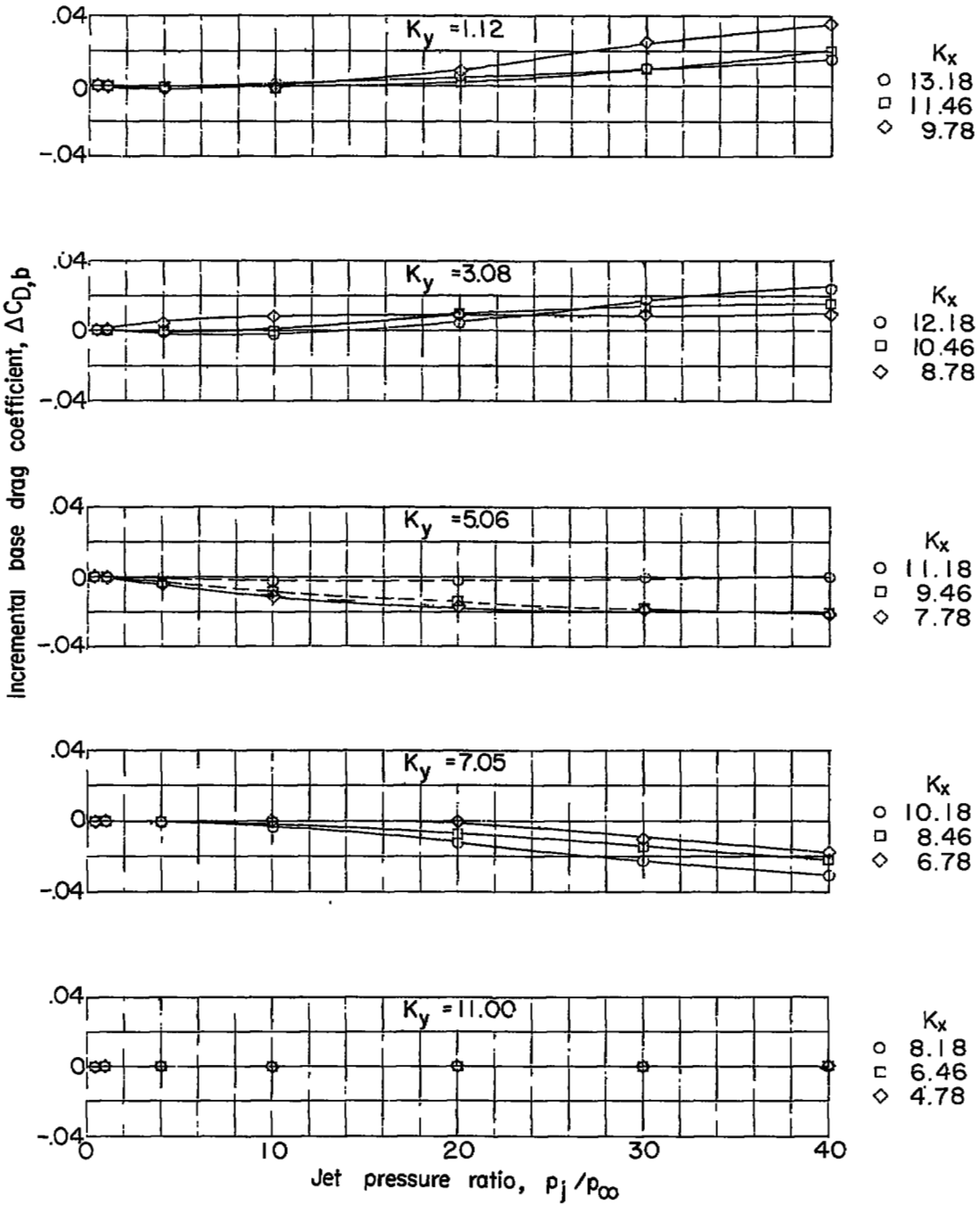

$K_z = 2.5$

(a) $M_\infty = 1.94$. Continued.

Figure 8.- Continued.

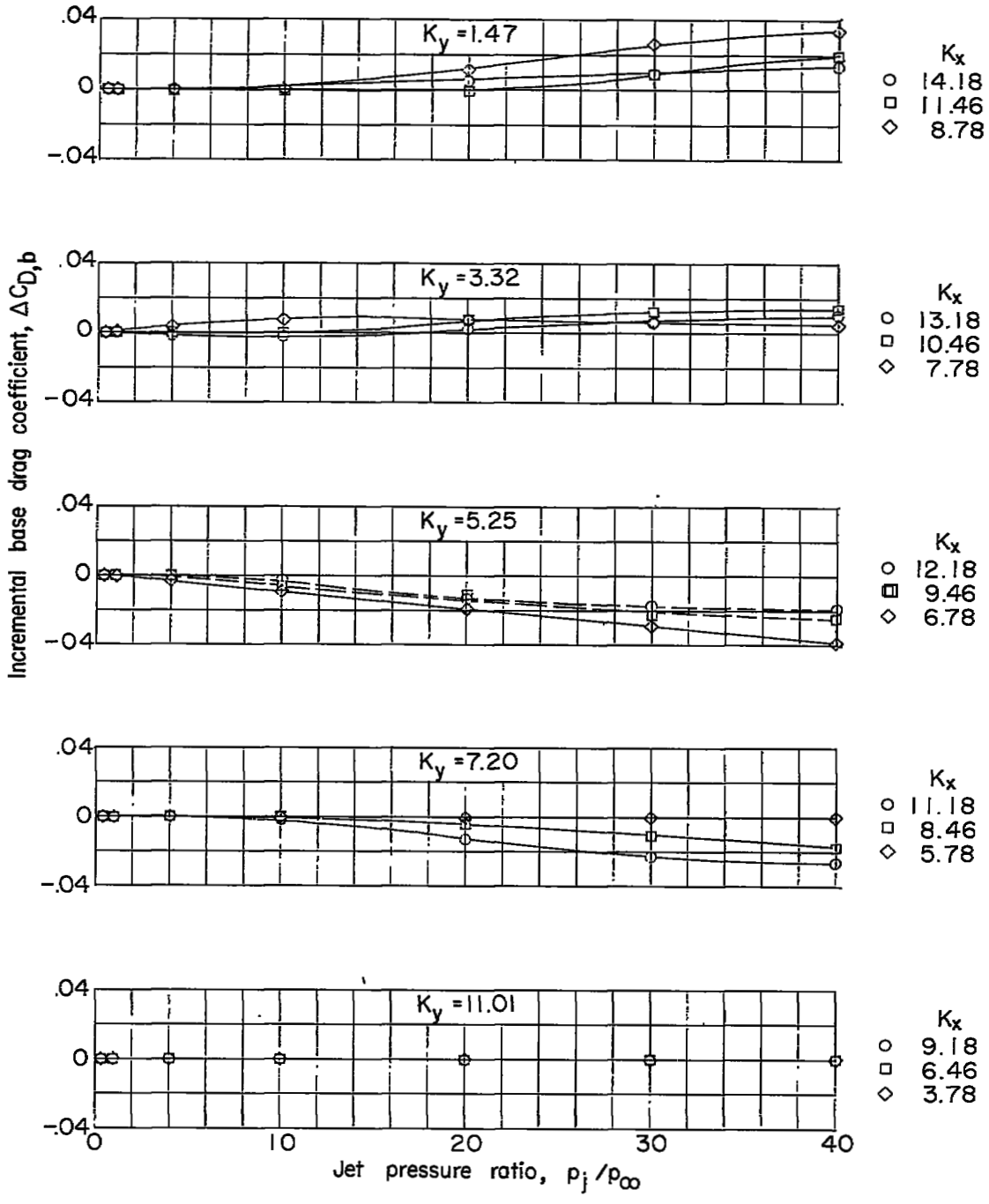

K_z = 3.5

(a) M_∞ = 1.94. Concluded.

Figure 8.- Continued.

[redacted]

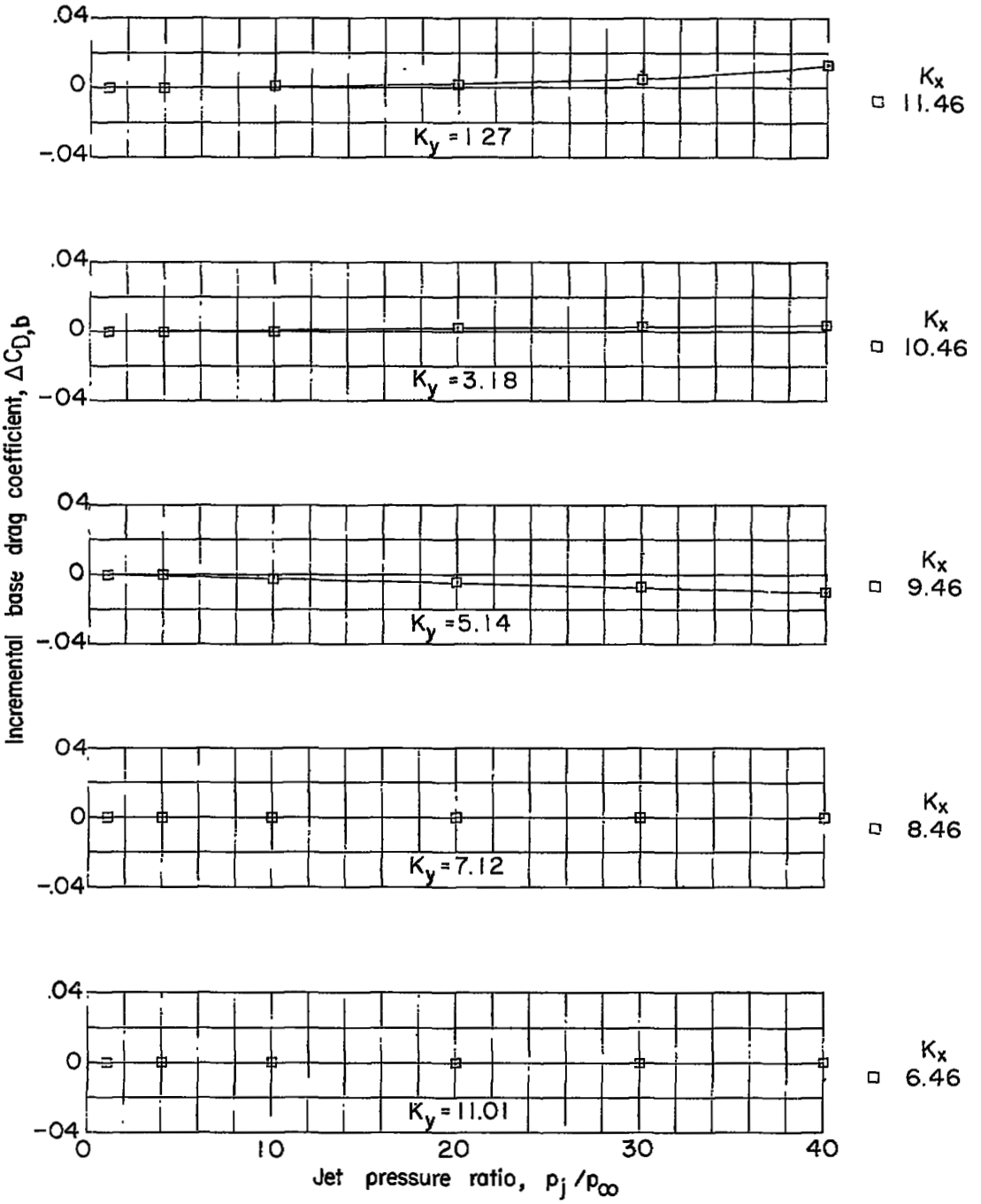

$K_Z = 0$

(b) $M_\infty = 2.41$.

Figure 8.- Continued.

[redacted]

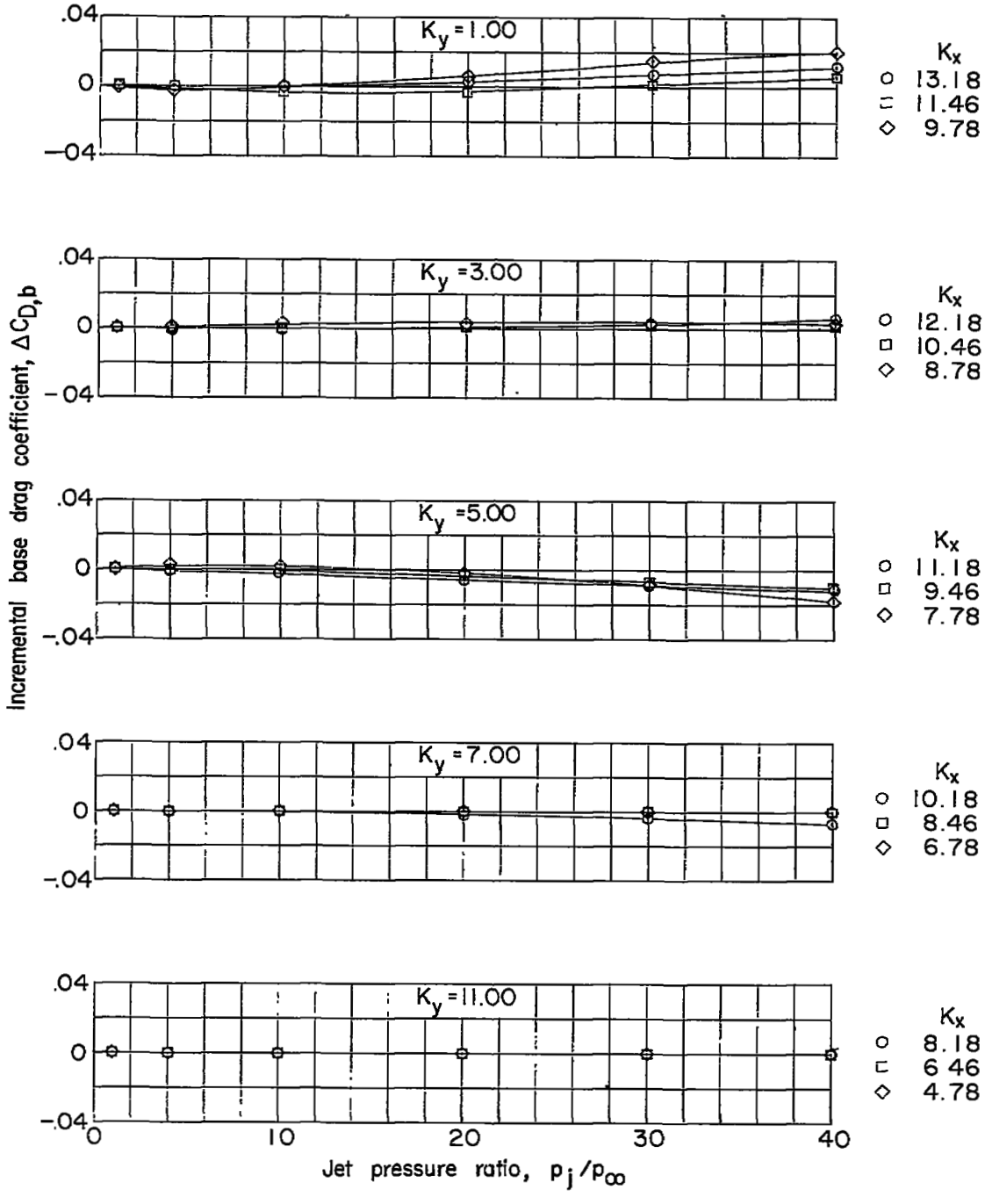

$K_z = 1.5$

(b) $M_\infty = 2.41$. Continued.

Figure 8.- Continued.

[redacted]

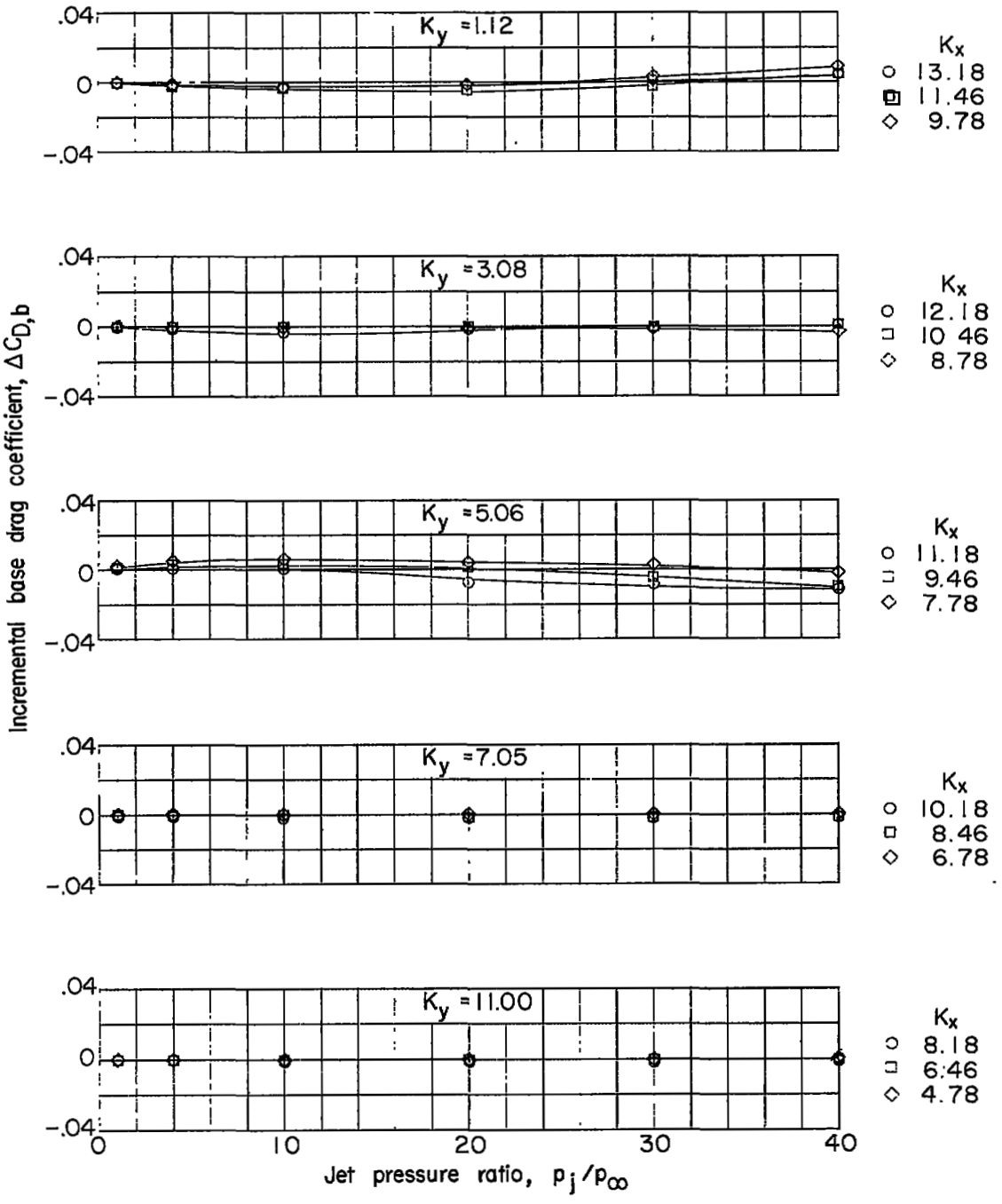

$K_z = 2.5$

(b) $M_\infty = 2.41$. Continued.

Figure 8.- Continued.

[redacted]

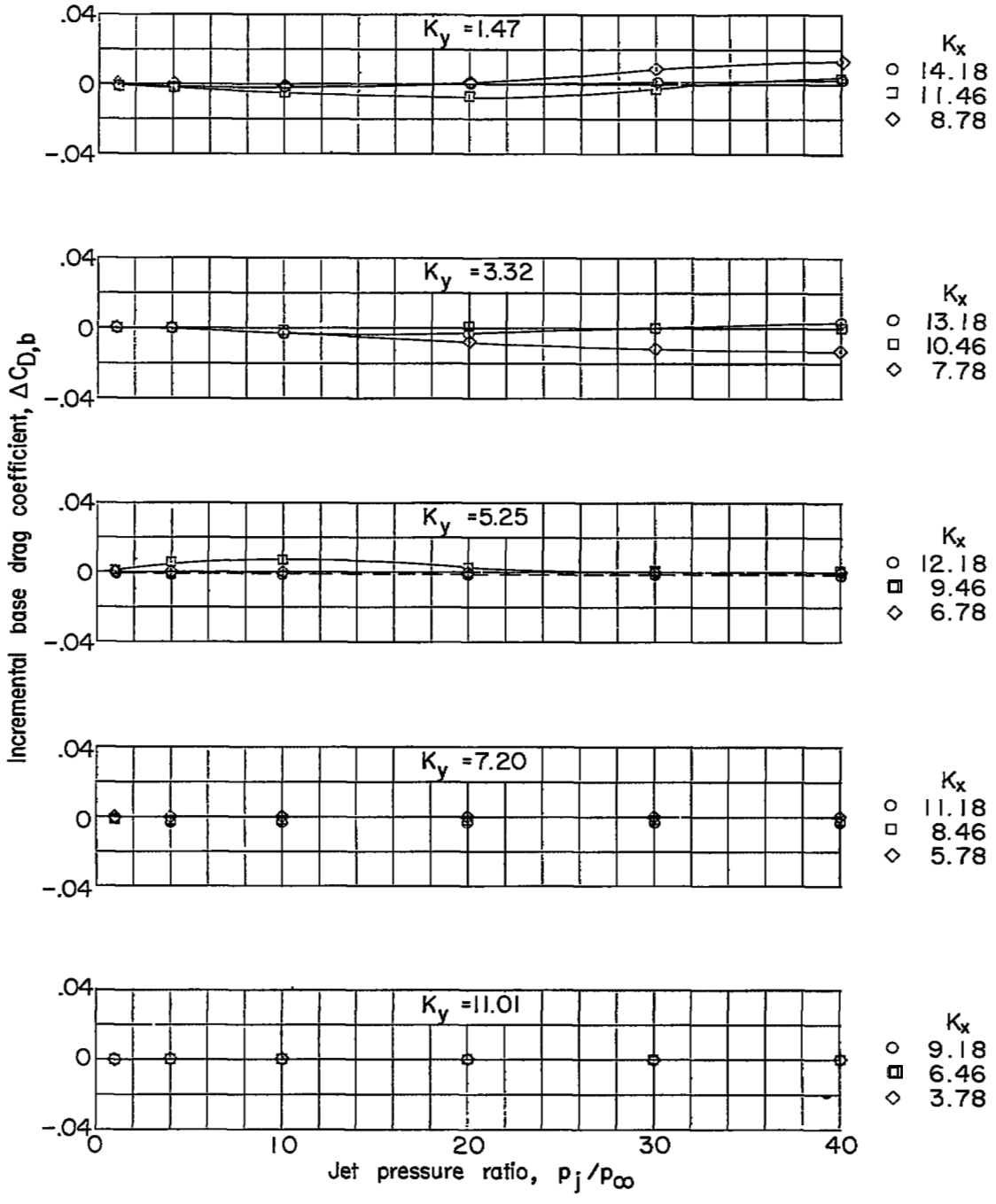

K_z = 3.5

(b) M_∞ = 2.41. Concluded.

Figure 8.- Concluded.

[redacted]

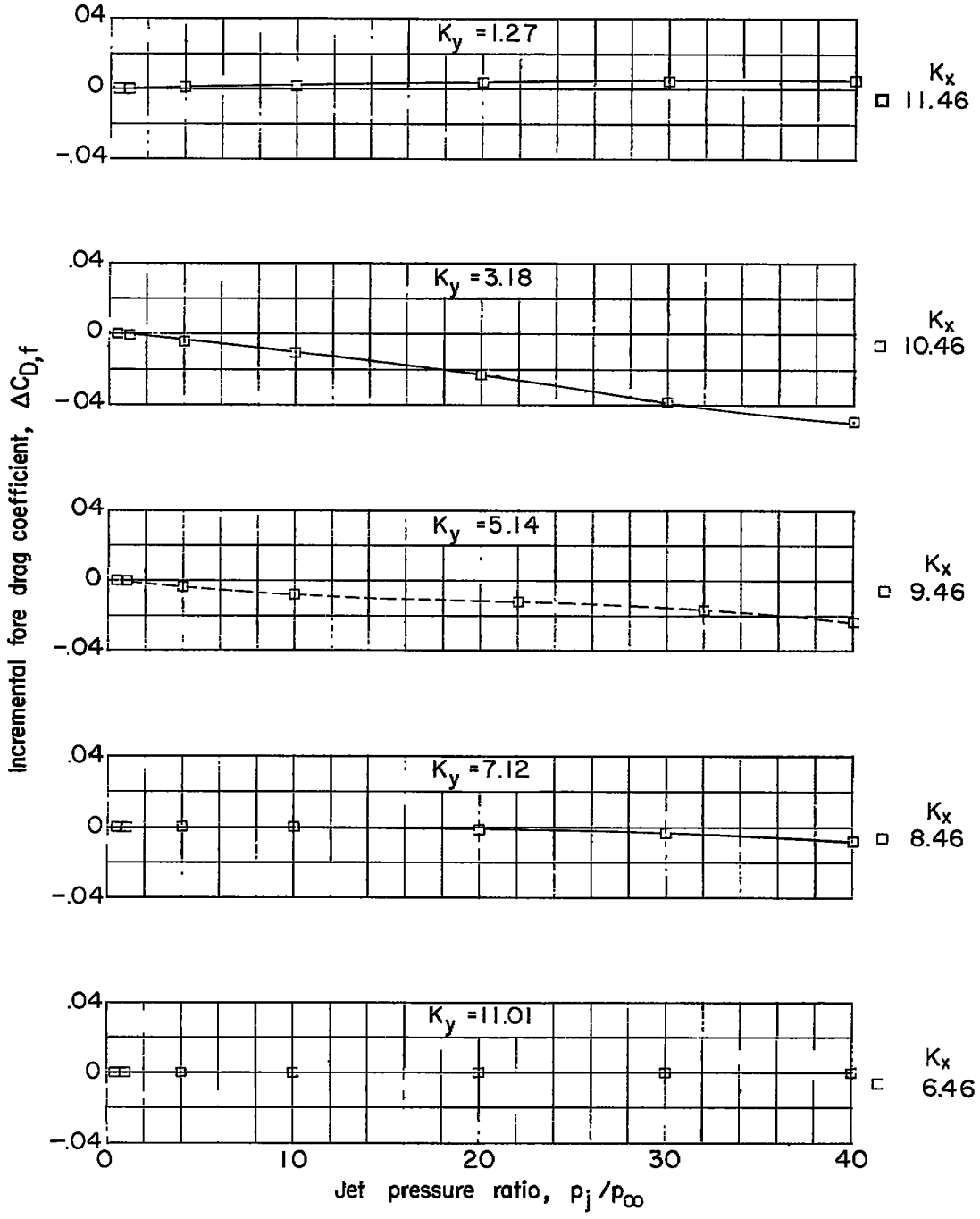

$K_z = 0$

(a) $M_\infty = 1.94$.

Figure 9.- Effects of the jet on incremental fore drag coefficients. Dashed curves are from interpolated data.

[redacted]

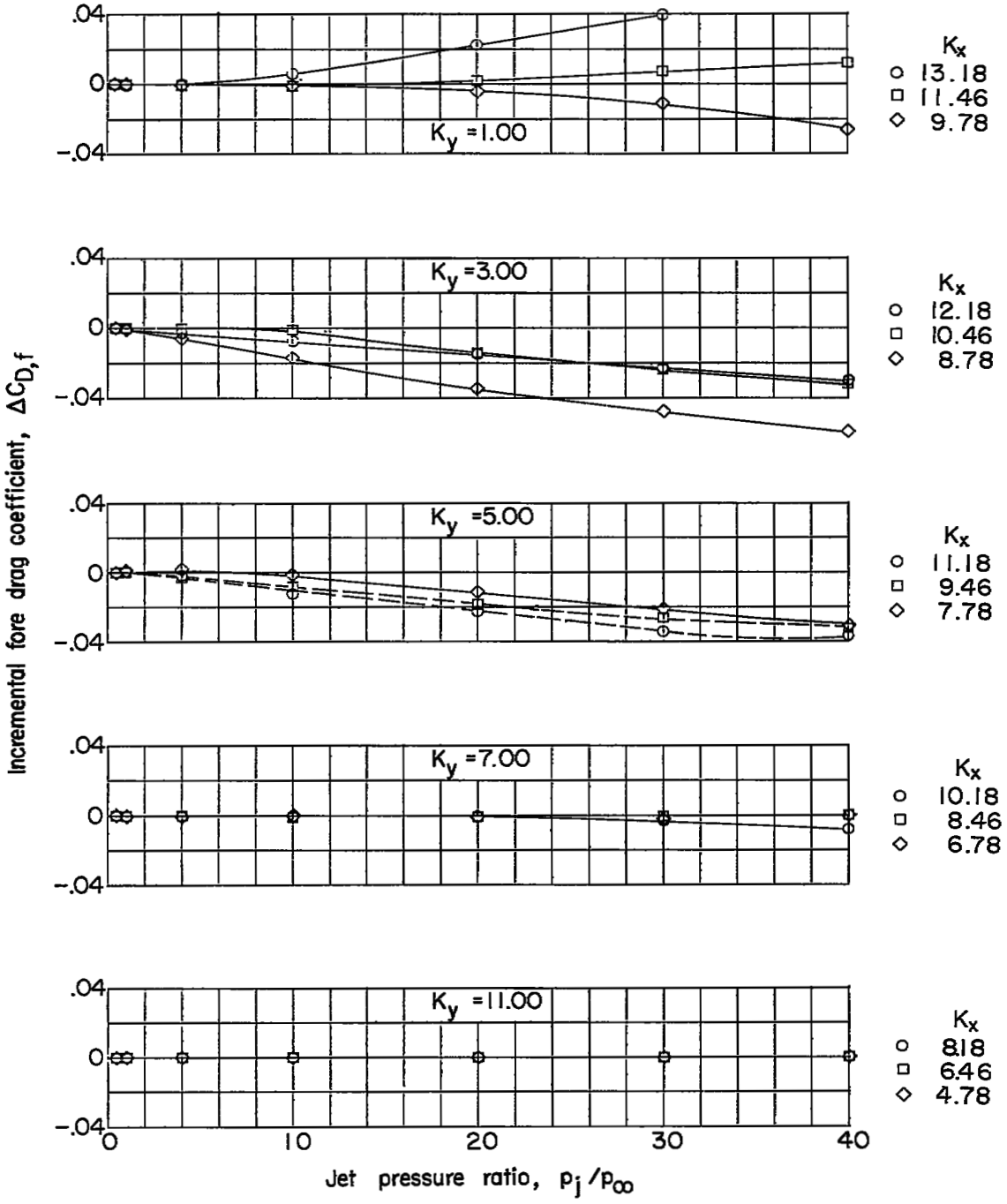

$K_z = 1.5$

(a) $M_\infty = 1.94$. Continued.

Figure 9.- Continued.

[redacted]

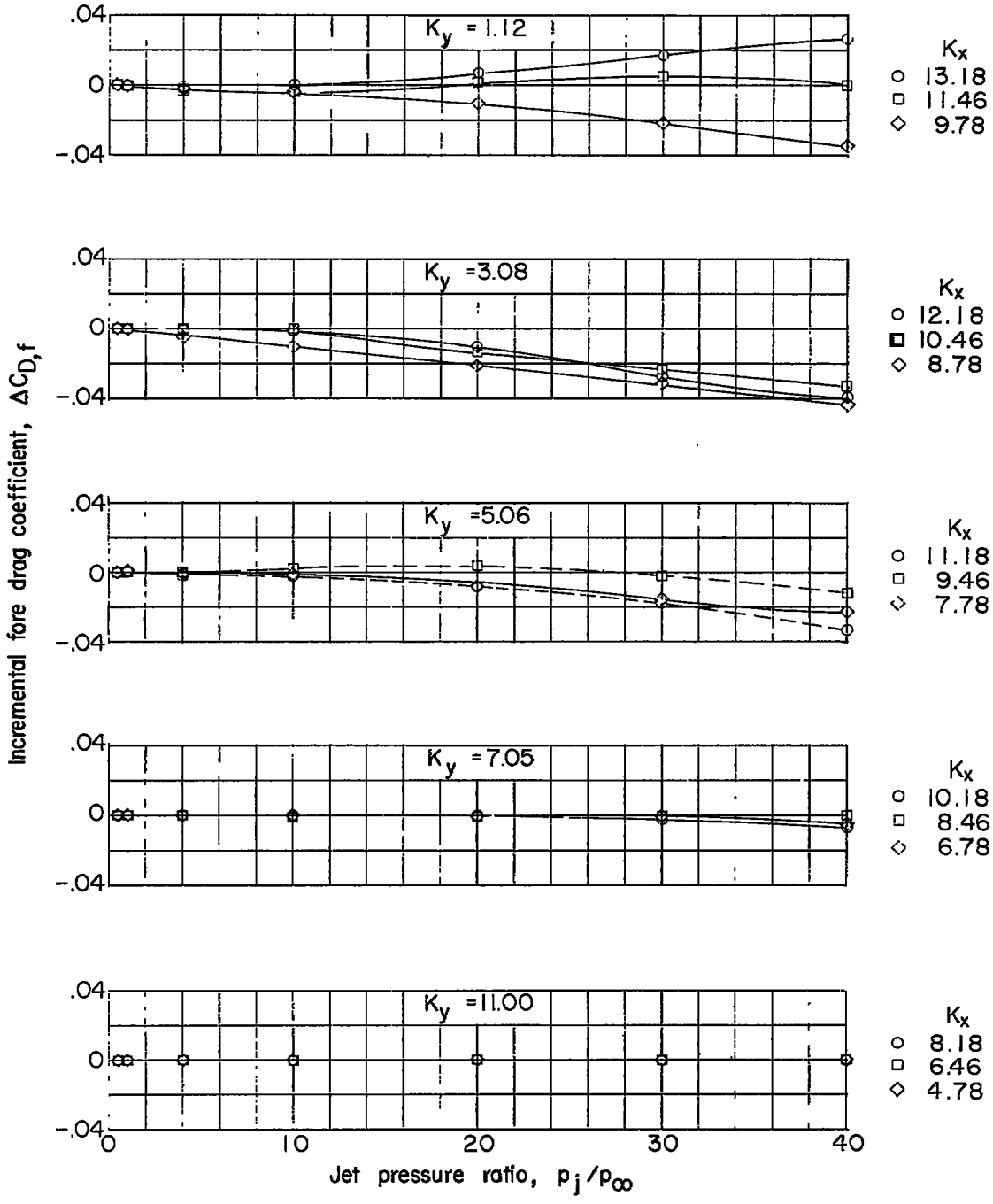

K_z = 2.5

(a) M_∞ = 1.94. Continued.

Figure 9.- Continued.

[redacted]

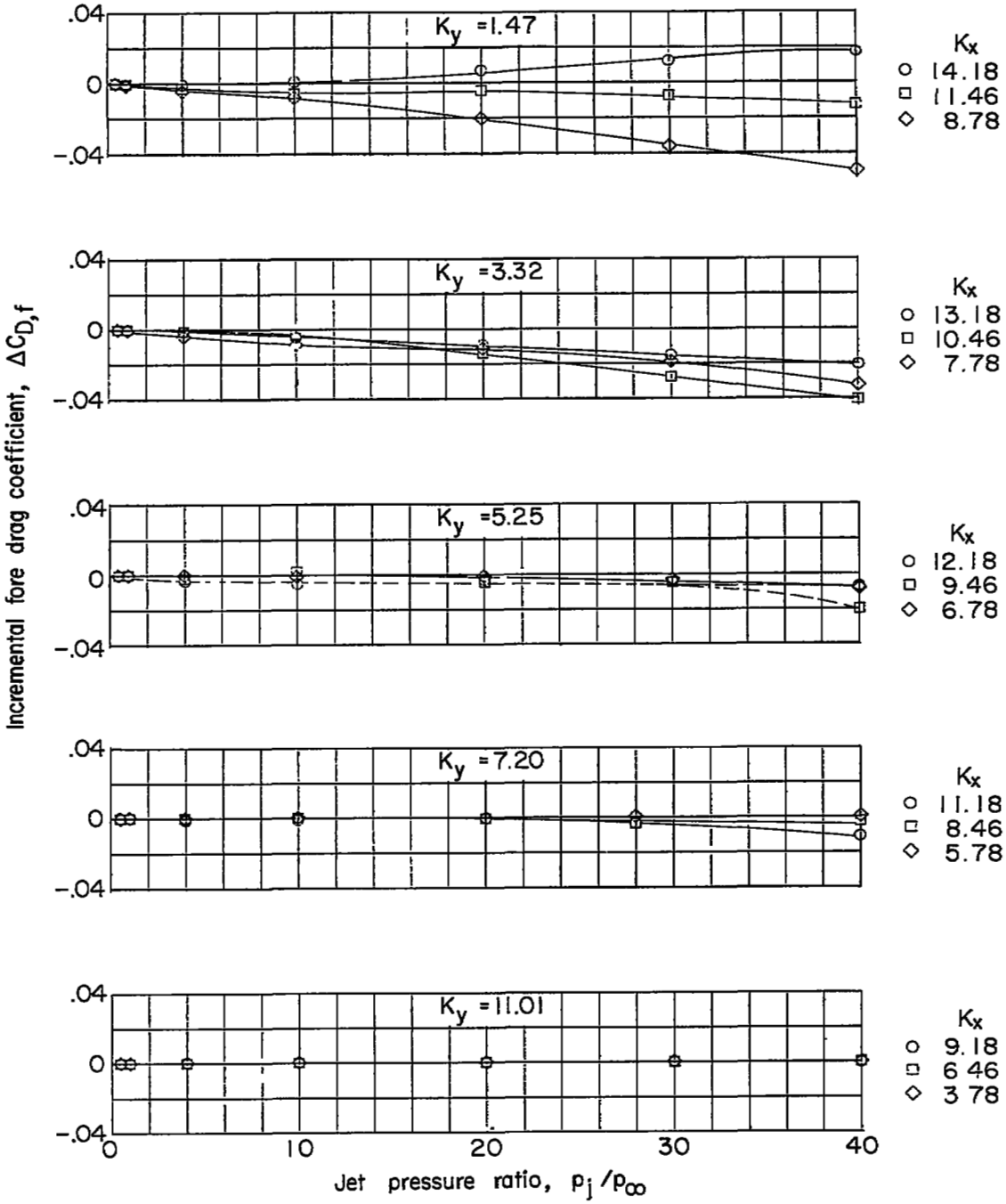

$K_z = 3.5$

(a) $M_\infty = 1.94$. Concluded.

Figure 9.- Continued.

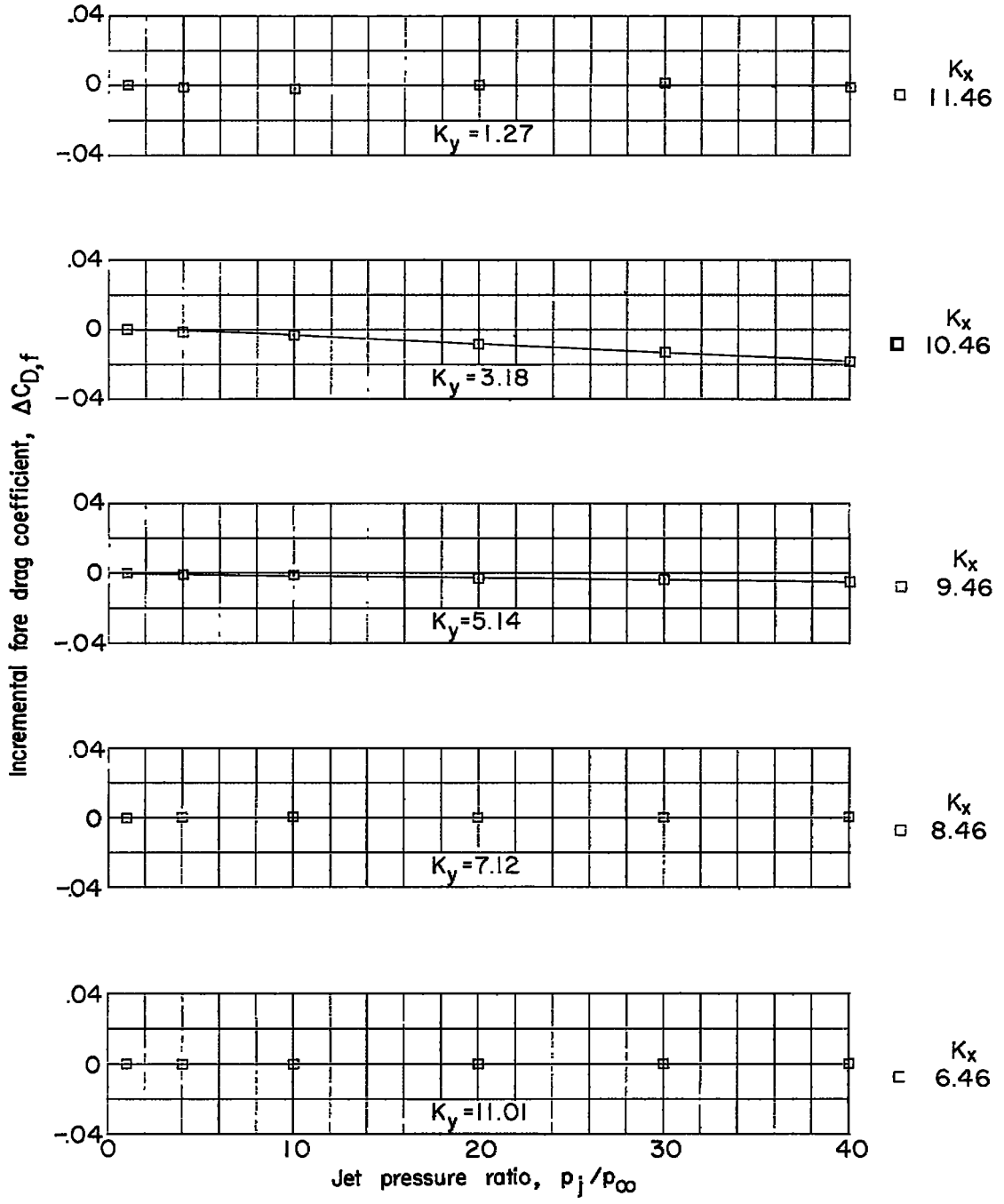

$K_z = 0$

(b) $M_\infty = 2.41$.

Figure 9.- Continued.

[redacted]

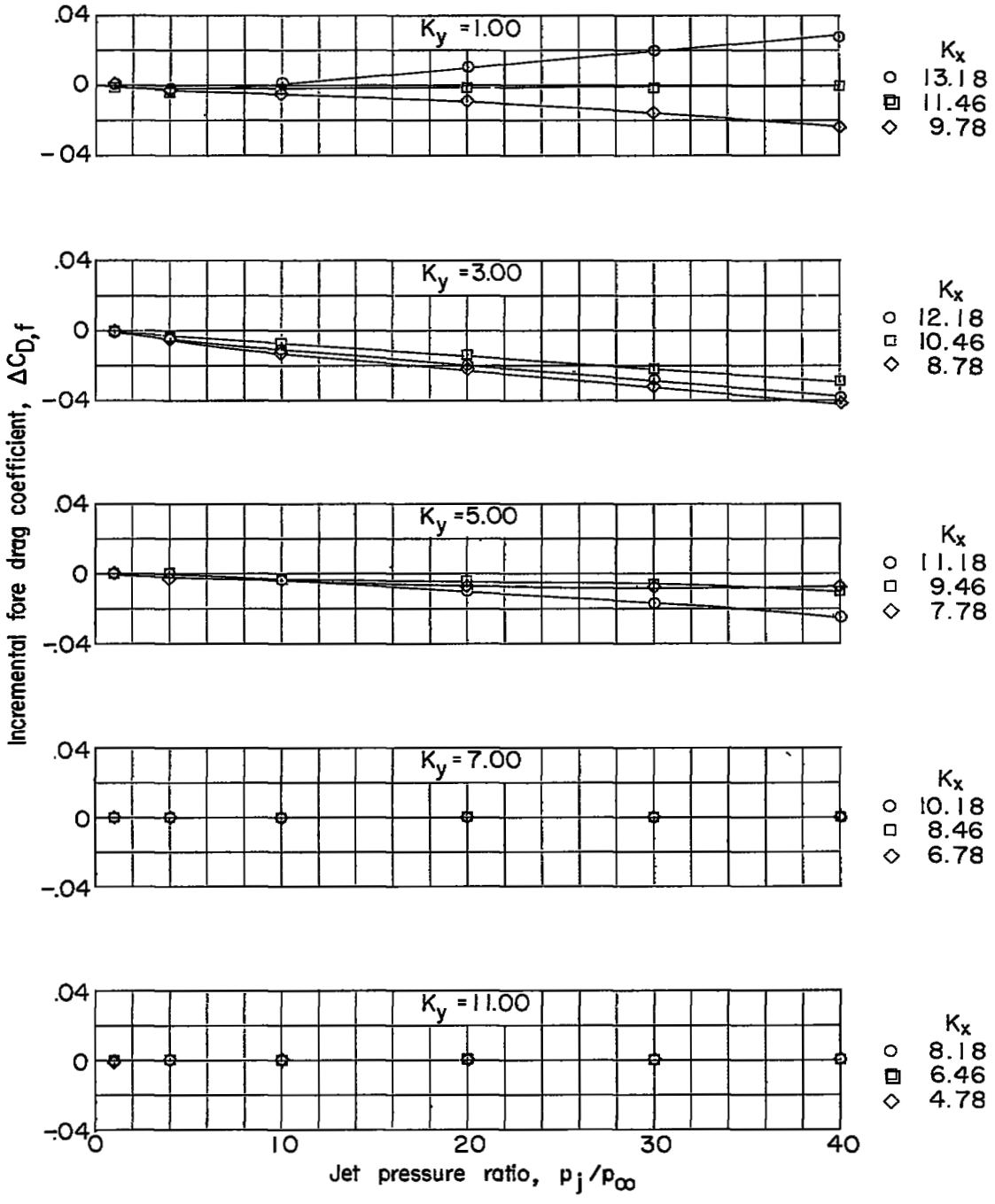

$K_z = 1.5$

(b) $M_\infty = 2.41$. Continued.

Figure 9.- Continued.

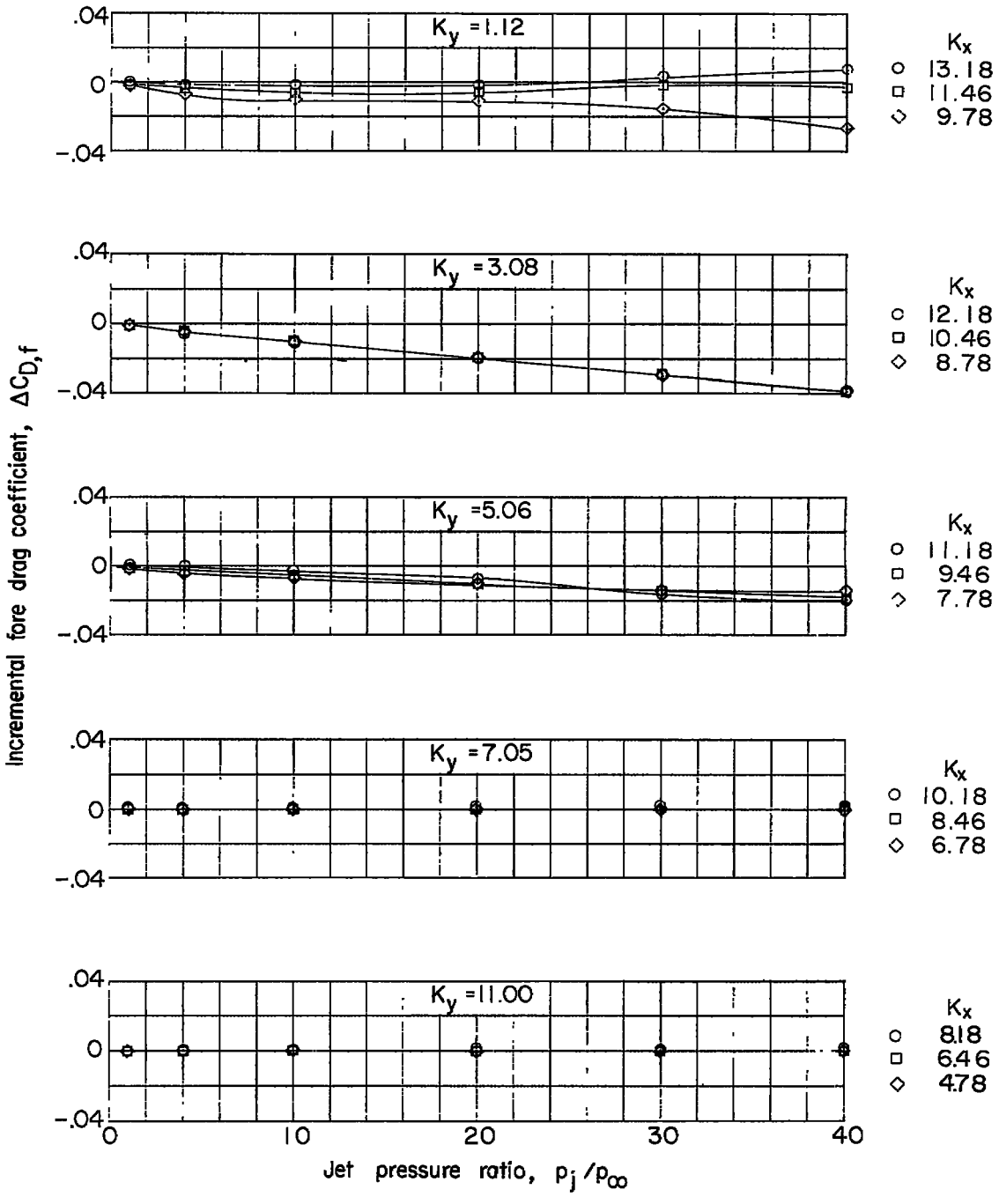

K_z = 2.5

(b) M_∞ = 2.41. Continued.

Figure 9.- Continued.

[redacted]

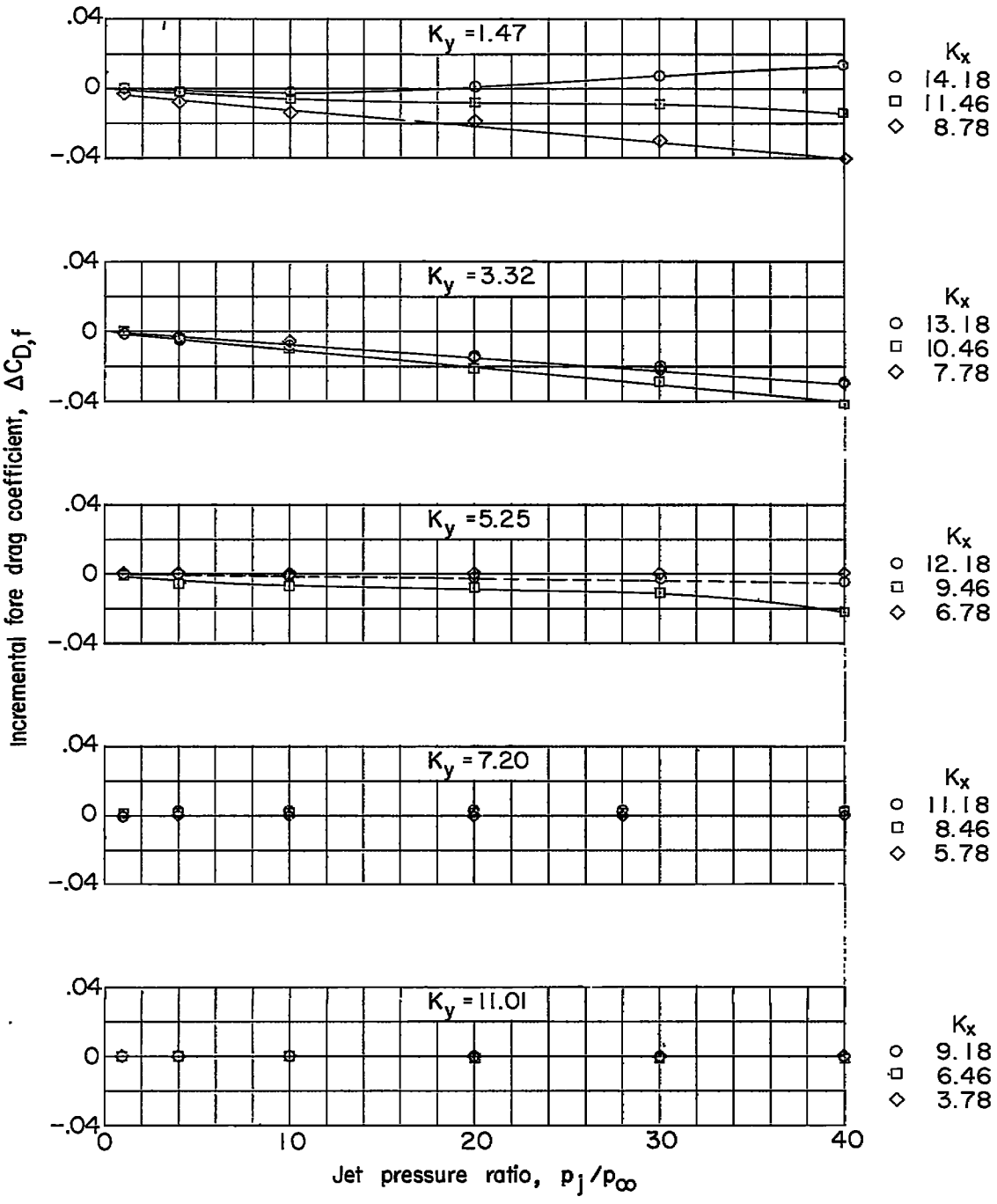

K_z = 3.5

(b) M_∞ = 2.41. Concluded.

Figure 9.- Concluded.

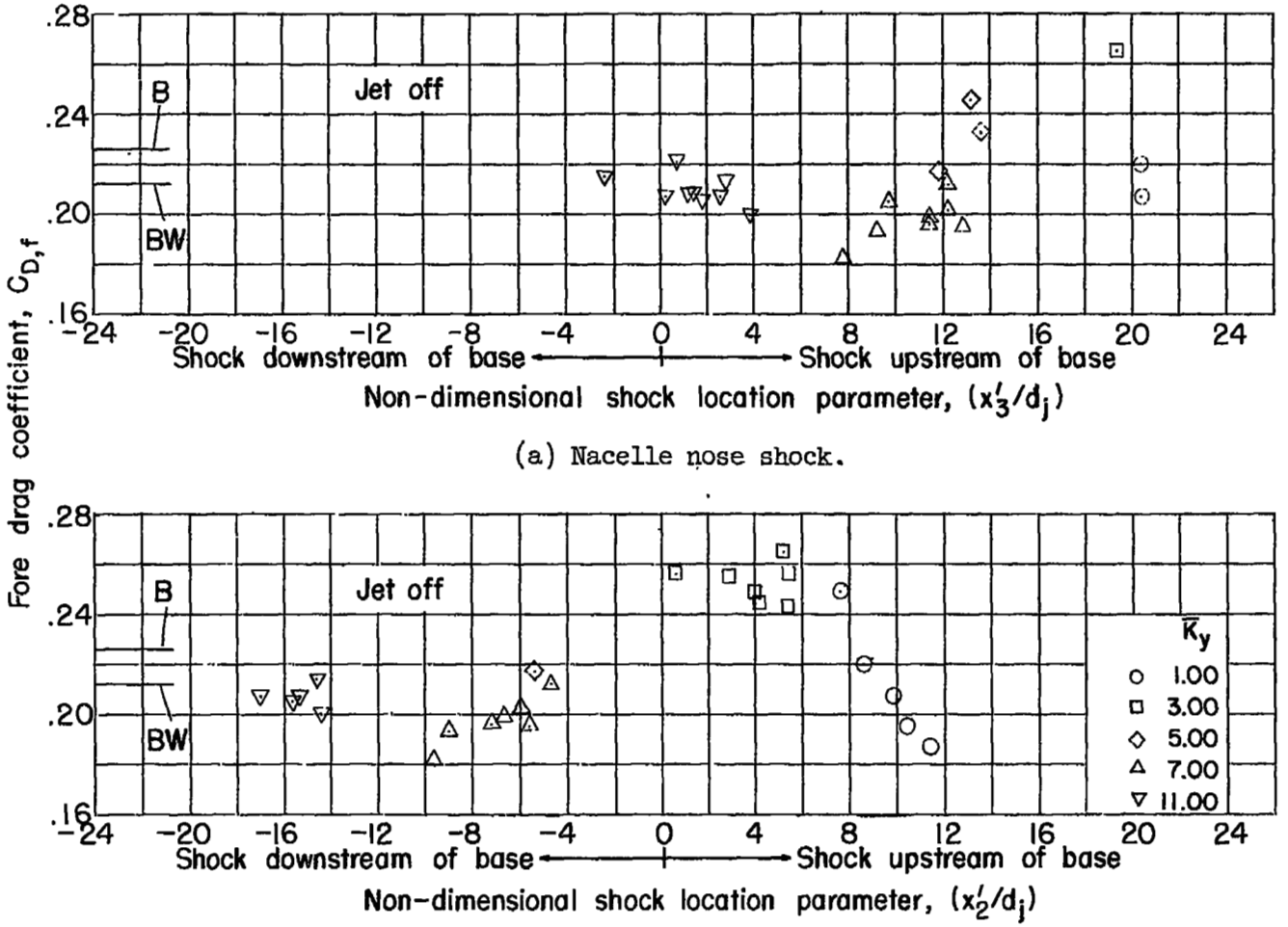

(a) Nacelle nose shock.

(b) Trailing shock.

Figure 10.- Changes in shock locations associated with changes in fore drag and incremental fore drag of the body; $M_\infty = 1.94$.

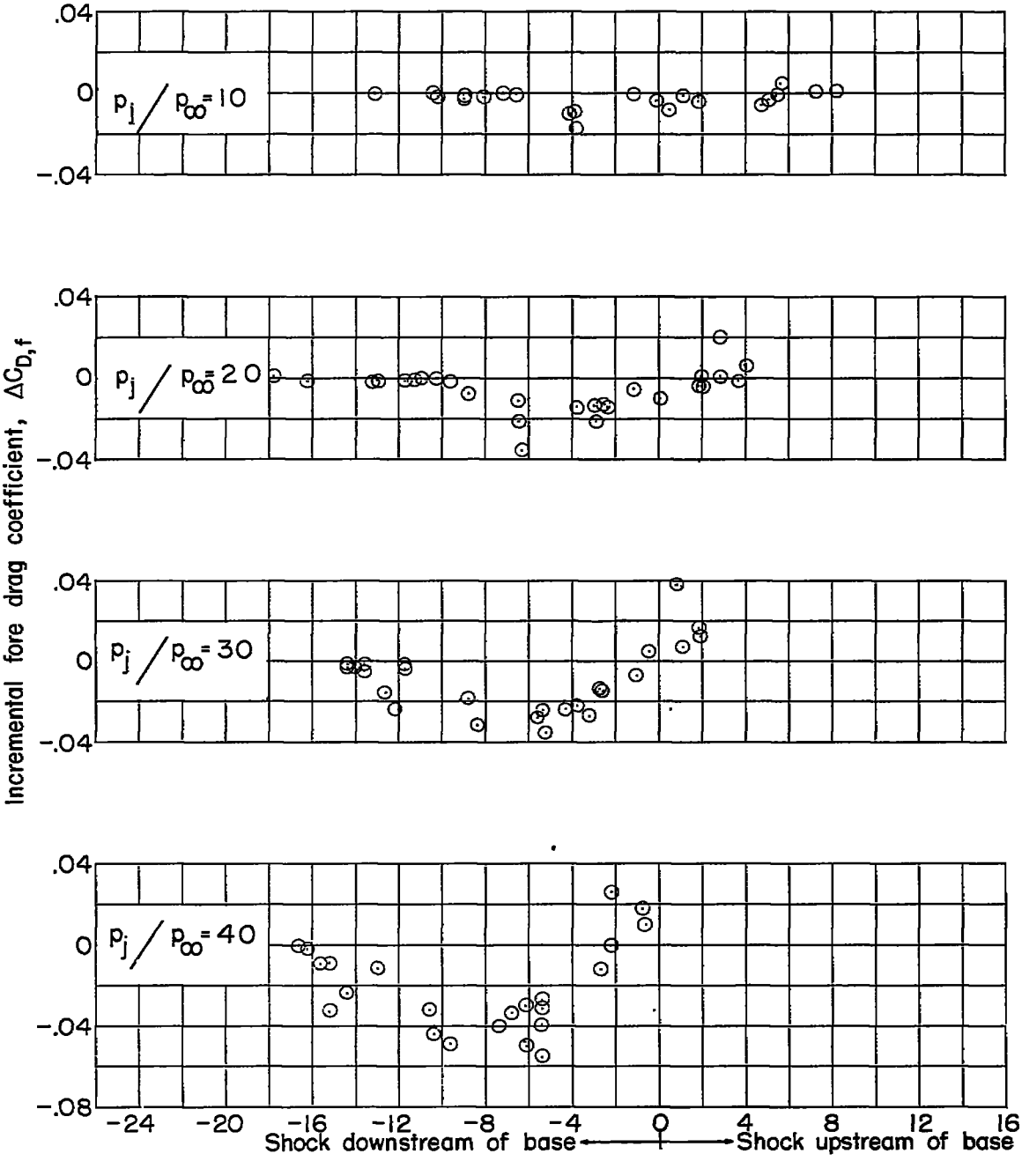

(c) Shock from within jet.

Figure 10.- Continued.

[redacted]

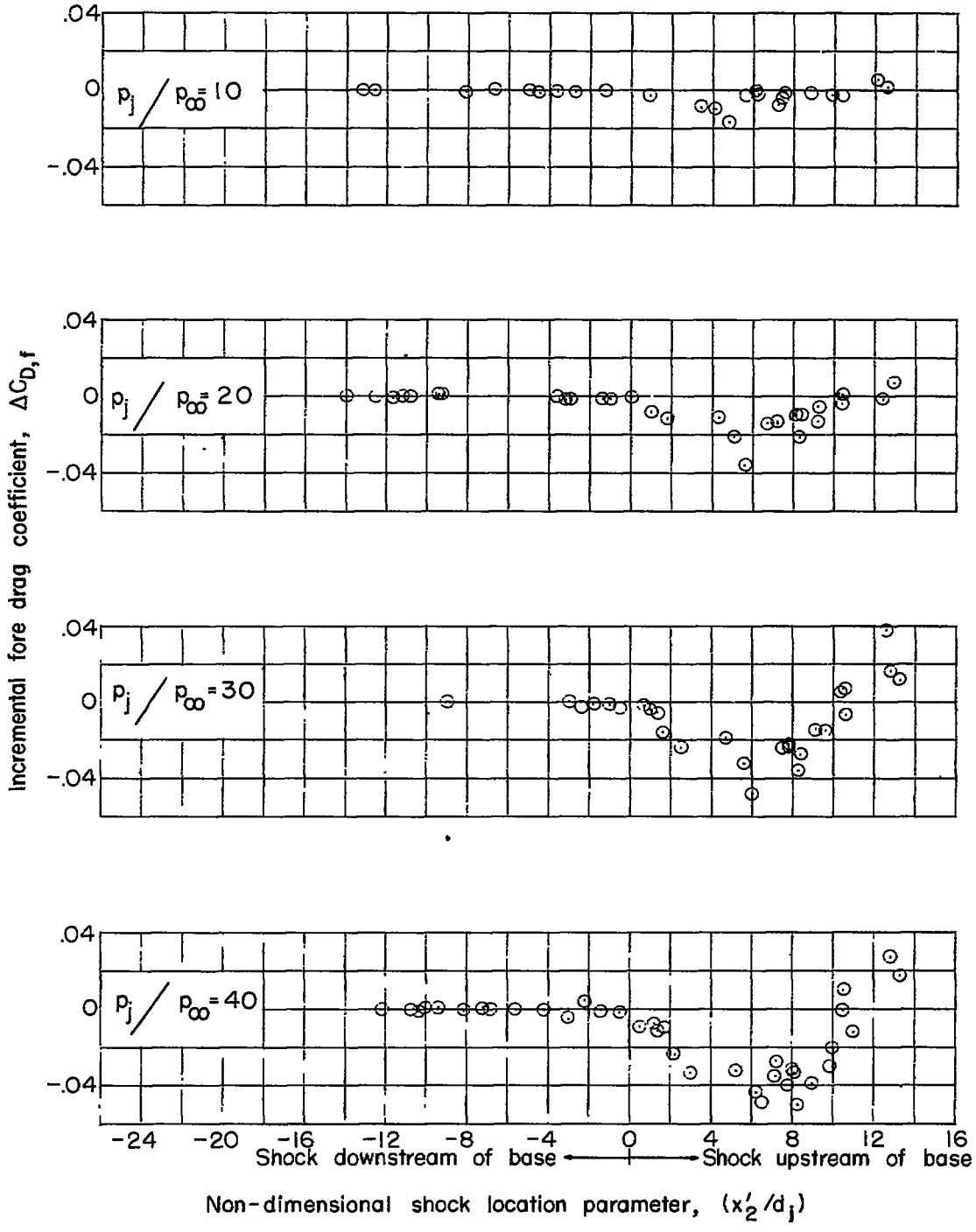

(d) Exit shock.

Figure 10.- Concluded.

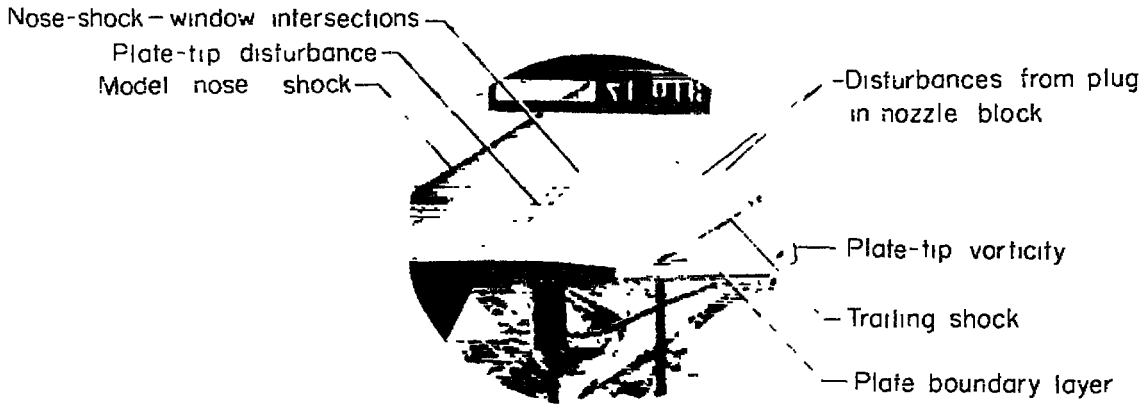

(a) Body alone.

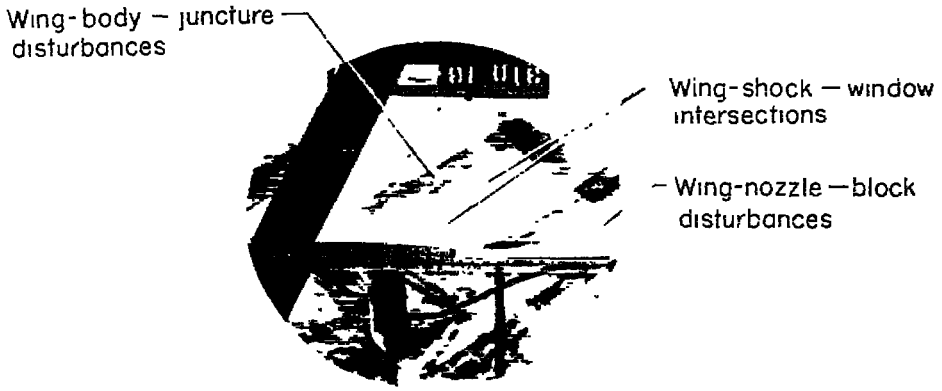

(b) Body-wing combination.

L-91752

Figure 11.- Schleren photographs of model buildup; $M_\infty = 1.94$.

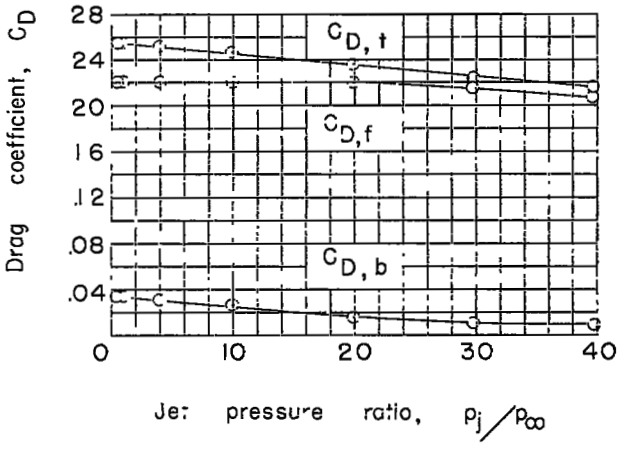

Jet off

$p_j/p_\infty = 1$ $p_j/p_\infty = 4$ $p_j/p_\infty = 10$

$p_j/p_\infty = 20$ $p_j/p_\infty = 30$ $p_j/p_\infty = 40$

(a) Model 2-C; $K_x = 8.96$, $K_y = 6.06$, $K_z = 2.50$. L-91753

Figure 12.- Comparisons of flow fields and measured body drag coefficients; $M_\infty = 1.94$.

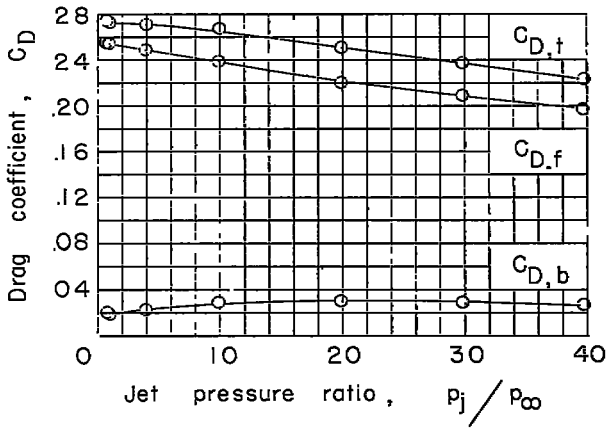

Jet off

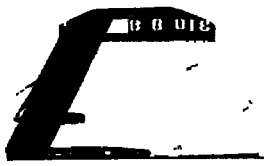

$p_j / p_\infty = 1$

$p_j / p_\infty = 4$

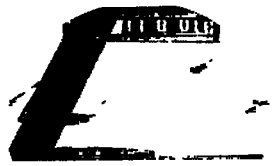

$p_j / p_\infty = 10$

$p_j / p_\infty = 20$

$p_j / p_\infty = 30$

$p_j / p_\infty = 40$

L-91754

(b) Model 3-B; $K_x = 8.78$, $K_y = 3.00$, $K_z = 1.50$.

Figure 12.- Continued.

[redacted]

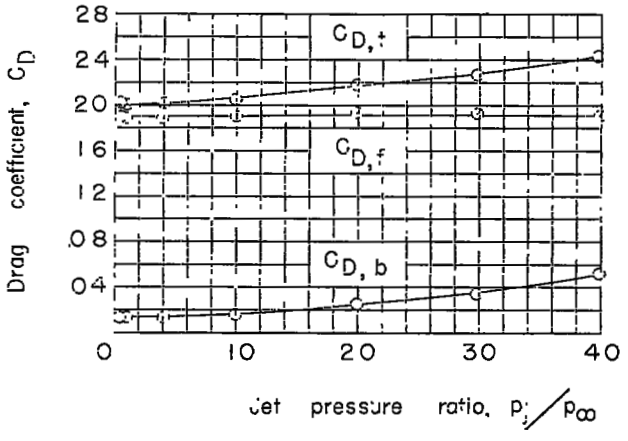

Jet off

$p_j / p_\infty = 1$ $p_j / p_\infty = 4$ $p_j / p_\infty = 10$

$p_j / p_\infty = 20$ $p_j / p_\infty = 30$ $p_j / p_\infty = 40$

L-91755

(c) Model 2-A; $K_x = 11.46$, $K_y = 1.27$, $K_z = 0$.

Figure 12.- Concluded.

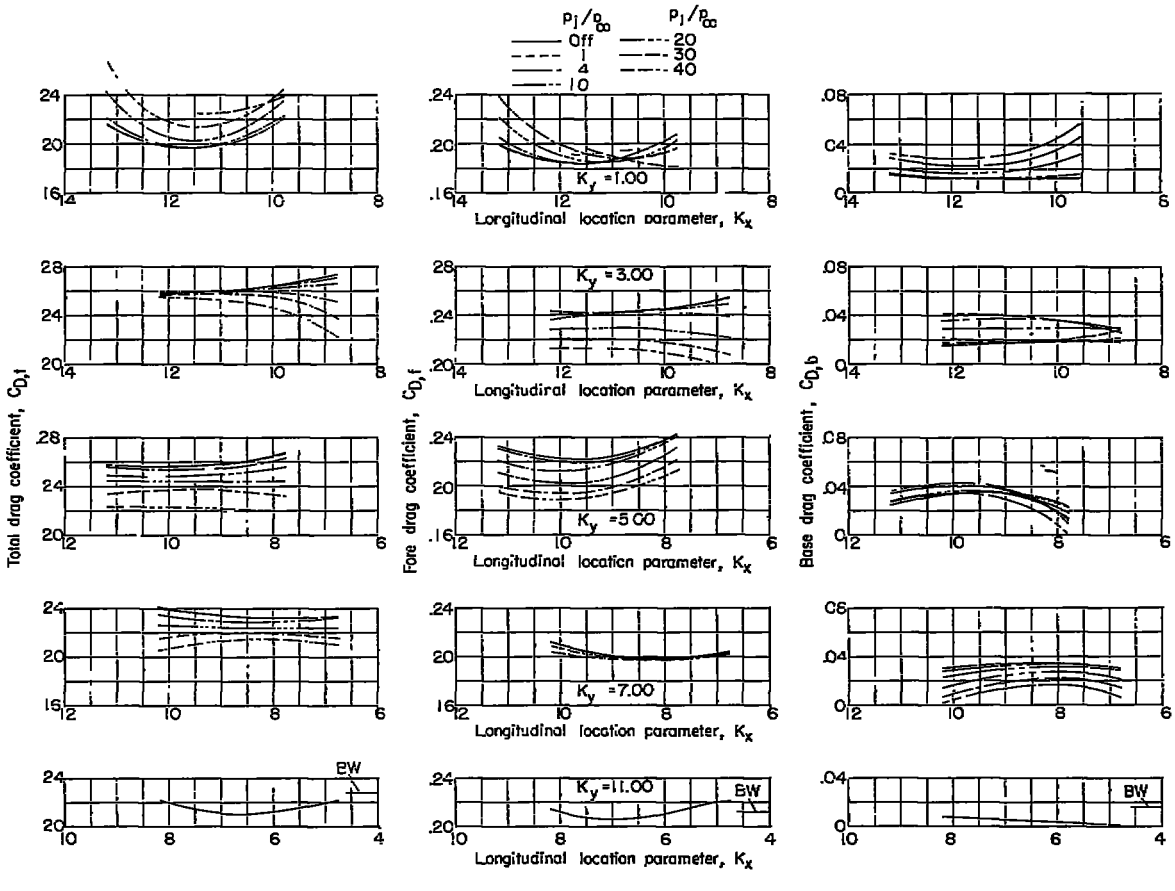

$K_Z = 1.5$

(a) $M_\infty = 1.94$.

Figure 13.- Variation of measured drag coefficients with longitudinal nacelle location.

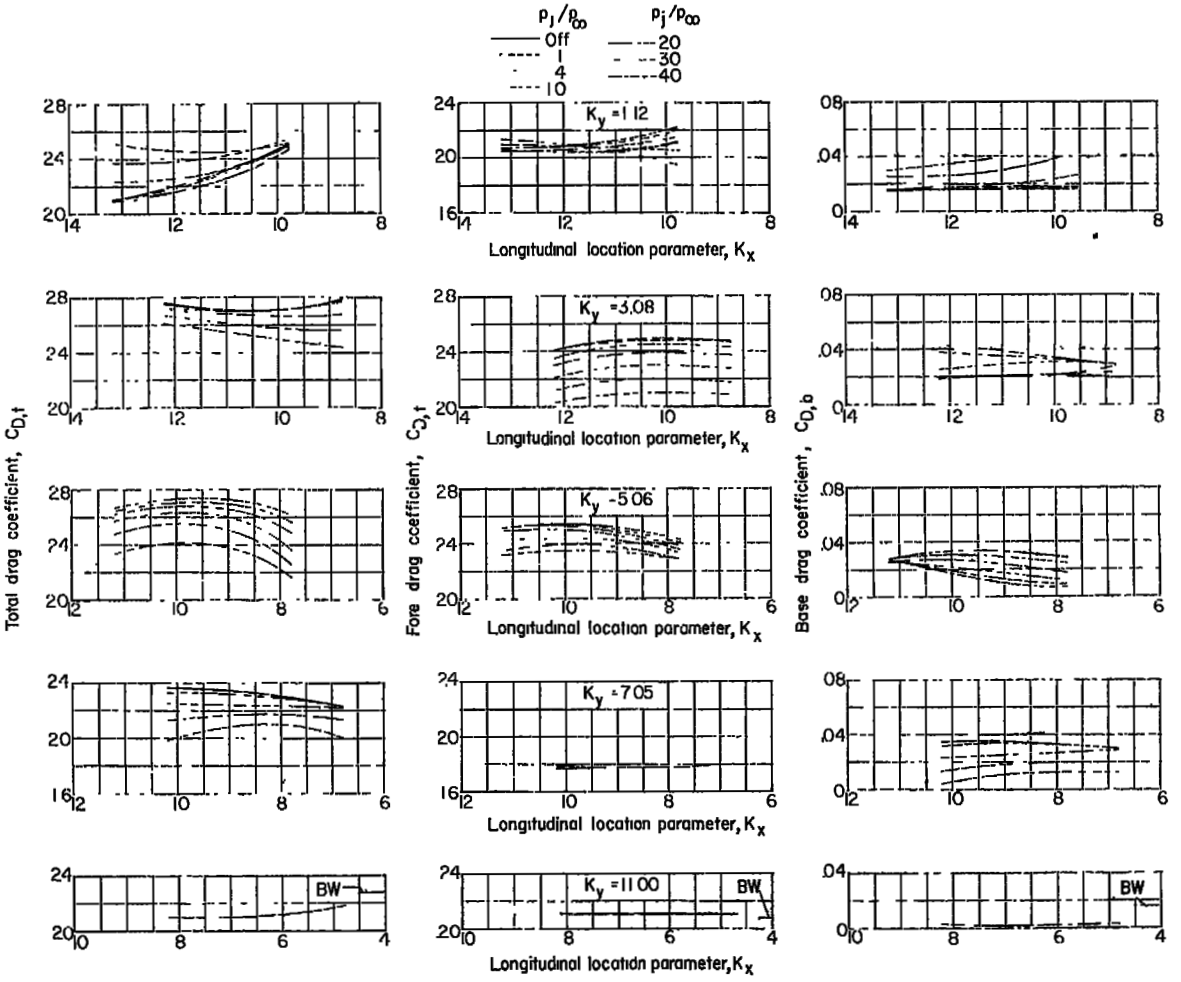

$K_Z = 2.5$

(a) $M_\infty = 1.94$. Continued.

Figure 13.- Continued.

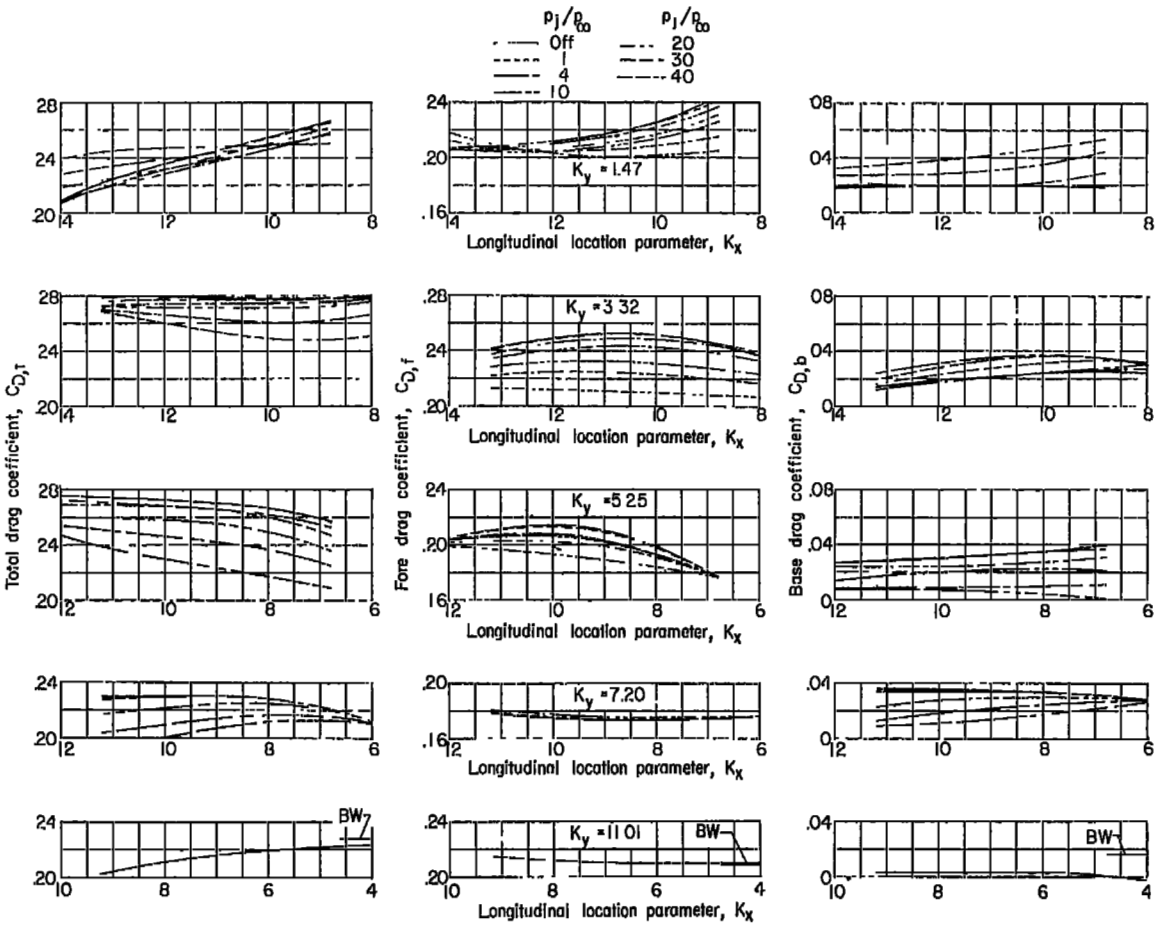

$K_Z = 3.5$

(a) $M_\infty = 1.94$. Concluded.

Figure 13.- Continued.

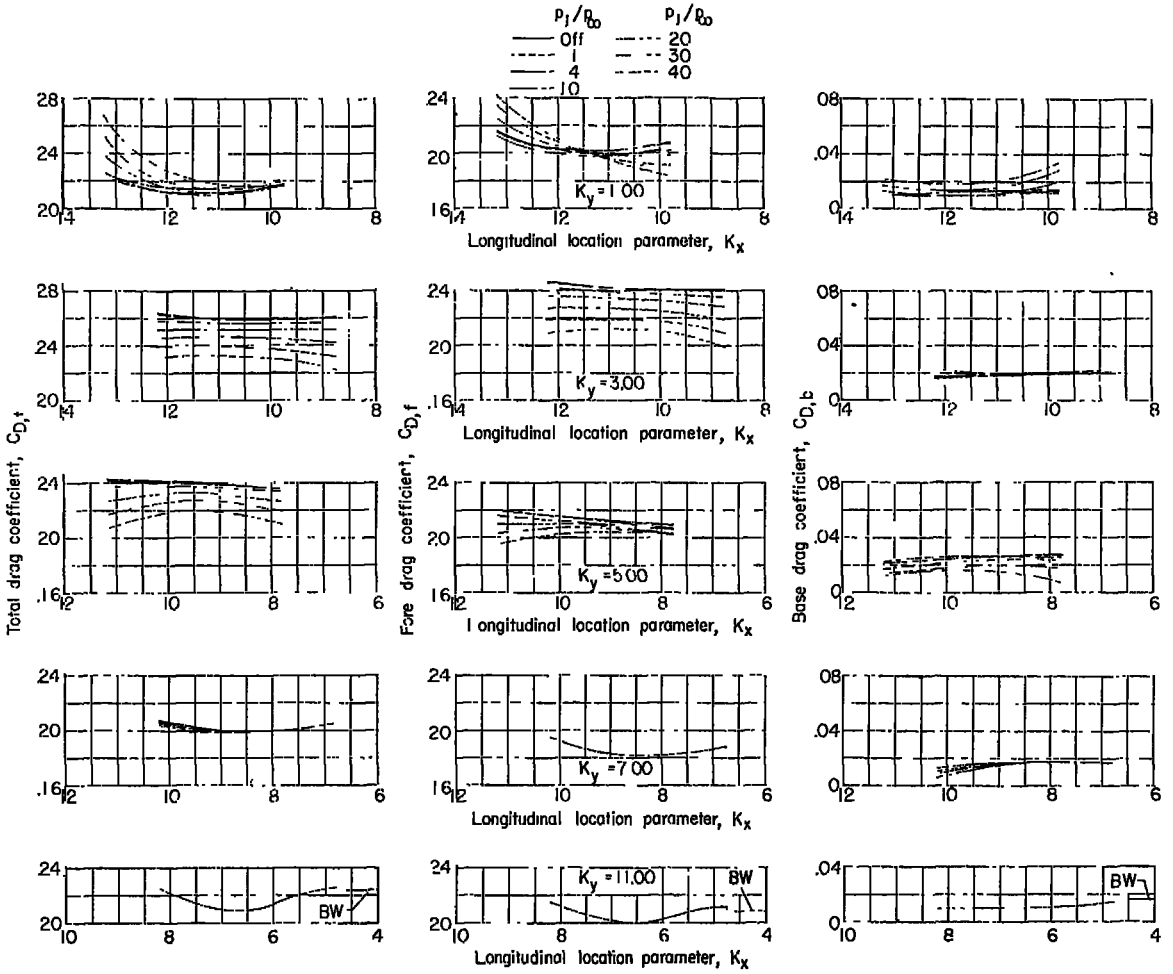

$K_Z = 1.5$

(b) $M_\infty = 2.41$.

Figure 13.- Continued.

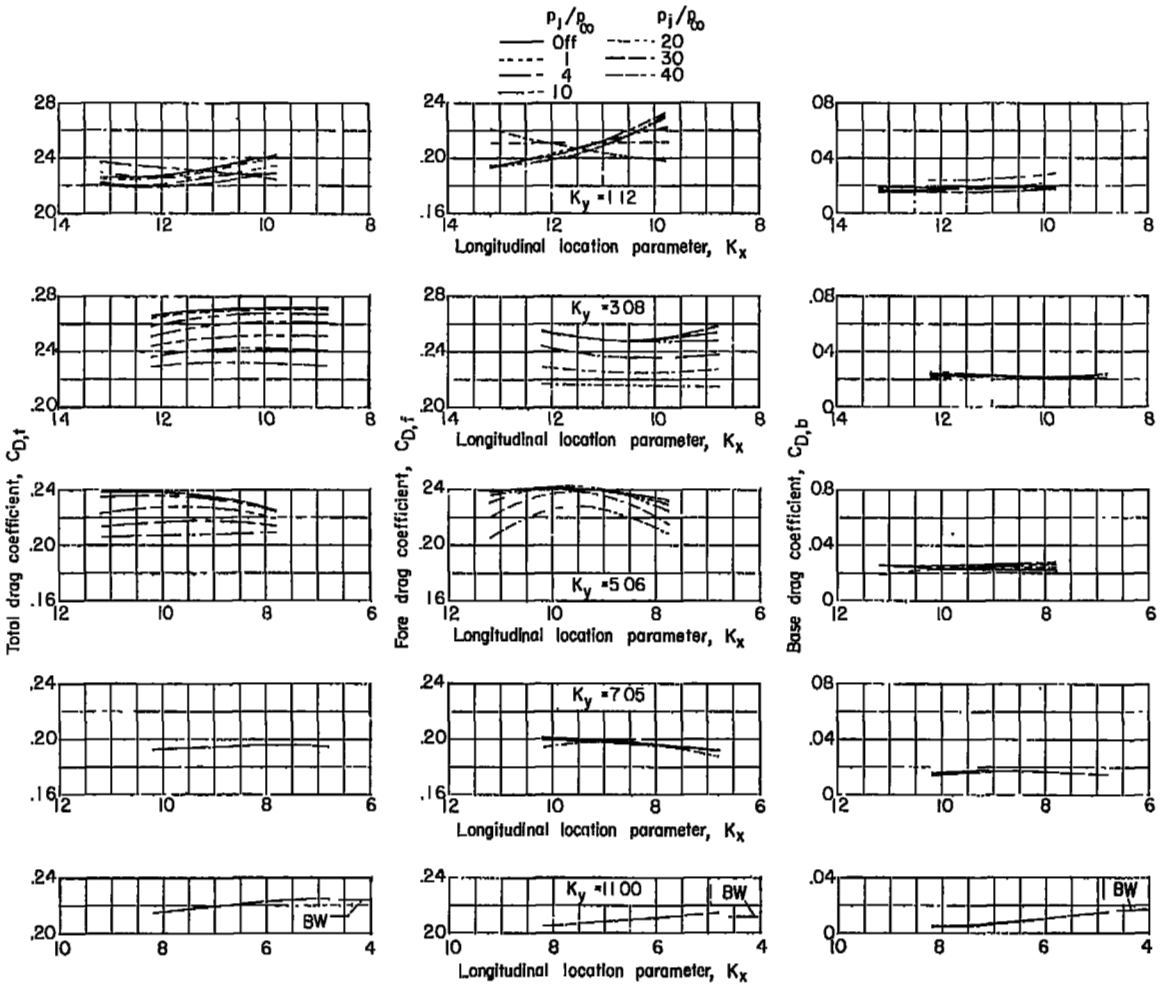

$K_Z = 2.5$

(b) $M_\infty = 2.41$. Continued.

Figure 13.- Continued.

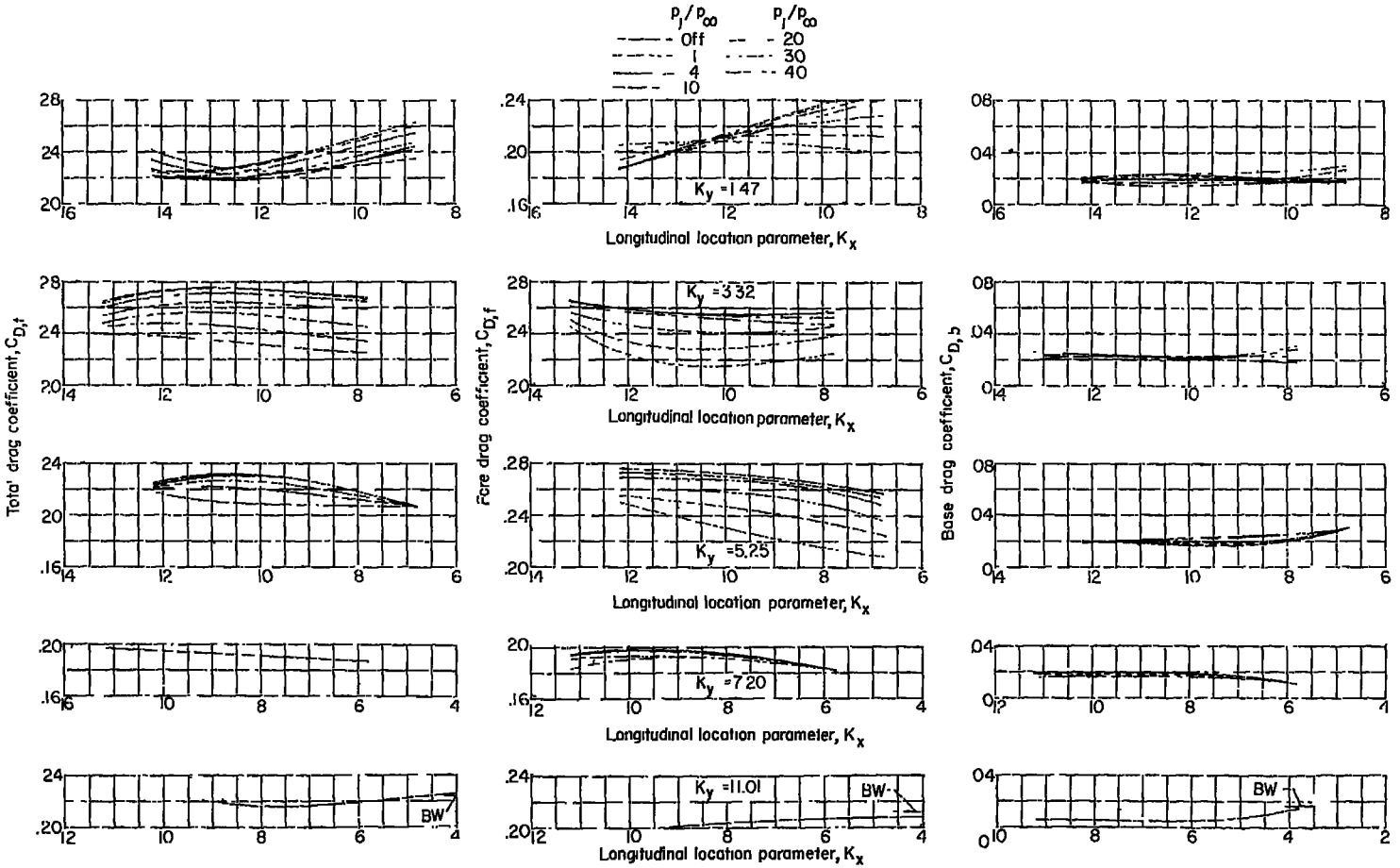

$K_Z = 3.5$

(b) $M_\infty = 2.41$. Concluded.

Figure 13.- Concluded.

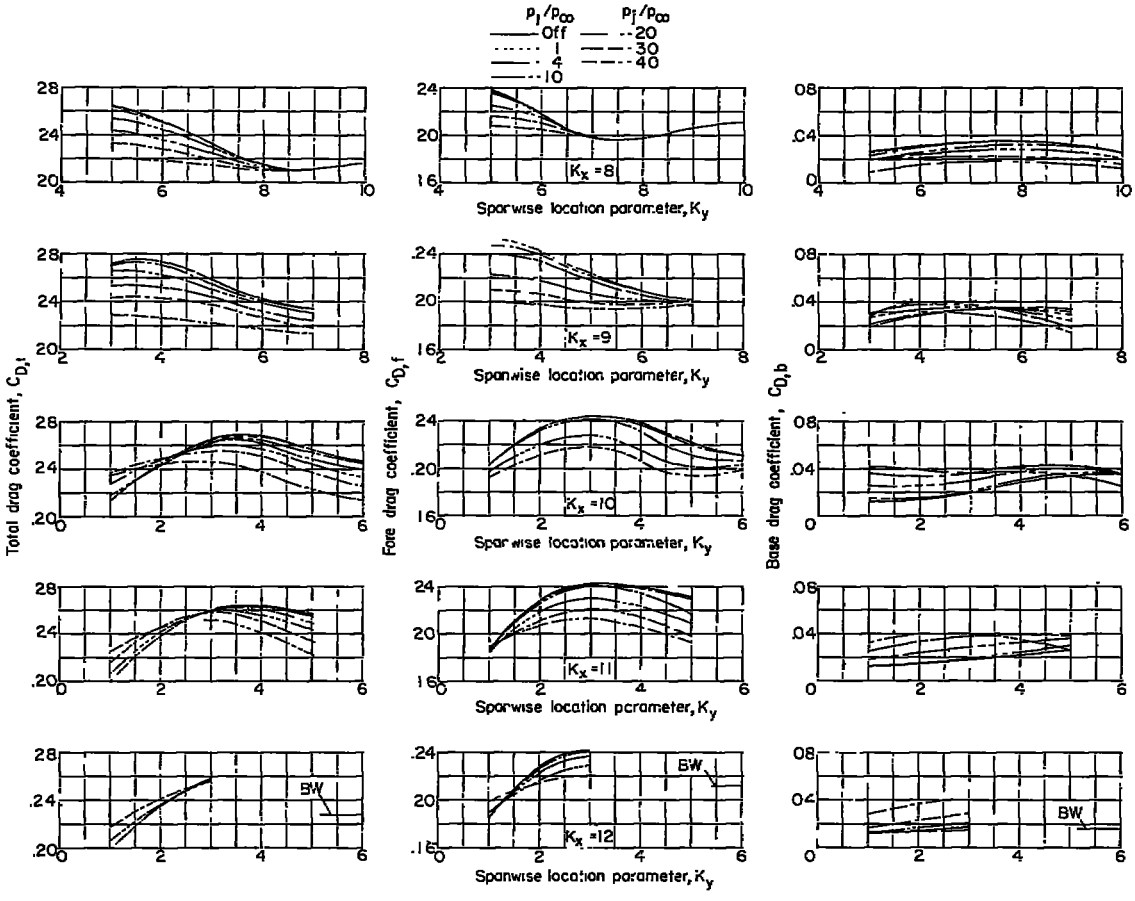

$K_Z = 1.5$

(a) $M_\infty = 1.94$.

Figure 14.- Variation of measured drag coefficients with spanwise nacelle location.

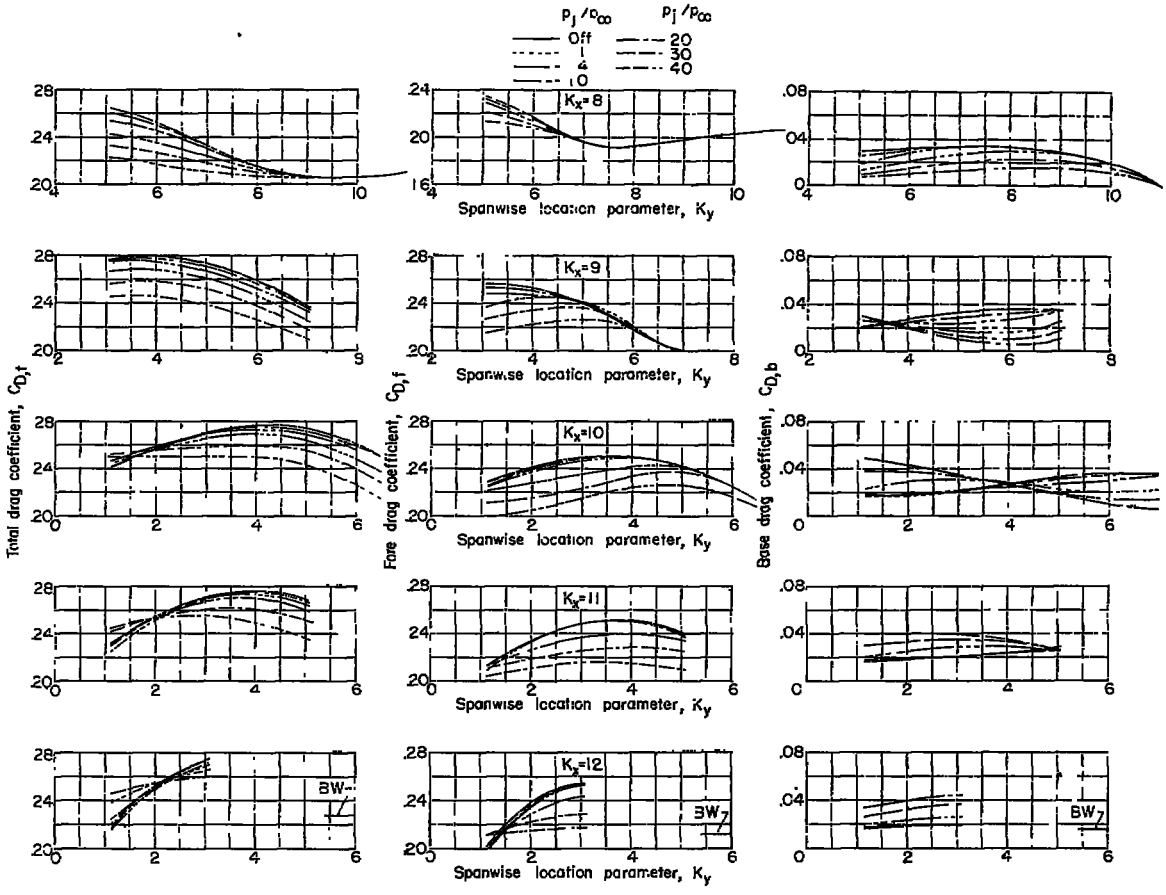

$K_z = 2.5$

(a) $M_\infty = 1.94$. Continued.

Figure 14.- Continued.

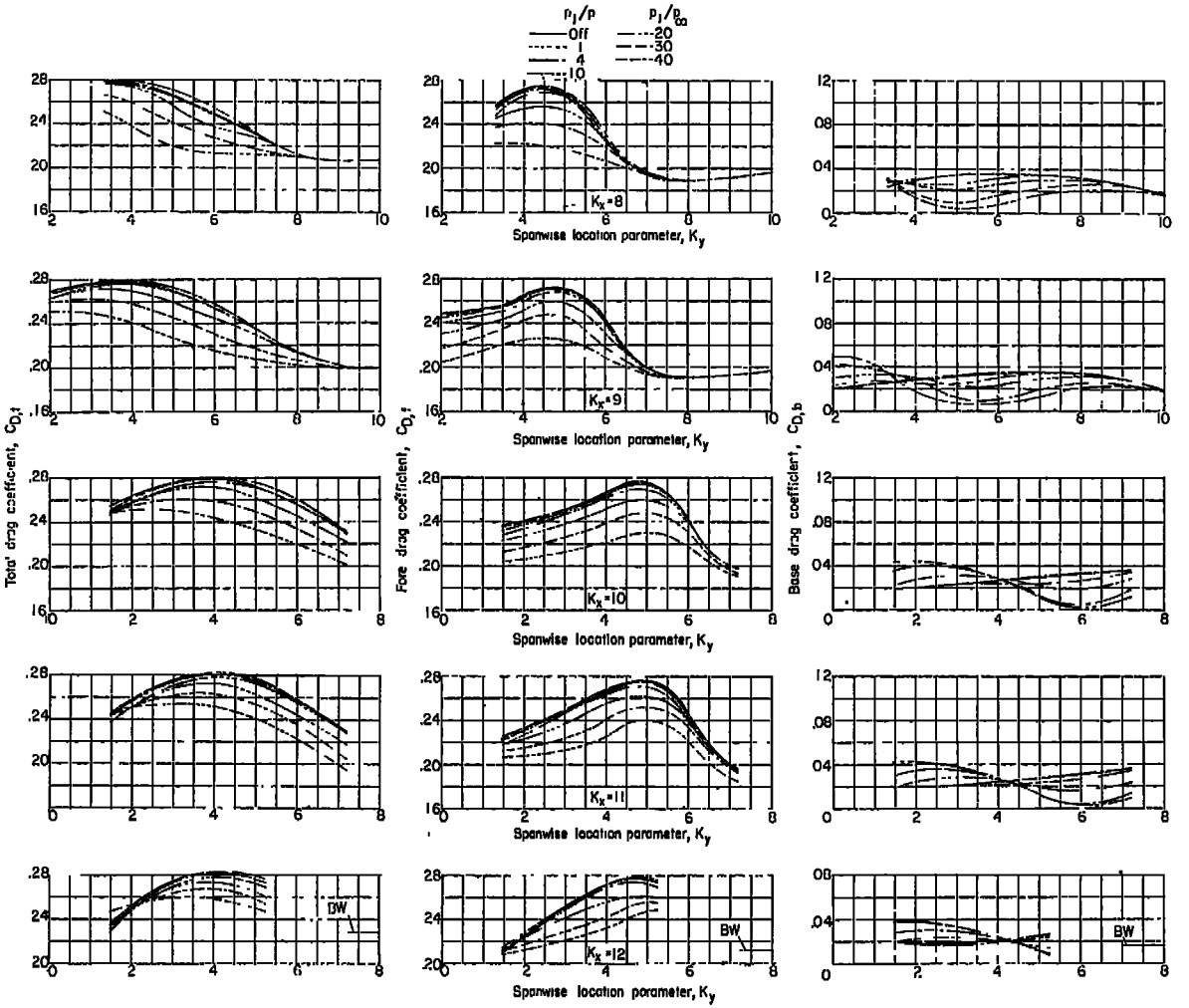

$K_Z = 3.5$

(a) $M_\infty = 1.94$. Concluded.

Figure 14.- Continued.

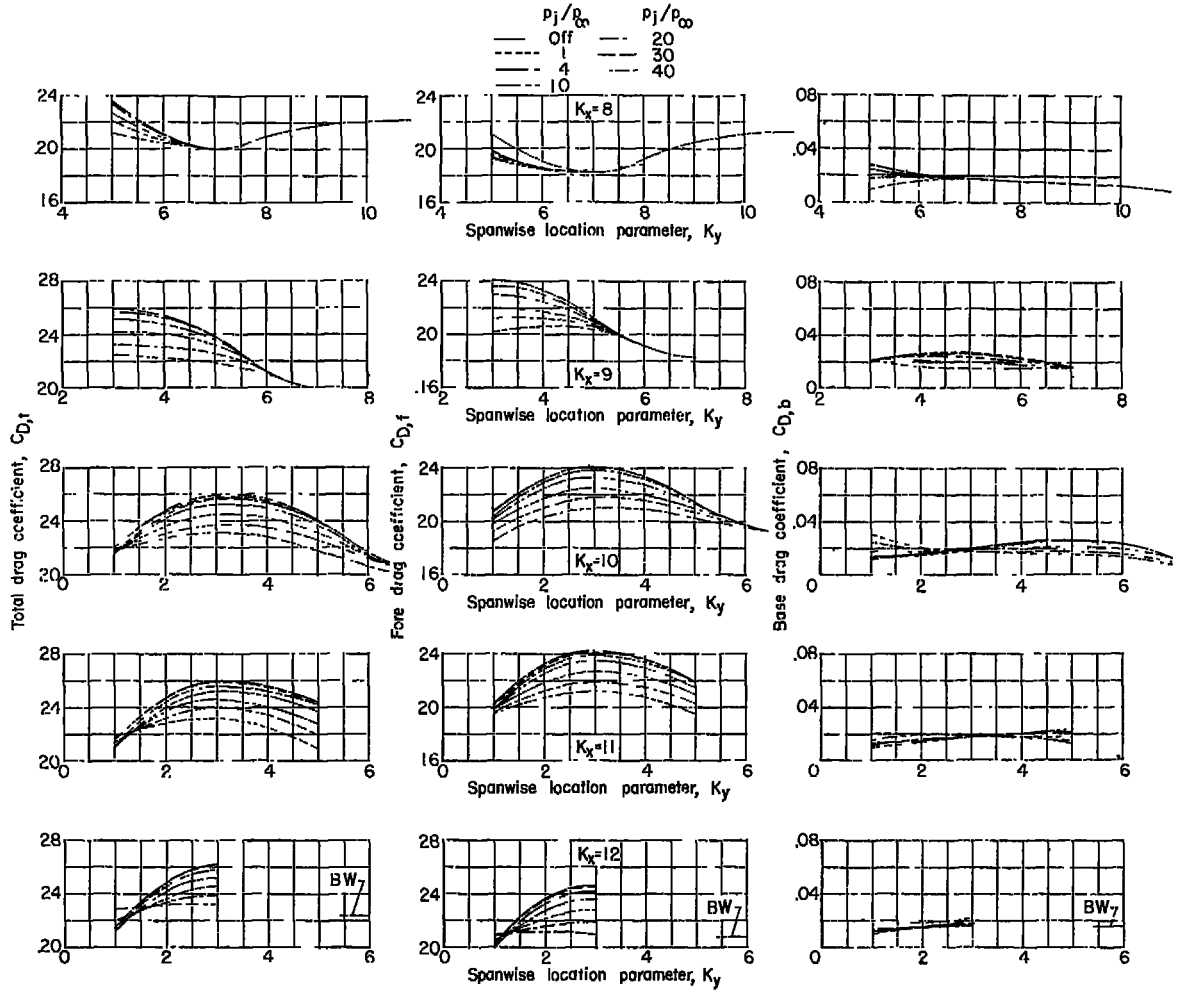

$K_Z = 1.5$

(b) $M_\infty = 2.41$.

Figure 14.- Continued.

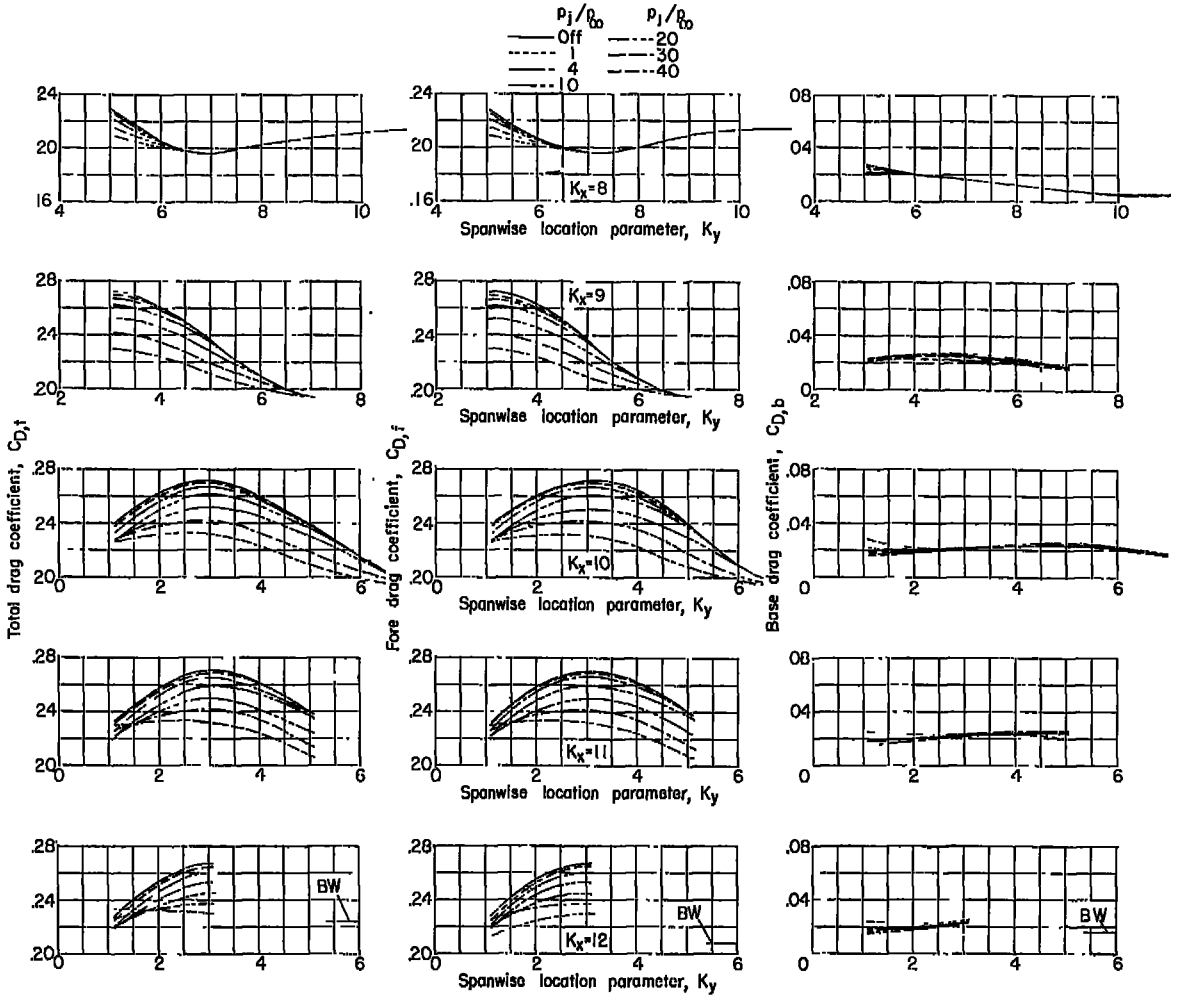

$K_Z = 2.5$

(b) $M_\infty = 2.41$. Continued.

Figure 14.- Continued.

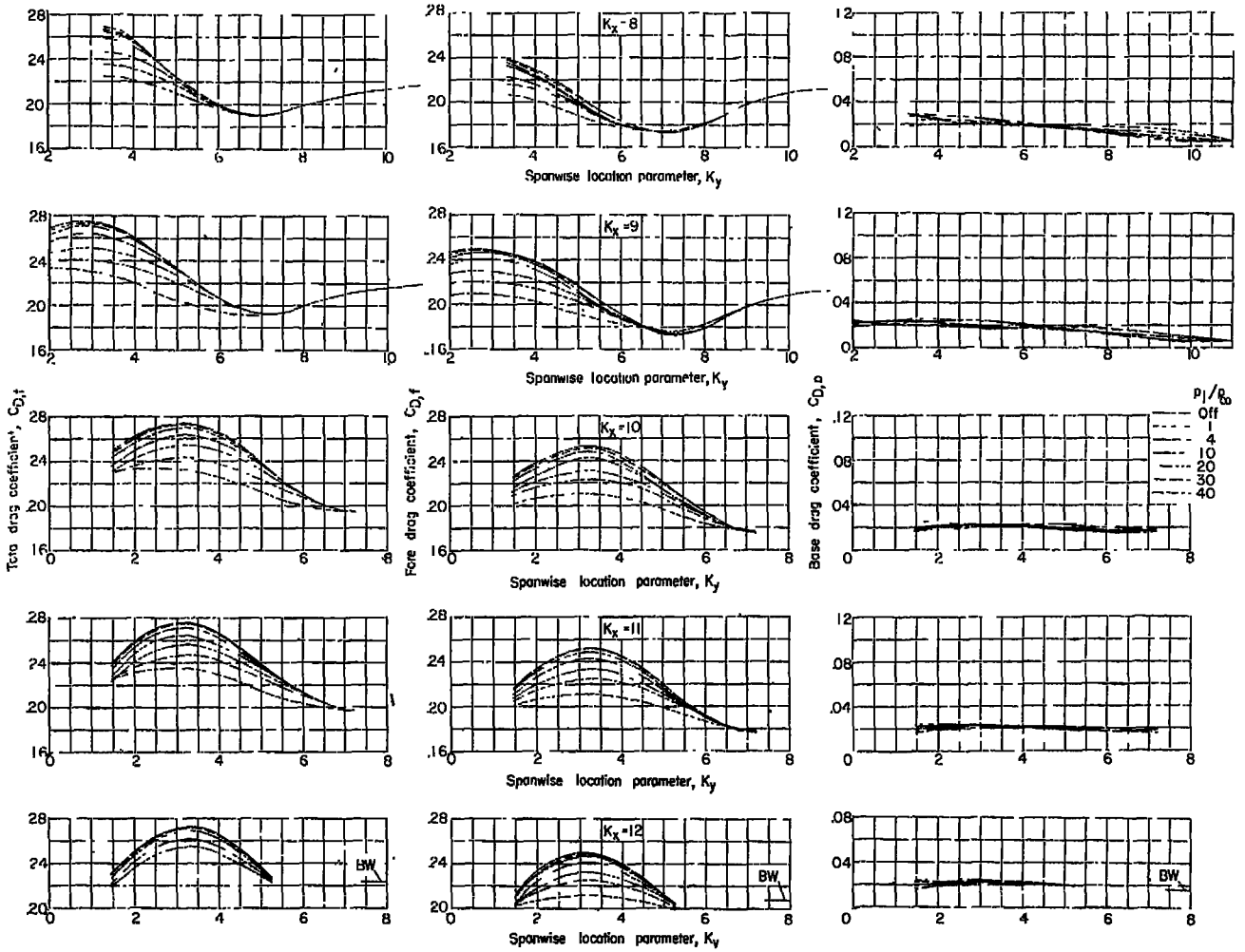

$K_Z = 3.5$

(b) $M_\infty = 2.41$. Concluded.

Figure 14.- Concluded.

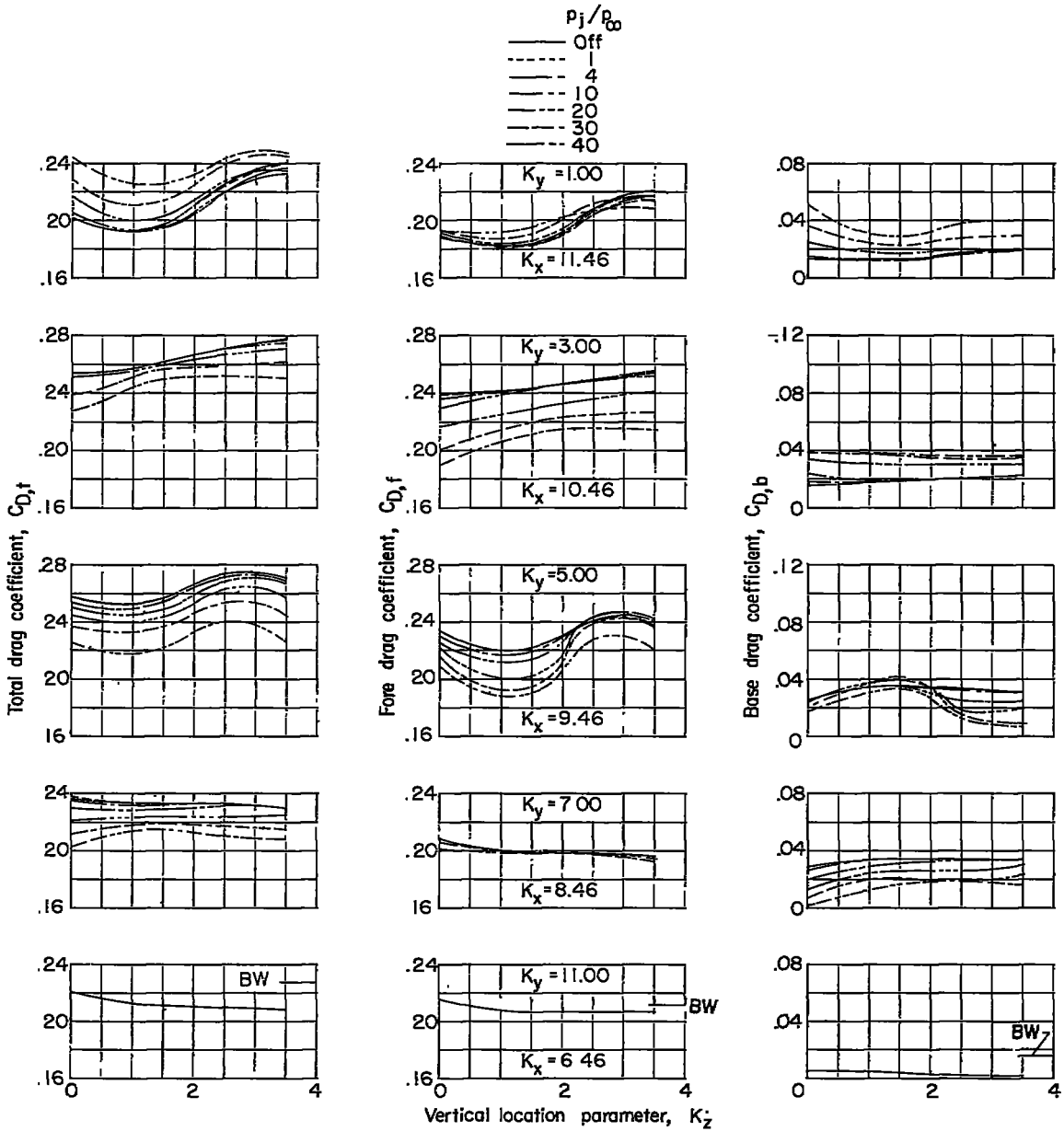

(a) $M_\infty = 1.94$.

Figure 15.- Variation of measured drag coefficients with vertical nacelle locations; unswept pylon.

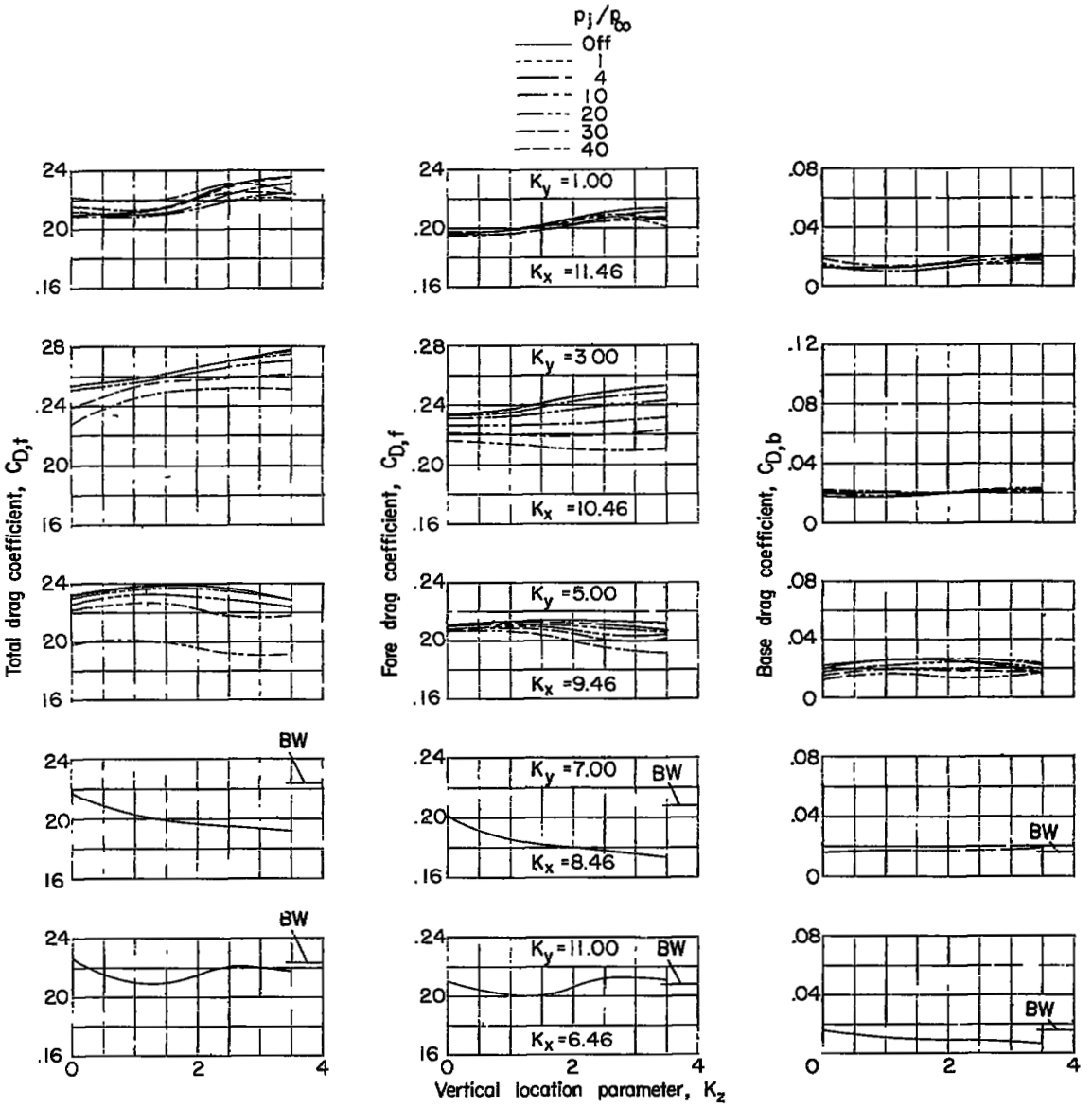

(b) $M_\infty = 2.41$.

Figure 15.- Concluded.

NACA - Langley Field, Va

LANGLEY RESEARCH CENTER
3 1176 01348 4747